Separation and Focusing of Magnetic Beads for Agglutination Tests

THÈSE N° 4996 (2011)

PAR

Rana AFSHAR GHASEMLOUY

EPFL

ÉCOLE POLYTECHNIQUE
FÉDÉRALE DE LAUSANNE

Suisse
2011

Abstract

Functional magnetic micro- and nanoparticles are used in bioanalytical applications as solid carriers for capture, transport and detection of biomolecules or magnetically labeled cells. Colloidal suspensions of such particles provide a large specific surface for chemical binding and therefore allow highly efficient interactions with target molecules in a sample solution. Controlled actuation and manipulation of these mobile substrates in the microfluidic format offers interesting new opportunities for on-chip bioassays with previously unmatched properties. Separation of functional magnetic particles or magnetically labeled entities is therefore a key feature for bioanalytical or biomedical applications and also an important component of lab-on-a-chip devices for biological applications.

In this thesis we present two novel integrated microfluidic magnetic bead manipulation devices. The first system consists of dosing of magnetic particles, controlled release and subsequent magnetophoretic size separation with high resolution. On-chip integrated soft-magnetic microtips with different shapes provide the magnetic driving force for the bead manipulation. The system is designed to meet the requirements of specific bioassays, in particular of on-chip agglutination assays for the detection of rare analytes, in which the latter can be quantified via the counting of the particle doublets.

In a second approach, magneto-microfluidic three-dimensional (3D) focusing of microparticles has been developed. In this system, magnetic microparticles from a dense plug are released into a single streamline with longitudinal inter-particle spacing. Plug formation is induced by a high-gradient magnetic field generated at the sidewall of a microchannel by a micromachined magnetic tip that is connected to an electromagnet. Controlled release of the microparticles is achieved using an exponential damping protocol of the magnetic retention force in the presence of an applied flow. Carefully balancing the relative strengths of the drag force imposed by the flow and the magnetic retention force moreover allows in-flow size separation of the microparticles. Adding subsequently a lateral sheath flow microchannel focuses the microparticles into a single stream situated within ± 5 μm from the channel center axis.

Our system for 3D focusing and in-flow separation of magnetic microparticles has been used for performing an immuno-agglutination assay on-chip. 3D focusing was of the basis of reliable in-flow counting of singlets and agglutinated doublets. We

demonstrated the potential of the agglutination assay in a microfluidic format using a streptavidin/biotinylated-bovine serum albumin (bBSA) model system. A bBSA detection limit of about 400 pg/mL (6 pM) is achieved.

Résumé

Les micro- et nanoparticules magnétiques sont utilisées dans les applications bioana-lytiques en tant que supports solides pour la capture, le transport et la détection de biomolécules ou de cellules. Les suspensions colloïdales de ces particules fournissent une grande surface spécifique pour la formation de liaisons chimiques et permettent donc des interactions hautement efficaces avec les molécules cibles dans un échantillon. La combinaison de l'actionnement contrôlé et de la manipulation de ces substrats mo-biles dans le format microfluidique offre des possibilités nouvelles et intéressantes pour des essais biologiques sur puce. La séparation des particules magnétiques ou des entités marquées magnétiquement est donc un élément clé pour la bioanalyse et les applica-tions biomédicales Particuliérment en ce qui concerne les dispositifs de laboratoire sur puce.

Dans cette thèse, nous présentons deux nouveaux microsystèmes magnétiques pour la manipulation des billes magnétiques dans des microcanaux. Le premier système se compose du dosage des billes magnétiques, de leur libération contrôlée et de leur séparation à haute résolution en fonction de leur taille. Des micropointes magnétiques intégrées de différentes formes fournissent la force magnétique pour la manipulation des billes. Le système est conçu pour répondre aux exigences des essais biologiques spécifiques, en particulier des tests d'agglutination sur puce pour la détection d'analytes rare, lors desquels ces dernières peuvent être quantifiées par la comptabilisation des doublets de particules.

Dans une deuxième approche, la focalisation magnéto-microfluidique tridimension-nelle des billes magnétique a été développée. Dans ce système, les billes magnétiques sont libérées à partir d'un amas dense dans une seule ligne de courant avec un espace-ment longitudinal entre elles. La formation d'un amas est induite par un fort gradient de champ magnétique généré au flanc d'un microcanal par une pointe magnétique reliée à un électro-aimant. La libération contrôlée des microparticules est réalisée en utilisant un protocole d'amortissement exponentiel de la force magnétique de rétention en présence d'un débit appliqué. Le réglage précis des grandeurs relatives de la traînée imposée par le flux et de la force magnétique de rétention permet par ailleurs une séparation granulométrique en flux des microparticules. L'ajout d'un liquide de gaine permet de concentrer les microparticules dans un flux unique situé dans $\pm\ 5\ \mu$m de l'axe central du canal.

Notre système pour la focalisation tridimensionnelle et la séparation des billes magnétique a été utilisé pour effectuer un test d'immuno-agglutination sur puce. La focalisation tridimensionnelle a été utilisée comme une méthode fiable pour la comptabilisation fiable en flux de singlets et doublets agglutinés. Nous avons démontré le potentiel du test d'agglutination dans un format microfluidique en utilisant un modèle basé sur l'interaction streptavidin/biotin-bovine sérum albumine(bBSA). Une limite de détection du bBSA d'environ 400 pg/mL (6 pM) est atteint.

Mots-clés: microfluidique, manipulation magnétique, immunoassay, Lab-on-a-chip, billes superparamagnétiques, test d'agglutination, séparation, focalisation tridimensionnelle

Acknowledgments

very well welcomed while I started my PhD, thanks to Elodie, Mina, Fred, Jean baptiste, Ulrike, Daniel, Nicolas, Raphaël, Marta, Raphaëlle, Lynda and venkat. All these years I had the pleasure to meet and share memorable moments with all of you: Hamideh, Jalil, Qasem, Rob, Anja, Tuna, Cumhur, Hui, Meng, Meena, Josias, Nicolas Abelé, Nina, bilge, Guillaume, Alessandro, Harsha, Oscar, Katrin, Loic, Vahid, Marc, Jonas, Cynthia, Marc, Damien and many others who will forgive me if their names are not flashing on my mind right now.

I cannot imagine living in Lausanne; let go doing a PhD without the friendship of these girls: Basira, Rana, Sahar. Hey girls, I enjoyed every single second of our "ver ver"s, you have always been there no matter what. I already miss calling you to ask for chat over a cup of coffee or a glass of wine in the city. You always had your own, different from the other one, way of making my PhD and non-PhD days enjoyable. Thank you girls.

There were a lot of moments during my master and PhD studies that I was sure I could never succeed if it wasn't for my sister and brother-in-law. Ana and Hamid, you know much better than me how a big part of this is because of you. A simple thank you is never enough for what you have done for me. The advices, the serious talks, the birthday dinners, ALL the weekends, the endless laughter, the calmness of your house,... (I cannot even count them all): I am thankful. Dyna who was born on one of the first days of my PhD, you are the endless source of joy when I needed to think about something else than the magnetic beads. Mani, for the "thank you" to you, I really don't need to use words, you know it already without really saying it. Your words and silence both were always placed exactly where they should be.

I am very thankful to my parents, you are the main reason of who I am today. You have always been a great support during different stages of my life. You were always ready to hear what I think and accept who I want to be, I am thankful not only for the help during the PhD but for the great persons that you are.

Table of contents

Table of contents

1

Introduction

1.1 The lab-on-a-chip concept

In the early nineties, the concept of lab-on-a-chip (LOC) or micro total analysis system (μTAS) was introduced by Manz et al. [1]. In recent years, considerable progress has been made in the field of miniaturization. It is possible to miniaturize most mechanical, fluidic, electomechanical, chemical or thermal systems. This miniaturization has given rise to many new fields and applications. One of them is microfluidics. Microfluidics has provided attractive solutions for many problems in chemical and biological analysis, especially for in-field use or point-of-care testing. Detailed overviews of the various topics related to microfluidic systems, such as sample preparation, sample injection, sample manipulation, small-volume reaction, separation and detection have been published and reviewed in [2, 3].

1.2 The DetectHIV project

1.2.1 HIV testing

This thesis was carried out in the frame of a European project, DetectHIV (# 037118, "Sensitive nanoparticle assay for detection of HIV"). In this project, the idea was to develop a platform for HIV diagnosis via p24 antigen detection.

An arsenal of laboratory methods is available to screen blood, diagnose infection, and monitor disease progression in individuals infected by HIV. These tests can be

classified into those that: detect antibodies, identify antigens, a combination of these two, detect or monitor viral nucleic acids, or provide an estimate of T lymphocyte numbers. ELISA is the most commonly used test to screen for HIV infection. Antibody can be detected in a majority of individuals three to four weeks after infection, using third-generation sandwich assays. The window period can be shortened to about two weeks using p24 antigen (Ag) assays or reduced to one week with the implementation of nucleic acid detection assays [4, 5]. The p24 protein is a viral capsid (core) protein that appears in blood during infection due to the burst of viruses during replication. The detection limit (25 pg/mL) of fourth-generation combination assays is close to that of the single Ag assays [6].

HIV-1 RNA detection using highly efficient amplification techniques such as polymerase chain reaction (PCR) has become the standard for monitoring antiretroviral therapies after diagnosis of the disease [7]. The p24 Ag assay sensitivity is inferior to PCR in detecting viral particles, but the presence of extraviral p24 Ag in most samples makes largely up for this. p24 Ag testing is similarly sensitive and specific in diagnosing pediatric HIV infection, in predicting CD4+ T cell decline and clinical progression at early and late stage of infection, and suitable for antiretroviral treatment monitoring.

The tests of HIV-1 RNA are very difficult to perform in developing countries. Therefore research has been guided to develop simple and cheap tests to monitor the disease [8]. The advantage of using p24 is the possibility of detection in early stages of the infection. The DetectHIV platform was aimed to perform a viral load test with only one reactant (grafted beads). The goal was to obtain a detection limit of 1 ng/ml in microtiter plate and 0.1 pg/ml for a test on a microfluidic chip. The platform should be tested with synthetic p24 samples and patient samples.

The aimed p24 test is based on an agglutination test, which forms aggregates of magnetic beads that are linked irreversibly via the protein. In the microfluidic system, the sample solution is transported through a suspension of magnetic beads that are magnetically retained in a microfluidic channel. The concentration of the formed aggregates is proportional to the p24 concentration in the sample solution.

1.2.2 Objectives of the project

The feasibility and high potential of a magnetic micro or nano-particles agglutination assay has been recently demonstrated in the bulk format (microtitre plate) [9, 10].

Immunoassays, where reactions occur both in solution and on a solid phase, offer the advantage of easy separation of chemical complexes from reactants. Biomolecule immobilization on a solid phase, such as micro- and nano-beads offers the potential to perform highly localized assays in a small volume.
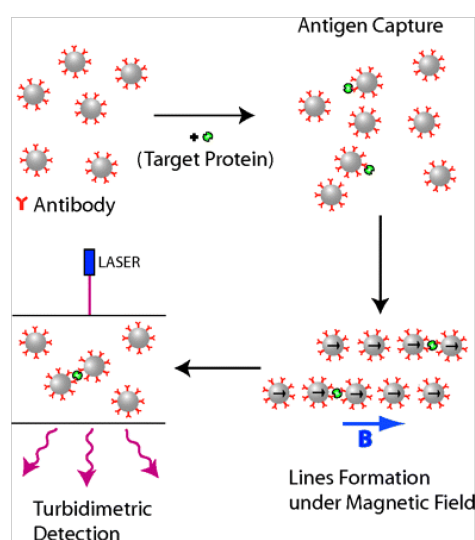
Figure 1.1: *Schematic diagram of the magnetic field-induced agglutination of colloidal magnetic beads into doublets and their detection by optical scattering.*

The DetectHIV project aims to develop an assay which is based on optically detecting the formation of a colloidal gel or aggregates of magnetic beads (agglutination test). The agglutination forms in a magnetic field under the presence of antigens that are able to link irreversibly two colloidal particles together. Therefore the particles are grafted with antibodies that bind specifically to the p24 Ag. The detection is achieved through simple optical absorbance measurements, owing to the strong optical scattering modification when passing from singlets to aggregated beads (Fig. 1.1). The main goal of DetectHIV is to perform the test on a microfluidic chip and to take advantage of the microfluidic approach.

A major objective of DetectHIV was the development of an actuation system for magnetic retention of magnetic beads in the microfluidic channel in the presence of the flow to offer the maximum exposure to the analyte solution for reaching the envisioned high sensitivity of the platform. Another objective was to develop an optical detection system integrated with microfluidic channels using polymer based waveguides on a microfluidic chip. The ultimate aim was to have the different developed functionalities on a single chip.

1.3   Scope of this thesis

For ultimate sensitivity, we have planned to use magnetic actuation to separate beads aggregates from the single magnetic beads, in order to enrich the fraction of aggregates of magnetic beads before the optical detection system. We present here a method for the separation of magnetic beads on-chip. The principal objective of this thesis, as defined by the DetectHIV project, was the design of a system allowing the separation and 3D focusing of magnetic nanoparticles in a microfluidic channel.

The first device is a novel integrated chip-based separation system that comprises an arrangement of distinct magnetic microtips adjacent to a microfluidic channel. It comprises three functions:

- Dosing of a specific amount of magnetic particles.

- Well-controlled release in the microchannel for possible detection.

- Continuous separation in the sample flow with high resolution.

In particular, we focus on the separation of bead singlets and doublets, which is an important feature for on-chip agglutination assays for the detection of rare antigens via particle coupling into doublets.

A second objective of this thesis was to perform a method for 3-dimensional focusing of magnetic beads. This approach is important for accurate optical detection with high sensitivity. A hydrodynamic 3D focusing method of beads was developed by another project partner, the realisation of a less complex system has been the objective of this thesis. In our second device, a pair of magnetic tips permits bead retention and controlled release near the channel wall, by controlled decrease of the local magnetic force in the presence of an applied flow. Combining subsequently the bead-containing flow with a lateral sheath flow through a secondary channel, focuses the beads along a single central line in the main micro-channel. Our system is designed to handle and control a very small amount of beads. 3D focusing of magnetic beads has not been reported before. In this device in-line separation of different sizes of magnetic beads has been performed.

The system of in-line separation and 3D focusing has been used as a new approach for performing an immuno-agglutination assay on-chip. 3D focusing allowed reliable

counting of singlets and agglutinated doublets. In-line separation for agglutination is a novel method that can be used not only for the separation of different sizes of particles but also for separation of single beads from aggregates. We show that this type of separation can be used as a method of detection in agglutination tests. We demonstrate the potential of the agglutination assay in a microfluidic format using a streptavidin/biotinylated-bovine serum albumin (bBSA) model system.

The thesis comprises the following chapters. Important magnetic concepts required for the manipulation of magnetic beads are explained in chapter 2. An introduction to different techniques of separation and 3-dimensional focusing of particles, especially magnetic bead based methods (state-of-the-art), is presented in chapter 3. At the end of chapter 3, some examples of magnetic bead based immunoassays, in particular agglutination tests are reported. In chapter 4, the engineering aspects of this work, fabrication of the platform for microfluidic and magnetic manipulations have been explained. The last part of the thesis summarizes the main results. In chapter 5, the results obtained with the separation of different sizes of magnetic beads and the aggregates are discussed. In chapter 6, magneto-microfluidic 3D focusing of magnetic beads is explained along with a new method for in-line separation of magnetic beads. The agglutination test on-chip is demonstrated using a model based on the streptavidin-biotin interaction in chapter 7.

2

Magnetic particles

2.1 Introduction

In this chapter we introduce the basics aspects related to magnetic particles and discuss the forces exerted on them in microfluidic environment. Magnetic particles can be manipulated using permanent magnets or electromagnets, independently of normal microfluidic processes. They can be used as a mobile substrate for assays. Using a simple magnet, they can be easily recovered from dispersion and by removing the magnet they can be re-dispersed. Using them in microfluidic environment offers the advantage of enhanced interaction of an analyte solution with the functionalized surfaces of the particles. Such particles are also called "beads" in literature, independent of their size [11].

2.2 Magnetic material properties

2.2.1 Magnetic field and magnetization

The origin of magnetic properties lies in the orbital and spin motions of electrons and how the electrons interact with each other [13]. Materials, depending on their interaction with an external magnetic field, can be classified as diamagnetic, paramagnetic, ferromagnetic, ferrimagnetic and antiferromagnetic, as is presented in Table 2.1 and Fig. 2.1.
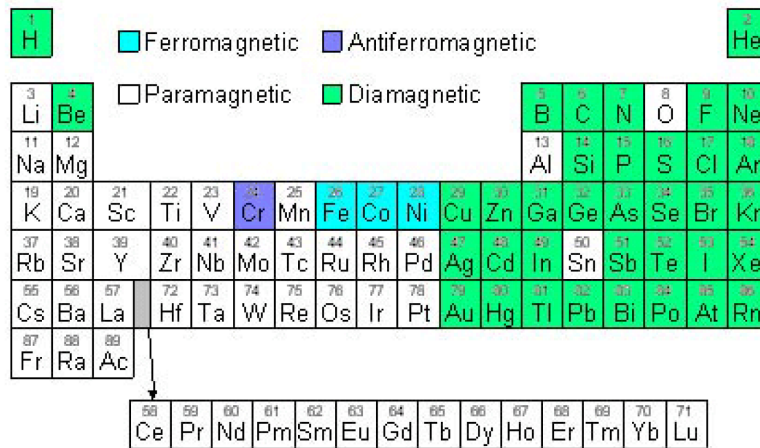
Figure 2.1: *Diagram of a periodic table showing elements colored according to the type of magnetism they show at room temperature [12].*

If a magnetic material is placed in a magnetic field of strength **H**, the individual atomic moments in the material contribute to its overall response, resulting in the magnetic induction **B**

$$\mathbf{B} = \mu_0(\mathbf{H} + \mathbf{M}) \tag{2.1}$$

where $\mu_0 = 4\pi \cdot 10^{-7} Vs/Am$ is the permeability of free space, and the magnetization $\mathbf{M} = \mathbf{m}/V$ is the magnetic moment per unit volume, where **m** is the magnetic moment of a volume V of the material. Materials may be classified in terms of their volumetric magnetic susceptibility χ_r, where
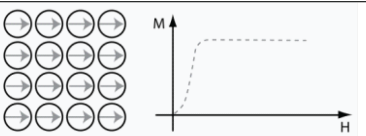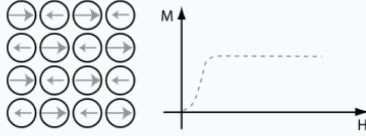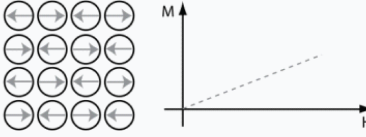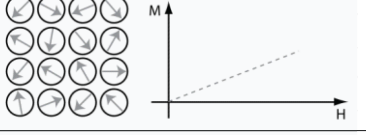
$$\mathbf{M} = \chi_r \cdot \mathbf{H} \tag{2.2}$$

describes the magnetization induced in a material by **H**. In SI units, χ_r is dimensionless, **B** is expressed in tesla (T), and both **M** and **H** are expressed in A/m. Combing these two equations results in

$$\mathbf{B} = \mu_0(1 + \chi_r)\mathbf{H} = \mu_0\mu_r\mathbf{H} \tag{2.3}$$

where $\mu_r \equiv 1 + \chi_r$ is the relative permeability of the material.

Table 2.1: *Classification of different types of magnetic properties [14].*

Magnetism type	Atomic and magnetic behavior		Susceptibility (χ_r)
Ferromagnetism		Atoms have parallel aligned magnetic moments within domains	- large (>> 1) - positive Fe ,~100,000
Ferrimagnetism		Anti-parallel aligned magnetic moments of different atom types do not cancel completely	- large (>> 1) - positive Ferrite, ~ 1000
Antiferromagnetism		Atoms have parallel and anti-parallel magnetic moments aligned in a regular pattern	small (<< 1) - positive Cr, $3.6 \cdot 10^{-6}$
Paramagnetism		Atoms have randomly oriented magnetic moments and there is negligible interaction energy between atomic magnetic	- small (<< 1) - positive Pt, $2.1 \cdot 10^{-5}$
Diamagnetism		Atoms have no Magnetic moment	- small ($|\chi_r| \ll 1$) - negative Cu, $-0.77 \cdot 10^{-6}$

2.2.2   Types of magnetic materials

Diamagnetism is due to the cooperative behavior of orbiting electrons when exposed to an applied magnetic field. Diamagnetic materials are composed of atoms which have no net magnetic moments (i.e. all the orbital shells are filled and there are no unpaired electrons). However, when exposed to a field, a negative magnetization is produced and as a result the susceptibility χ_r is negative.

When electrons are paired together, their opposite spins cancel the magnetic moments. Therefore, no net magnetization exists. In paramagnetic materials, some of the atoms or ions in the material have a net magnetic moment due to unpaired electrons in partially filled orbitals. In the presence of a field, there is a partial alignment of the atomic magnetic moments in the direction of the field, resulting in a net positive magnetization and positive susceptibility χ_r. The magnetization becomes zero when the field is removed.

In ferromagnetism, the atomic moments exhibit very strong interactions. These interactions are produced by electronic exchange forces and result in a parallel or
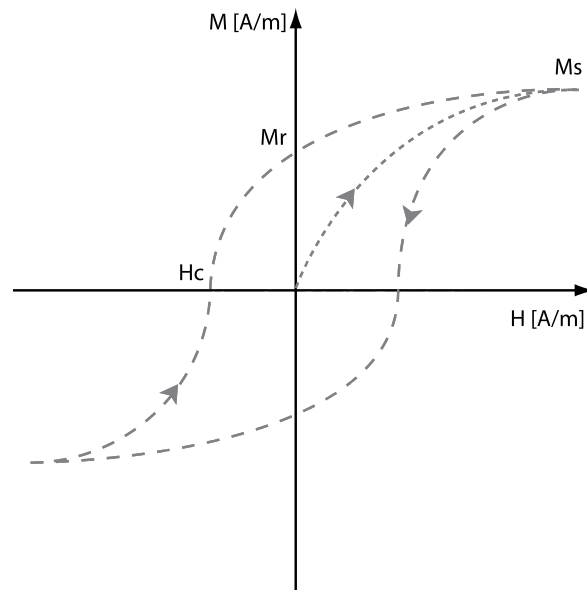
Figure 2.2: *Magnetic hysteresis loop (broken line). After initial magnetization from the unordered state up to saturation (small dashed line), the material will retain a magnetization M_r even in the absence of an external field. Only at the application of the coercitive field H_c, the net magnetization of the material will return to zero. M_s is the saturation magnetization.*

antiparallel alignment of atomic moments. Parallel alignment of moments results in a large net magnetization, even in the absence of a magnetic field. Eventhough electronic exchange forces in ferromagnets are very large, thermal energy eventually overcomes the exchange and produces a randomizing effect. This occurs at a particular temperature called the Curie temperature T_C. Below the Curie temperature, the ferromagnet is ordered and above it, disordered.

In ionic compounds, such as oxides, more complex forms of magnetic ordering can occur due to the crystal structure. They are categorized in the group of ferrimagnetism or antiferromagnetism.

2.2.3 Ferromagnetism

Ferromagnetism is of interest in the present context. Parts of the magnetic actuation system in our device, such as a magnetic core or microtips, are made of ferromagnetic materials. Furthermore, magnetic particles often have ferromagnetic cores with high susceptibility in order to generate a strong interaction with external magnetic fields. The atomic moments in ferromagnetic materials exhibit very strong interactions. These
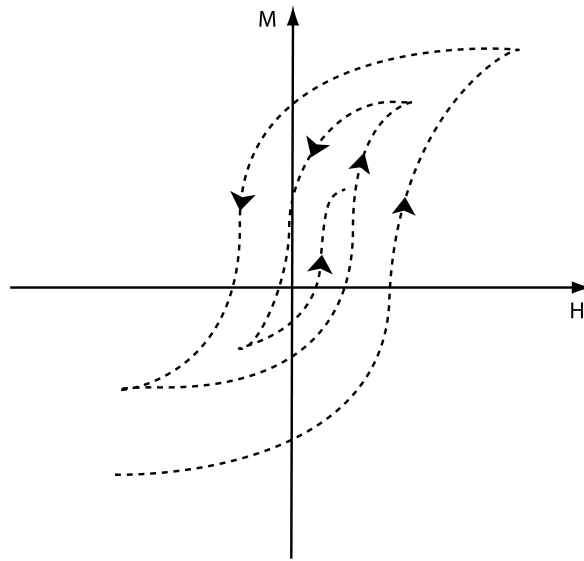
Figure 2.3: *Demagnetization curve of a ferromagnetic material by applying a damped external magnetic field to decrease the remanent magnetization.*

materials exhibit parallel alignment of moments resulting in large net magnetization even in the absence of a magnetic field. They can keep a memory of an applied field, even when the latter is removed. As a consequence, the plot of the variation of the magnetization **M** with the magnetic field **H** shows a hysteresis loop (schematically shown in Figure 2.2).

The loop is characterized by the saturation magnetization M_s, remanence M_r and coercivity H_c. The saturation magnetization is the maximum induced magnetization that can be obtained in an external magnetic field. Beyond this field, no further increase in magnetization occurs. Upon reducing the field to zero, the magnetization does not go to zero, but persists as a remanence M_r. When increasing the field in the negative direction, a point is reached where the induced magnetization becomes zero. The field at this point is called the coercivity H_c. Increasing the field further in the negative direction results in saturation again, but in the negative direction.

The hysteresis loop can be explained by understanding the magnetic domains. A magnetic domain is a region, in which the magnetic fields of atoms are grouped together and aligned. Ferromagnetic domains are small regions in the ferromagnetic material in which all of the magnetic dipoles are parallel to each other. When it is in its demagnetized state, the magnetization vectors in different domains have different orientation, and the total magnetization average is zero. The process of magnetization

orientates all the domains in the same direction. When the field is applied, the domain whose magnetization is closest to the field direction starts to grow at the expense of the other domains. Eventually the applied field is sufficient to eliminate all domain walls, leaving a single domain. While the magnetic field is removed, the domain walls will not fully reverse to their original positions, as a result the magnetization curve shows hysteresis.

Demagnetization of ferromagnetic materials is important for practical applications. Fig. 2.3 shows the path through successive hysteresis loops for returning the material back to the unmagnetized state. By reducing gradually the external filed, the demagnetization adopts smaller values with increasing number of field reversals. In the second loop, the applied field is not large enough to reach the saturation. Some domains stay oppositely oriented. At the end, domains are randomly orientated, and the magnetization is reduced to a value close to zero.

2.3 Superparamagnetic particles

2.3.1 Mono-domain nanoparticles

Small mono-domain nanoparticles are of particular interest. They are single domain, because they have a dimension that is of the order or smaller than the typical thickness δ of a magnetic domain wall given by [11]

$$\delta = \sqrt{\frac{JS^2\pi^2}{Ka}} \tag{2.4}$$

with J being a magnetic exchange constant, S the total spin quantum number of each atom, a the inter-atomic spacing, and K the magnetic energy density of the magnetic material. For iron, assuming that $S=1$, and with $J = 2.16 \cdot 10^{-21}$ J, $a = 2.86 \cdot 10^{-10}$ m total spin quantum number of each atom, and $K = 4.2 \cdot 10^4$ J/m^3, one calculates a domain wall width of 42 nm.

The magnetic energy of a nano particle is given by

$$E_{mag} = K\frac{4}{3}\pi r^3 \tag{2.5}$$

r being the radius of a spherical particle.

Mono-domain magnetic nanoparticles become superparamagnetic, i.e. their time-averaged magnetization without magnetic field is zero when their magnetic energy E_{mag} is lower than about ten times the thermal energy $k_B T$ (k_B the Boltzmann constant). At the order of tens of nanometers or less, one can see superparamagnetism, where the magnetic moment of the particle is free to fluctuate in response to thermal energy, while the individual atomic moments maintain their ordered state relative to each other. At room temperature, ($k_B T = 4.0 \cdot 10^{-21}$ J) a maximum radius of 18 nm may be estimated for a superparamagnetic spherical particle of maghemite (above that volume it would ne paramagnetic).

The underlying physics of superparamagnetism is founded on an activation law and a corresponding relaxation time τ of the net magnetization of the particle [15, 16]:

$$\tau = \tau_0 exp \frac{E_{mag}}{k_B T} \tag{2.6}$$

For non-interacting particles the pre-exponential factor τ_0 is of the order $10^{-10} - 10^{-12}$ s and only weakly dependent on temperature [17].

If $\tau << \tau_m$ (characteristic measurement time), the flipping is fast relative to the experimental time window and the nanoparticles appear to be superparamagnetic; while if $\tau >> \tau_m$ the flipping is slow and quasi-static properties are observed. This is so-called 'blocked' state of the system.

2.3.2 Types of superparamagnetic beads

In the frame of this project, we used magnetic beads that show superparamagnetic behaviour. The diameter of suspended beads is typically in the range of 100 nm to a few μm. These beads are built up from a matrix of mono-domain nanoparticles embedded in a non-magnetic matrix. In order to generate superparamagnetic behaviour in such "large" beads, the nanoparticles have to be dispersd sufficiently to avoid interaction in the matrix. This is schematically shown in Fig. 2.4.

Fig. 2.4a shows the magnetic moments of the iron oxide nanoparticles that are randomly oriented before application of the magnetic field. With application of the
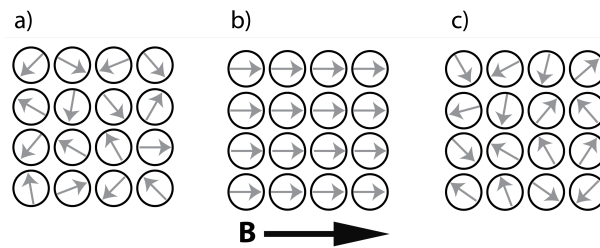
Figure 2.4: *Superparamagnetic behavior of a group of non interacting nanoparticles of ferromagnetic material in the absence and presence of an external magnetic field.*

field all the moments are aligned in the direction of the field (Fig. 2.4b). While the field is switched off; the bead returns to its initial state (Fig. 2.4c) without keeping the remanecence. The resulting hysteris-free magnetization curve of a multi-core superparamagnetic bead is shown in Fig. 2.5.
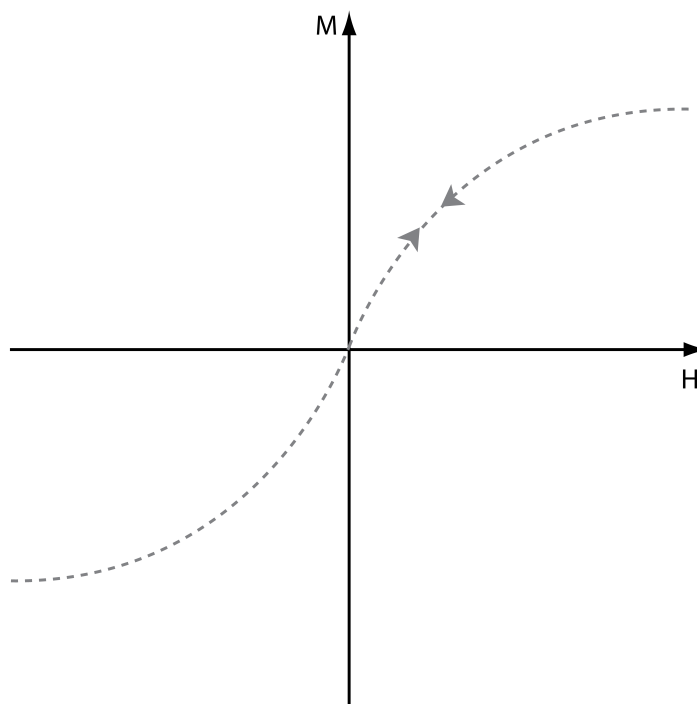
Figure 2.5: *The hysteresis-free variation of M with changing H, showing superparamagntic behaviour.*

A typical magnetic bead has a magnetic core of superparamagnetic material surrounded by a non magnetic coating which can be functionalized with different materials (e.g. proteins or a DNA sequence). Iron oxides such as magnetite (Fe_3O_4) or maghemite ($\gamma - Fe_2O_3$) are more stable against oxidation, so they are used as material in the fabrication of superparamagnetic microparticles.
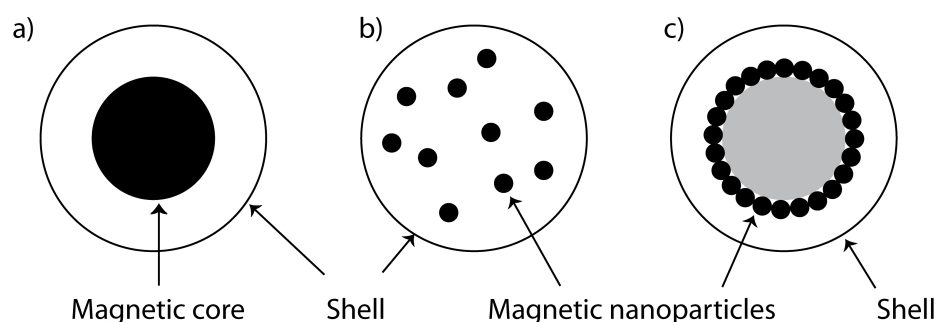
Figure 2.6: *Various types of magnetic particles a) Magnetic core-polymer shell, b) magnetic multicores homogeneously dispersed within the polymer matrix, c) magnetic nanoparticles located on the surface of a polymer core.*

Various methods and materials were used for magnetic bead synthesis [18]. Magnetic properties of the microspheres are mostly determined by the selection of the magnetic material, its concentration, and distribution inside the non-magnetic matrix. Various preparation methods provide magnetic polymer microspheres differing in morphology (Fig. 2.6), including magnetic core-polymer shells (Fig. 2.6a), magnetic multicores homogeneously dispersed within a polymer matrix (Fig. 2.6b), or magnetic nanoparticles located on the surface of a polymer core ("strawberry" morphology, Fig. 2.6c) [19]. The advantage of a polymer shell surrounding the magnetic core is the possibility of surface functionalization and subsequent immobilization of target biomolecules [11].

2.4 Forces on a magnetic bead in solution

2.4.1 Magnetic force

Magnetic beads can be magnetically manipulated using permanent magnets or electromagnets. This degree of freedom is the basis of the enhanced exposure of the functionalized bead surface to the surrounding liquid, due to the increased relative motion of the bead with respect to the fluid.

The magnetic force acting on a point-like magnetic dipole or "magnetic moment" **m** in a magnetic induction **B** can be written as a function of the divergence of the magnetic induction [13, 20].
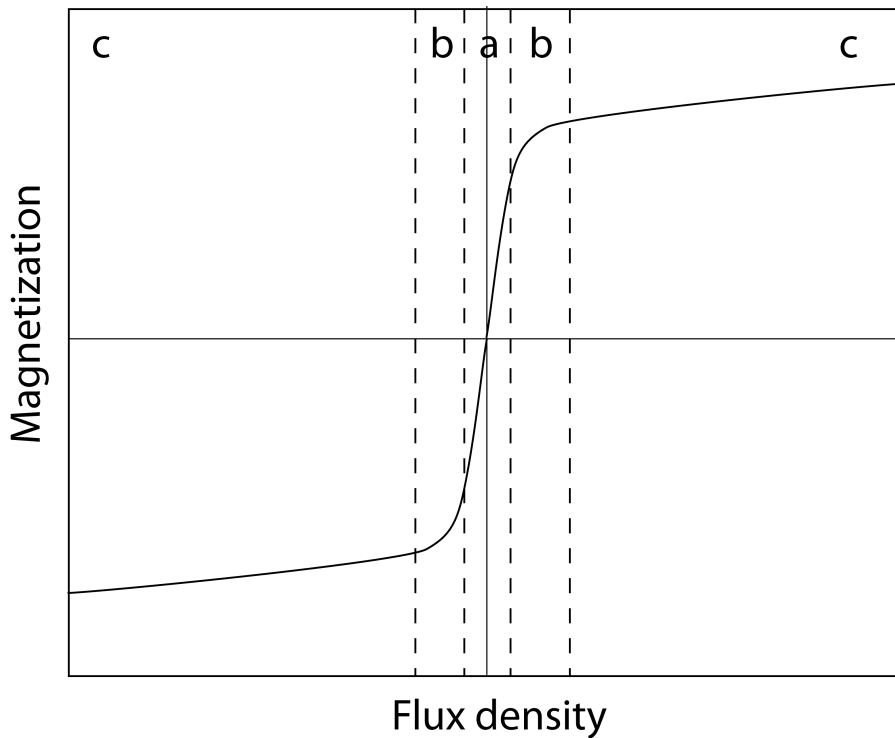
Figure 2.7: *Magnetization curve of a Dynabead MyOne. Three regions are distinguishable considering the relation between flux density **B** and magnetization **M**: a) linear b) non-linear. c) saturation (constant magnetization)*

$$\mathbf{F}_m = (\mathbf{m} \cdot \nabla)\mathbf{B} \tag{2.7}$$

Fig. 2.7 shows a typical magnetization curve for Dynal MyOne beads. In this graph the magnetizaton **M** is proportional to the magnetic flux density **B**. Three typical regions are distinguishable. In the first region (Fig. 2.7a), the bead magnetization is proportional to the applied magnetic flux density, in contrast to the second region (Fig. 2.7b) where the relation between magnetization and magnetic flux density is not linear. In the third region (Fig. 2.7c) (saturation region), the magnetization of the bead is almost constant due to saturation.

In our case, as we use weak magnetic fields, we assume that the magnetic moment of the bead is proportional to the intensity of the magnetic induction **B**. We can describe the moment at small fields (corresponding to the region (a) in Fig. 2.7) by the linear relation:

$$\mathbf{m} = V_m \mathbf{M} = V_m \frac{1}{\mu_0} \Delta \chi \mathbf{B} \tag{2.8}$$

with $\mathbf{M}$ the magnetization of the particle, $\Delta \chi$ the difference in magnetic susceptibility between the magnetic particle and the surrounding liquid medium, μ_0 is the vacuum permeability and V_m is the magnetic volume of the particle. Using standard vector calculations Equation 2.7 becomes:

$$\mathbf{F}_m^b = (\mathbf{m} \cdot \nabla)\mathbf{B} = V_m \frac{\Delta \chi}{2\mu_0} \nabla \mathbf{B}^2 \tag{2.9}$$

where $\mathbf{F}_m^b$ is the magnetic buoyant force which takes into consideration the susceptibility of the medium. It is important to recognize that a magnetic field gradient is necessary to have a translation force on a magnetic bead, a uniform field gives rise to torque without any transational action.

2.4.2 Other forces

Viscous drag force

Manipulation of magnetic particles with the help of a permanent magnet or coil can result in a translating magnetic force on magnetic particles in a microfluidic environment, while the liquid solution is static. The hydrodynamic drag force is the consequence of the difference of velocity between the particle and the fluidic environment.

When a spherical particle is moving in a fluid, it is subjected to a drag force exerted by the fluid depending of the flow regime, which is determined by the Reynolds number (Re) [21]:

$$Re = \frac{vL}{\nu} \tag{2.10}$$

where L is the typical dimension of the system, v is the mean flow velocity, and ν is the kinematic viscosity of the fluid. The value of the Reynolds number defines the ratio between inertial and viscous forces. Depending on the Reynolds number, different flow regimes can be characterized, such as turbulent or laminar flow [22, 23]. In microchannels, the flow regime is normally laminar, where viscous forces are dominant.
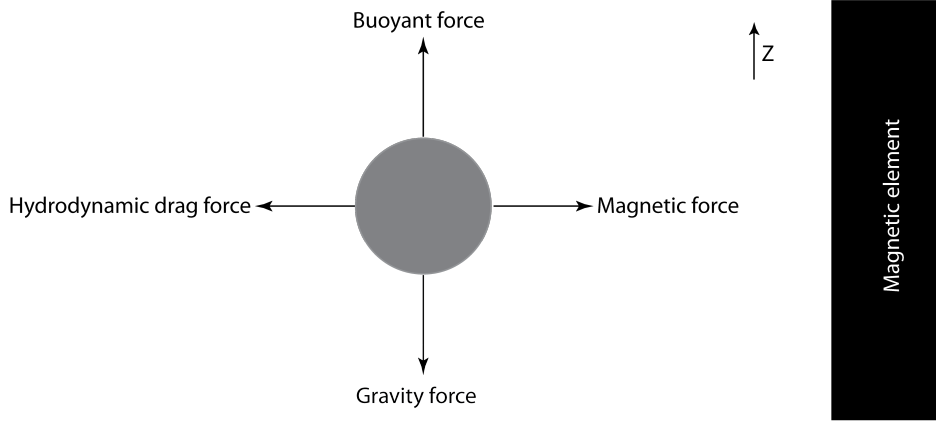
Figure 2.8: *Schematic illustration of a magnetic particle in a liquid solution under the influence of a magnetic force, hydrodynamic drag force, buoyant force and gravity force.*

In the laminar flow regime, the drag force can be expressed as [11]

$$\mathbf{F}_d = 6\pi\eta r\Delta\mathbf{v} \qquad (2.11)$$

where η is the dynamic viscosity ($\eta = \frac{\nu}{\rho}$) of the medium, Δv is the relative speed between the fluid and the particle and r is the radius of the bead. Equalizing equation 2.11 and equation 2.9 allows us to determine the maximum speed of a particle in a liquid when exposed to magnetic force.

By combining Eqs. 2.9 and 2.11 (with $\mathbf{F}_m^b = \mathbf{F}_d$ for steady state conditions), we can derive the magnetophoretic drift velocity $\mathbf{v}_m$ of a particle in a non-uniform magnetic field

$$\mathbf{v}_m = \frac{1}{6\pi}\frac{\Delta\chi V_m}{\eta r}\frac{\nabla\mathbf{B}^2}{2\mu_0} = \xi_m\frac{\nabla\mathbf{B}^2}{2\mu_0} \qquad (2.12)$$

where ξ_m has been defined as the magnetophoretic mobility, which summarizes particle and medium properties. According to Eq. 2.12, the magnetophoretic mobility of particles with identical magnetic properties is proportional to the square of the particle diameter and to the relative susceptibility. The design of our size-dependent magnetic separation device relies on this feature.

Buoyant and gravity forces

Figure 2.8 gives a schematic illustration of a magnetic particle in a solution under the influence of a magnetic force, hydrodynamic drag force and buoyant force $\mathbf{F}_b$. The effective force acting on the bead in the z-direction is given by

$$\mathbf{F}_b = -m_b g \mathbf{e}_z \tag{2.13}$$

with the gravitation constant g.

The "buoyant mass"

$$m_b = V(\rho_{bead} - \rho) \tag{2.14}$$

represents the effective mass of the magnetic bead by taking into account the density difference of the bead ρ_{bead} and the surrounding fluid ρ [21].

Electrostatic and electrodynamic forces

Electrostatic and electrodynamic (van der Waals) forces are the other group of forces acting on a magnetic bead in a microfluidic environment. Intractions between permanent electrical dipoles and induced dipole in solutions give rise to the van der Waals forces [18].

In the same time, if ions are present in the solution, both beads and the surface of the channels become charged through adsorption of ions. This charge is neutralized by mobile ions of opposite charge also present in the solution, thus forming the well-known double layer. When the double layers of two surfaces overlap, an electrostatic interaction occurs, resulting in either a repulsive or an attractive force.

While changing the pH , it is possible to obtain repulsive electrical force conditions between the beads and the substrate surface, considering combined van der Waals and electrostatic forces.This is important, if one wants to avoid the issue of unwanted particle sticking to the microfluidic channel. It is possible to coat the microchannel wall with proteins or polymers to avoid sticking of beads or molecules, but it adds to the complexity of the system.

Brownian forces

When the size of the magnetic bead is in the submicrometer range, stochastic Brownian forces become relatively more important, as the magnetic (and gravitational) forces, being proportional to r^3, are fastly decreasing. The diffusion coefficient D of the bead is given by [18]:

$$D = \frac{k_B T}{6\pi\eta r} \tag{2.15}$$

For example, a MyOne Dynabead has a diffusion coefficient in water of 4.8×10^{-13} $\mathrm{m^2/s}$ at room temperature, after 1 s of diffusion, the bead will have moved an average distance of 0.7 $\mu\mathrm{m}$. Taking a magnetic nanoparticle with radius of 100 nm instead, the diffusion coefficient becomes 2.4×10^{-12} $\mathrm{m^2/s}$, resulting in a more than 2 times increased diffusion.

3

State-of-the-art

3.1 The concept of lab-on-a-chip

The most important advantages of using microfluidic systems are the following:

- Quantities of sample and reagents to be used can be very small .

- Reaction times are fast (diffusion lengths are of the order of the microfluidic channel dimension).

- They have a large surface-to-volume ratio.

This results in portability, low-cost, low consumption of power, versatility in design, high potential for parallel operation and for integration with other miniaturized devices. Microfluidic chips have proven to be ideal tools to precisely handle small volumes of samples, such as proteins or DNA solutions, as well as cell suspensions.

Different technologies have been developed to realize a microfluidic chip [2]. The first microfluidic chips have been made of glass and silicon. They have been replaced by different kinds of polymers allowing for low-cost microfabrication processes [24]. Polymers like polydimethylsiloxane (PDMS) are widely used. PDMS chips are fabricated using replication molding. The following attractive of PDMS make it a suitable material for miniaturized biological studies: PDMS is inexpensive, flexible and optically transparent and therefore compatible with many optical detection methods. It is impermeable to water, non-toxic to cells and permeable to gases. A major advantage

of PDMS over glass and silicon is the ease with which it can be fabricated and bonded to other surfaces. For the development of new bioassays, rapid prototyping in PDMS represents a critical advantage.

Employing micro- and nanoparticles in microfluidic channels offers the possibility of taking advantage of their high surface-to-volume ratio. Functional magnetic micro- and nanoparticles are used in bioanalytical applications as solid carriers for capture, transport and detection of biomolecules or magnetically labeled cells. Colloidal suspensions of such particles provide a large specific surface for chemical binding and therefore allow highly efficient interactions with target molecules in a sample solution [25]. Controlled actuation and manipulation of these mobile substrates in the microfluidic format offers interesting new opportunities for on-chip bioassays with previously unmatched properties [11, 26].

3.2 Non-magnetic separation methods of particles

One of the key functions required for microsystems used for biomedical applications is to separate specific cells or molecules from complex biological matrices. Various physical properties, including size [27, 28], motility [29], electric charge [30], electric dipole moment [31, 32], optical qualities [33, 34], and magnetic properties have been exploited for this purpose.

3.2.1 Hydrodynamic separation

Mainly because of the small dimension of channels in microfluidic circuits and the importance of the associated viscous forces, the flow stays in the laminar regime. Using this property, with different microchannels design and control of hydrodynamic flow, microparticles can be forced to different flow stream-lines and separate them.

Pinched flow fractionation is a good example of hydrodynamic separation of particles [28, 35]. Two laminar streams are pumped through a narrow channel section before entering a wider channel (Fig. 3.1). The sample stream contains a suspension of patricles with two different sizes, while the lower carrier stream contains a buffer solution. The microparticles are pushed against the wall in the pinched channel part as
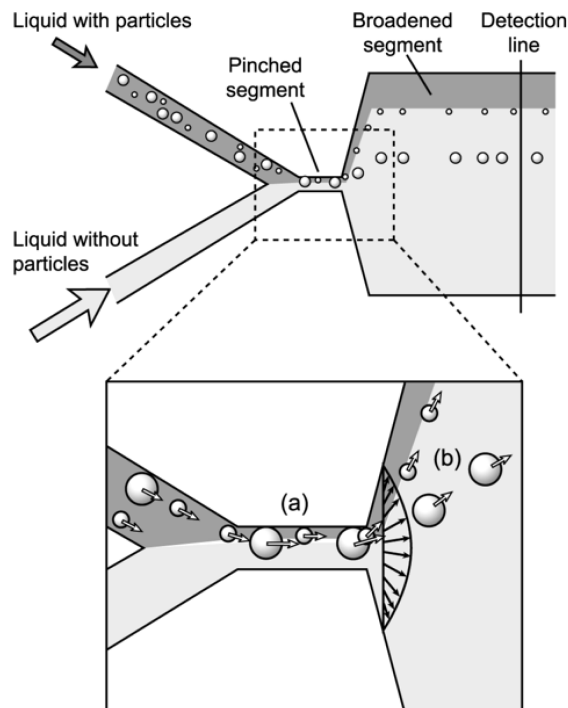
Figure 3.1: *Principle of pinched flow fractionation. a) In the pinched segment, particles are aligned to one sidewall regardless of their sizes by controlling the flow rates from two inlets. b) Particles are separated according to their sizes by the spreading flow profile at the boundary of the pinched and the broadened segments. The incoming liquid containing particles is dark-colored [28, 36].*

.

the flow rate of the carrier stream is higher than the one of the sample stream. Small particles stay in a flow stream close to the wall, while the centre of the gravity of the larger particles is further away from the wall. When the fluid enters the wider channel, the laminar flow carries the two particles along different streamlines. The particles are then separated across the width of the wide channel. The dimensions of the pinched segment have implications on the applicable size range and a significant amount of fine-tuning is necessary for the separation of sub-micron particles [36].

Flow around obstacles can also be used to separate particles or DNA molecules [27]. In this method, the separation process uses laminar flow through a periodic array of micrometer-scale obstacles (Fig. 3.2) . Each row of obstacles is shifted horizontally with respect to the previous row by $\Delta\lambda$, where λ is the center-to-center distance between the obstacles (Fig. 3.2a). Fluid emerging from a gap between two obstacles will encounter an obstacle in the next row and will bifurcate as it moves around the obstacle. Because the Reynolds number is low (flows are laminar) the streams in each lane do not cross or
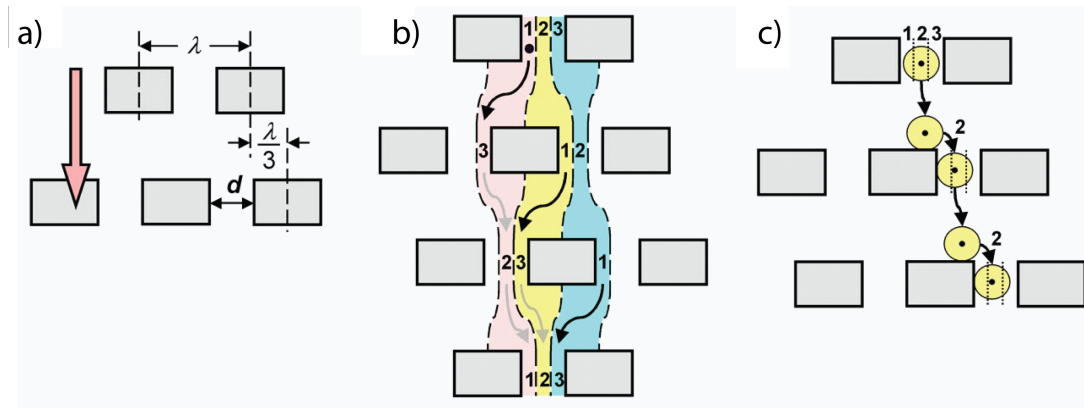
Figure 3.2: *a) Geometric parameters defining the obstacle matrix. A fluid flow is applied in the vertical direction (orange arrow). b) Three fluid streams (red, yellow, and blue) in a gap do not mix as they flow through the matrix. Small particles following streamlines will thus stay in the same lane. c) Trajectory of a particle with a radius that is larger than lane 1 [27].*

mix (Fig. 3.2b). Particles that are smaller than the lane width will follow the streamlines, starting from any of the lanes they will go back to the original lane assignment after three rows, so that net migration is in the average flow direction. In contrast to the smaller particles, a particle with a radius larger than the width of lane 1 at a gap will behave differently in the array. This is because the center of the particle cannot "fit" into lane 1 in a gap. As such a particle from lane 2 in one gap moves into the subsequent gap, expecting to move through the gap in lane 1, the particle will be "bumped" and its center will thus be displaced into lane 2 (Fig. 3.2c).

The geometry of the obstacles determines the separation efficiency and imposes some limitations for the range of particle sizes. Using hydrodynamic separation methods, labeling of sample components is not necessary [36].

3.2.2   Electrical separation

Microchannels offer a high surface-to-volume ratio resulting in good heat dissipation. Thus high electrical fields can be used in microfluidics, as the produced heat mostly is not a critical issue. Electrical fields have been used in various ways for separation, e.g. in combination with obstacles, for the separation of charged molecules, such as DNA or proteins. Fig. 3.3 i shows a "DNA prism" which was developed by Huang et al. [38], consisting of a regular array of posts over which an electrical field could be
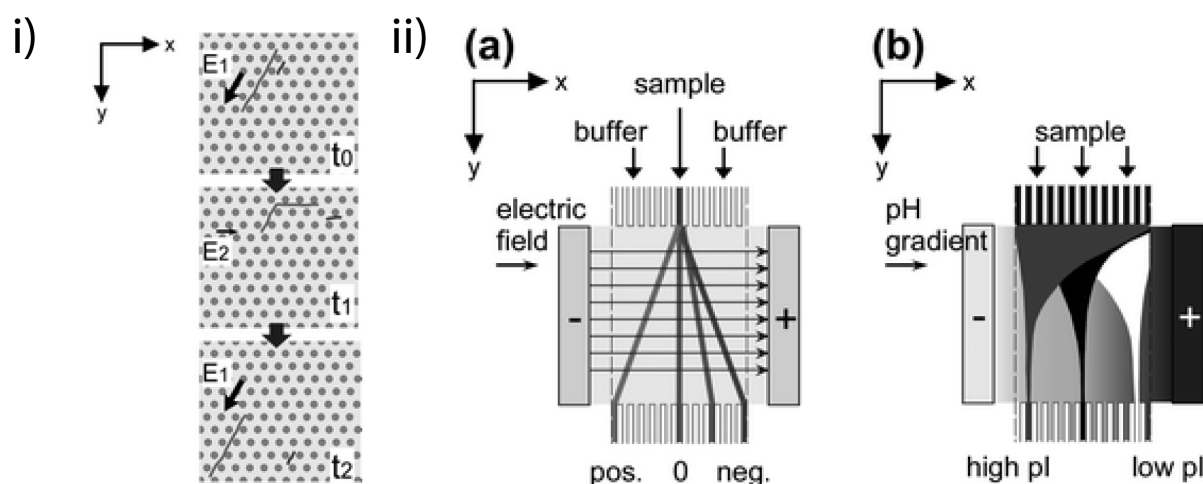
Figure 3.3: *i) "DNA prism" separation in which DNA molecules of different length are separated [37]. ii) Free-flow separation method using a shallow separation chamber with flow pumped in the y-direction. ii.a) Free-flow electrophoresis device applying a homogeneous electrical field orthogonal to the direction of the flow. Charged samples are deflecting ending on their charge-to-size ratio. ii.b) Free-flow isoelectric focusing using a pH gradient. Amphoteric samples migrate until they have reached the pH that equals their isoelectric point [36].*

applied diagonally (E_1) or parallel (E_2) to the posts. By continuously switching between the two fields, the separation of DNA molecules based on their molecular mass could be achieved.

Another form of electrical separation is free-flow electrophoresis. Free-flow electrophoresis is performed in a shallow chamber (Fig. 3.3ii). Buffer and sample solutions are continuously pumped into this chamber through numerous inlet channels and collected via outlet channels. Perpendicular to the direction of flow, a homogeneous electrical field is applied. Charged molecules are thus subjected to two flow vectors: the hydrodynamic flow in the y-direction and the electrophoretically induced motion in the x-direction [39–44]. Charged sample components are deflected from the direction of the laminar flow depending on their charge-to-size ratio, whereas neutral components follow the direction of the flow (Figure 3.3ii.a). In free-flow isoelectric focusing, a pH gradient is generated over the separation chamber. Amphoteric samples, such as proteins, are injected over the entire width of the chamber. They migrate until they exhibit zero net charge, i.e. until they have reached the pH that equals their isoelectric point (Figure 3.3ii.b) [36].

Another principle is separation using dielectrophoresis (DEP). When subjected to an electrical field, a particle or cell becomes polarised. If the electrical field is inhomoge-
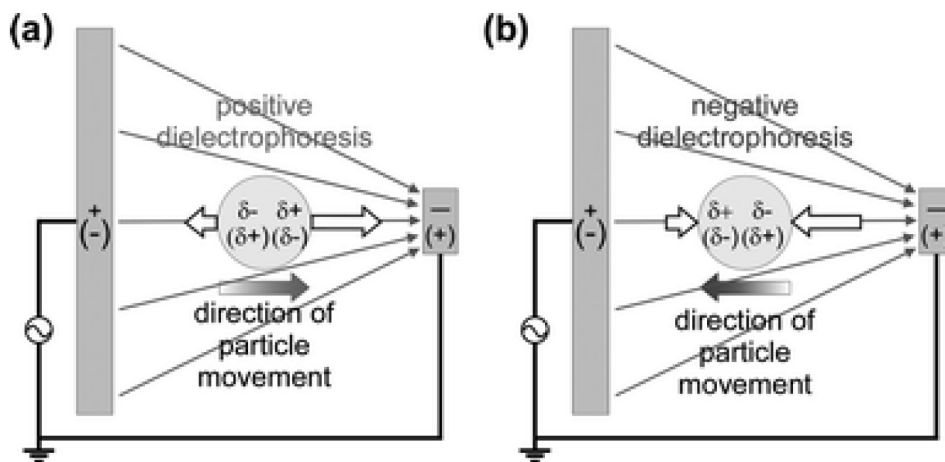
Figure 3.4: *The principle of dielectrophoresis (DEP): a) Positive DEP (larger polarisability of the particle than the surrounding medium). b) Negative DEP (the particle is less polarisable than the surrounding buffer medium) [36].*

neous, then the electrostatic forces on the two ends of the dipole are not equal and a movement is induced. Positive DEP occurs when the particle exhibits a larger polarisability than the surrounding medium. Positive DEP is directed towards the stronger electrical field (Figure 3.4 a). Negative DEP occurs if the particle is less polarisable than the surrounding buffer medium. Negative DEP forces the particle away from areas of high field intensity towards areas of low intensity (Figure 3.4 b).

3.2.3   Separation by acoustic forces

Continuous flow separation of particles and biological cells can also be performed with acoustic forces generated from ultrasonic waves. For this, a standing sound wave must be generated over the cross section of a microchannel, i.e. orthogonal to the direction of the flow. Usually the wave is tuned, such that the node is in the centre of the channel and two anti-nodes at the edges. Such waves can be generated, for example, with piezoelectric transducers. Particles or cells subjected to the sound wave experience a force, either towards the node or towards the anti-node. The acoustic force on a particle depends on the properties of the acoustic field, as well as on the properties of the particle and its surrounding medium [45, 46].

This method is not applicable to small nanoparticles, because the acoustic force is proportional to the volume, thus too small to manipulate them. Besides the fabrication

of the chip, actuators should be integrated near the channel which normally needs a more complicated fabrication process.

3.2.4 Separation by optical forces

Optical fields can also be used to arrange, guide or deflect particles in appropriate light-field geometries by means of an optical interference pattern (optical lattice). The response of a microscopic dielectric object to an applied light field can affect the kinetic motion of the particle. The strength of the interaction with the lattice sites depends on the optical polarizability of the particles (size, refractive index).
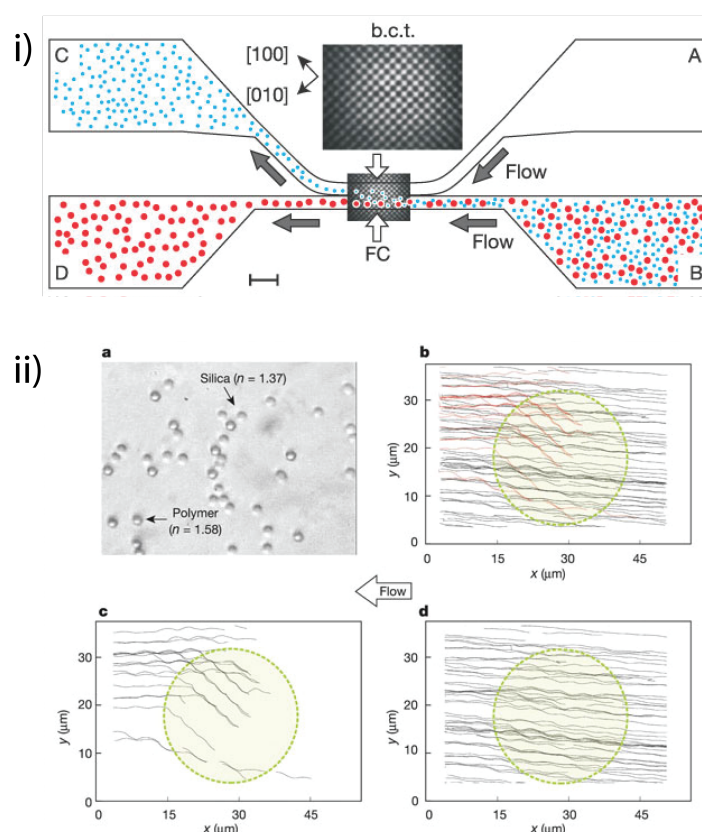
Figure 3.5: *i) The concept of optical fractionation which shows the optical lattice with the microfludic chamber . ii) Separation of silica and polymer particles by their index of refraction [47].*

MacDonald et al. used a five-beam interference pattern to sort co-streaming particles in microfluidic flows [47]. Figure 3.5.i describes the concept for the optical separation device. When a flow of mixed particles is passed through the opical lattice, selected

particles are strongly deflected from their original trajectories while others pass straight through largely unhindered, depending upon their sensitivity to the optical potential. Figure 3.5.ii demonstrate the separation; a co-streaming mixture of same-sized (2 μm diameter) silica and polymer spheres passes through our optical lattice. Polymer (n = 1.58) and silica spheres (n = 1.73) in water flow from through the optical lattice, Polymer trajectories are shown in red (Fig. 3.5.iib), and silica trajectories in black, with a green circle indicating the xy range over which the optical lattice is most intense. The polymer tracks show a deflection in excess of 45° while the silica tracks are only slightly modulated by the optical lattice (Fig. 3.5.ii c&d).

3.3   Magnetic separation

3.3.1   Separation concept

Magnetic separation, i.e. isolation or sorting of magnetic objects, including magnetically labeled cells, is a key feature of biomedical and bioanalytical applications and is currently an expanding lab-on-a-chip research area. In separation devices, high magnetic field gradients are required to generate the magnetic separation force [48]. Magnetic sorting and separation can be carried out at high-throughput using virtually any biological sample with minimal power requirements, and without damaging the sorted entities [49–51].

Separation of particles with different magnetophoretic mobility was investigated by Zborowski et al [52, 53]. These authors developed a quadrupolar magnetic device that produces a constant magnetic migration velocity inside a microfluidic circuit with two concentric cylinders. Among many applications, continuous immunomagnetic sorting of CD34+ progenitor cells was demonstrated with this system (Figure 3.6) [54].

Other approaches take advantage of magnetic split-flow thin fractionation in a planar device or magnetic field-flow fractionation in a capillary channel [55–57]. Magnetic thin fractionation is a newly developed family of split-flow techniques for separating magnetically susceptible particles. Particles with different degrees of magnetic susceptibility can be separated into two fractions by adjusting perpendicularly applied magnetic forces and flow rates at inlets and outlets.
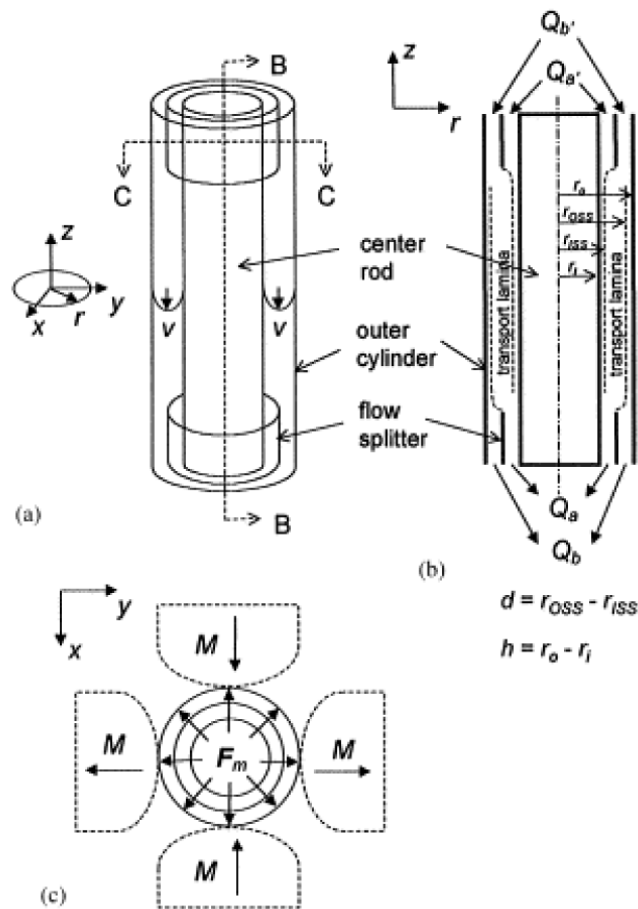
Figure 3.6: *Schematic view of the quadrupole magnetic flow sorter (QMS) separation element: a) Flow channel showing fluid velocity profile in the annulus. b) Longitudinal section of flow channel as shown in a). c) Cross-section through magnetic poles and flow channel, as indicated in a) showing radial magnetic forces [52].*

.

3.3.2 Microfluidic applications

In literature, magnetic separation may refer to batch type separation or continuous flow separation. Microfluidic approaches using external or integrated magnetic elements have been proposed for both techniques. In batch-type approaches, magnetic particles are generally extracted from a sample solution and immobilized on a solid surface [58–63].

Smistrup et al. use arrays of soft magnetic elements to separate magnetic particles from the flow. The soft magnetic elements placed on both sides of the channel are magnetized by an applied external magnetic field and provide magnetic field gradients attracting magnetic beads. Flows with two differently functionalized magnetic beads

and a separating barrier flow are introduced simultaneously at the two channel sides and the centre of the microfluidic channel, respectively. The beads have been attracted to the needle-like tips and stopped. The system is designed to perform a selective on-chip DNA hybridization assay but does not allow for continuous separation (figure 3.7) [62, 64].
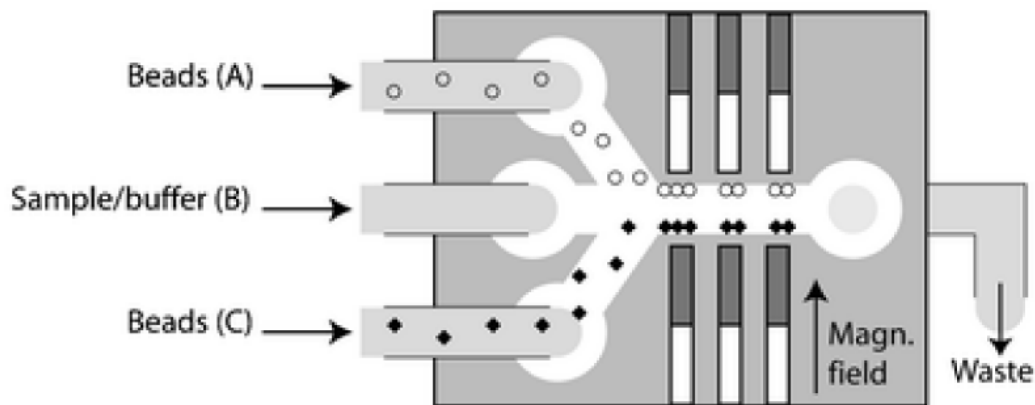
Figure 3.7: *Schematic illustration of the microsystem and the fluid connections to the three inlets A-C. The two types of beads are introduced through inlets A and C, respectively, and separated by a buffer flow through inlet B. The applied magnetic field and the magnetized magnetic elements with captured beads are indicated [62].*

Continuous magnetophoretic separation in the microchip format has been demonstrated by several authors. Different methods to generate high local magnetic gradients in microfluidic channels, i.e. to produce high magnetic separation force, have been proposed. A recent review on continuous flow separation in microfluidic systems also includes magnetic separation methods [36]. For instance, the field gradient and force may simply be controlled by adjusting the distance of an external permanent magnet from the microchannel. A magnetic force-based multiplexed immunoassay was proposed using this method [65].

Arrays of micro-sized magnetic elements or stripes were used to alter the flow direction of particles and magnetically labeled leukocytes in microfluidic chambers [66, 67]. If electromagnets are used, captured particles can be released for further processing or detection. In-plane electromagnets for magnetic particle displacement were formed by co-fabrication of metallic wires and a microchannel [68]. A similar principle was applied by using current lines buried under the microchannel [69]. An on-

chip bead separator using a novel magnetic interconnection technology in a Si substrate has also been designed [70].

In other approaches, red and white blood cells could be separated from whole blood based on their native magnetic properties (Figure 3.8) [71–73]. The required high magnetic gradients were achieved by integrated ferromagnetic or soft-magnetic elements embedded adjacent to a microfluidic channel. Such device was also used for the isolation of suspended breast cancer cells in peripheral blood [74].

Xia et al. designed a high-gradient field concentrator consisting of an electroplated NiFe comb-like structure on one side of a microchannel (Figure 3.9) [75]. Continuous separation of beads with a diameter of 1.6 μm or magnetically labeled *E. coli* bacteria bound to magnetic nanoparticles from the laminar flow path of the sample flow with high throughput was demonstrated. This system focused on efficient extraction of magnetic entities, whereas in our system size separation was the key issue. Although with a microfabricated NiFe comb and an external magnet, a three times higher gradient could be achieved in comparison to the external magnet alone, the authors mentioned that using an external magnet without field concentrator did not generate enough force to pull the particles to the desired location.

3.3.3 Size separation

On-chip free-flow magnetophoresis and continuous size-separation was introduced by Pamme et al. [76–78]. Separation of magnetic from non-magnetic particles and separation of different magnetic particles from each other (different size and/or different magnetization) have been performed using a small permanent magnet. Magnetic microparticles may be deflected from the direction of laminar flow by a perpendicular magnetic field depending on their magnetic susceptibility, size and on the flow rate. Separation of 2.8 and 4.5 μm superparamagnetic particles [76], as well as cells labeled with magnetic nanoparticles in a flow chamber (6 mm x 6 mm) has been performed prior to collection in 16 outlet channels (100 μm wide) (Fig. 3.10) [77].

In continuous flow, magnetic particles were deflected from the direction of laminar flow by a perpendicular magnetic field depending on their magnetic susceptibility and size and on the flow rate. Magnetic particles could thus be separated from each other
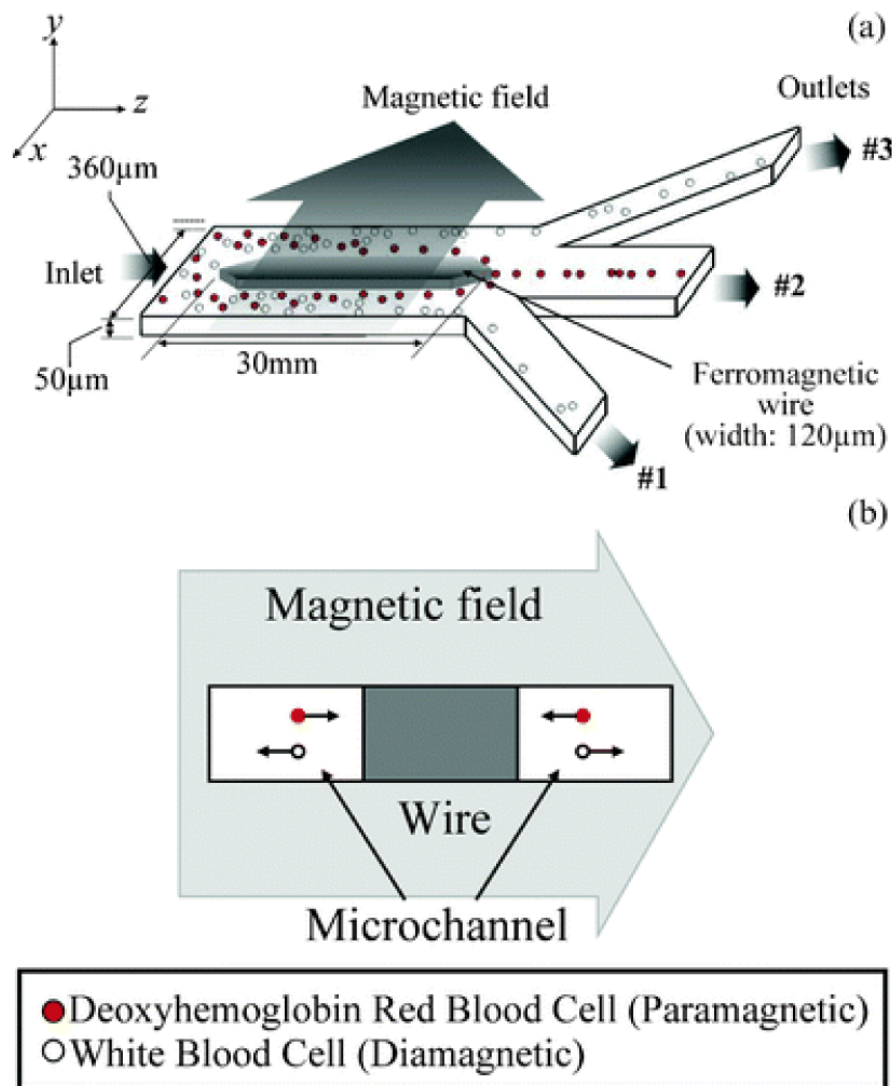
Figure 3.8: *Illustrations of the single-stage magnetophoretic microseparator with a rectangular ferromagnetic wire placed inside the microfluidic channel: a) Perspective view of the microchannel that has one inlet and three outlets. b) Cross-section view of the microchannel [71].*

and from nonmagnetic materials. Furthermore, agglomerates of magnetic particles were found to be deflected to a larger extent than single magnetic particles [76].

The same system has been used for continuous sorting of cells loaded with magnetic nanoparticles. Cells were passed through the microfluidic chamber and were deflected from the flow direction by means of a magnetic field, just like the beads. Two types of cells were studied, mouse macrophages and human ovarian cancer cells (HeLa cells).
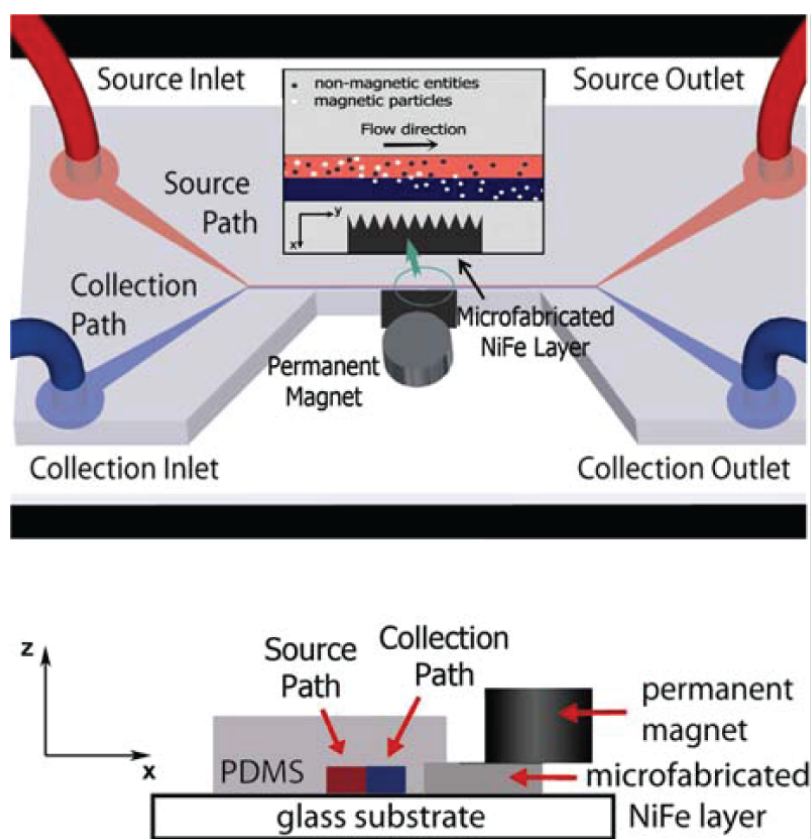
Figure 3.9: *Schematic depiction of the combined micro-magnetic microfluidic separation device that contains a microfabricated layer of soft magnetic NiFe material adjacent to a microfluidic channel with two inlets and outlets; both 3D (top) and cross-sectional (bottom) views of the microdevice are illustrated. The upper inset shows how magnetic beads flowing in the upper source path are pulled across the laminar strained boundary into the lower collection path, when subjected to a magnetic field gradient produced by the microfabricated NiFe layer located along the lower side of the channel. The fluid flow is in the y-direction, the magnetic field gradient across the channel is in the x-direction, and the channel height is in the z-direction [75].*

.

The deflection was dependent on the magnetic moment and size of the cells as well as on the applied flow rate. Furthermore, the separation of magnetic and non-magnetic cells was demonstrated using the same microfluidic device [78].

The concept has been used by Peyman et al. to perform a continuous flow immunoassay [79]. Beads are deflected through the chamber and they are introduced to different reagents and washing steps, thereby performing a sandwich immunoassay using this technique.
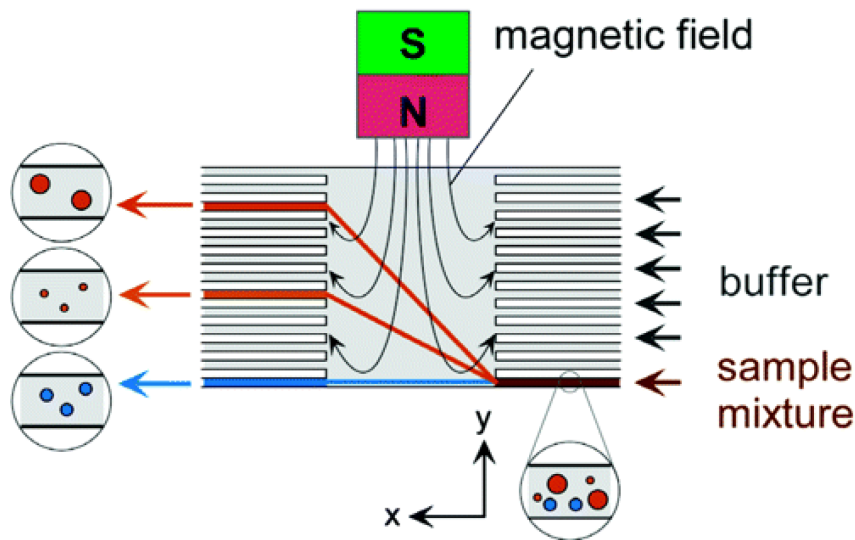
Figure 3.10: *The principle of free-flow magnetophoresis. Magnetic particles are deflected from the direction of laminar flow depending on their size and magnetic susceptibility [76].*

.

More recently, Kim and Park [65] used a similar setup for an immunoassay based on magnetic nanoparticles as labels. Superparamagnetic 50 nm nanoparticles and fluorescent 1 μm polystyrene beads are functionalized with specific antibodies. When target analytes react with the polystyrene beads and superparamagnetic nanoparticles simultaneously, the superparamagnetic nanoparticles can be attached onto the microbeads by an antigen-antibody complex. In the PDMS microfluidic channel, only the microbeads conjugated with superparamagnetic nanoparticles via the antigens consequently move to the high gradient magnetic fields. In this study, the magnetic force-based microfluidic immunoassay is successfully applied to detect the rabbit IgG and mouse IgG as model analytes. The lowest concentration of rabbit IgG and mouse IgG measured over the background is 244 pg/mL and 15.6 ng/mL, respectively [65]. The resolution of this system, however, appears to be limited by the use of an external permanent magnet positioned near the chamber and by the width of the inlet channel.

3.4 Three-dimensional focusing of particles

It is particularly attractive to implement an individual bead analysis approach on-chip, like used in a cytometer, for accurate discrimination, counting or quantitative detection,

instead of analyzing the average signal from a larger particle or cell population [80]. Such approach, however, requires three-dimensional (3D) focusing of the particle suspension into a single focused stream for reliable detection. Particles should indeed pass one-by-one, in-line and with a constant speed through the illumination spot of a laser or sensitive zone of an optical or impedimetric detector that is directly interfacing with the microchannel [81–84]. The requirement of a very narrow focused particle stream is particularly important for detecting small cells or micrometer-size beads.

3D hydrodynamic focusing in a microfluidic device may be realized in a variety of ways, as was summarized in a recent review [85]. The various particle focusing approaches in microfluidic devices may be classified as sheath flow focusing and sheathless focusing. Sheath flow focusers use one or more sheath fluids to pinch the particle suspension and focus the suspended particles. Sheathless focusers typically rely on a force to manipulate particles to their equilibrium positions. This force can be either externally applied or internally induced by channel topology.

3.4.1   Sheath flow focusing

Both horizontal and vertical laminar sheath flow focusing concepts have been proposed, requiring a multilayer chip design with several fluidic inlets and eventually with different microchannel heights [86–89].

Yang et al. presented a microfluidic device using a sample injection nozzle centered in a microfluidic channel realized using complex 3D lithography [90]. Watkins et al. developed an electrical microcytometer, in which T-cells were forced by a sheath flow to the bottom of a microchannel where they passed just over electrical detection electrodes [83]. A high-throughput microfluidic flow cytometer was presented by Simonnet et al. [81] (Fig. 3.11). This device was made of a single cast of PDMS on a SU-8 master microstructure. Adjusting the hydrostatic pressure applied to four fluidic inlets, together with the variation of the microchannel's geometrical parameters resulted in a focused 10 μm-wide stream of particles or cells. This approach was developed further to allow studying of biochemical kinetics based on a highly confined 3D sample flow with a lateral dimension below 0.5 μm [91].

Mao et al. took advantage of Dean flow in a curved channel for focusing 7-8 μm polystyrene particles in the vertical direction, thus eliminating a complex multilayer chip
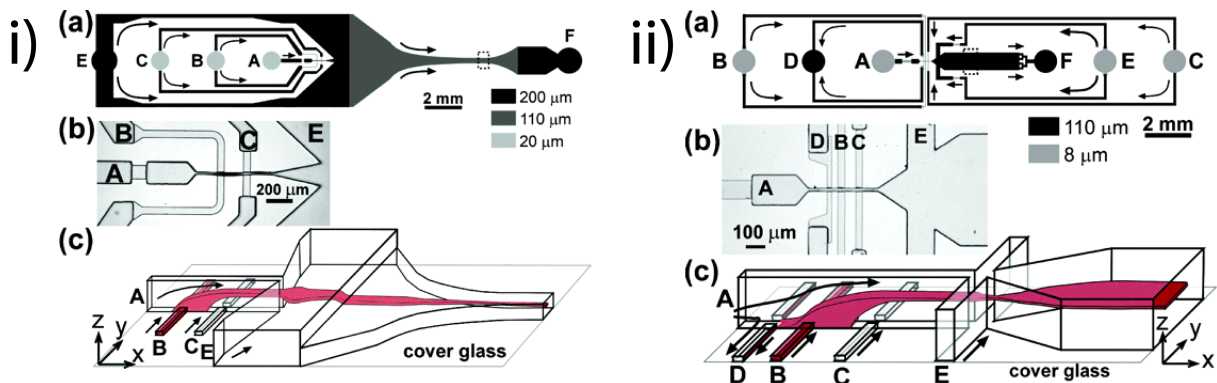
Figure 3.11: *This high-throughput 3D focusing device has fluorescence detection accuracy comparable with that of a commercial flow cytometer. Arrows show the direction of the flow. Capital letters indicate various ports and channels connected to these ports. i) a) Schematic drawing of the microchannel network; the small dashed line box indicates the cytometry channel. Gray scale coding of the channel depths is shown below the drawing. A suspension of particles is injected into port B; flow focusing in the out-of-plane (z) direction is provided by the liquids injected into ports A (focusing from the top) and C (focusing from the bottom); flow focusing in the in-plane direction is provided by the liquid injected into port E. Port F is the device outlet. b) Micrograph of the 3D focusing element. c) Schematic diagram showing the structure of the flow in the device, from the 3D focusing element to the cytometry channel. ii) High-resolution device that allows imaging the particles with a high numerical aperture microscope objective. a) Schematic drawing of the microchannel network; the respective roles of the ports are the same as in Fig. i). b) Micrograph of the 3D focusing element. The 110 μm deep channels have darker boundaries than the 8 μm deep channels. c) Schematic diagram showing the structure of the flow in the device, from the 3D focusing element to the imaging region [81].*

design. In this work, lateral focusing prior to detection was achieved by conventional sheath flow focusing [93], whereby the focused beam had a diameter of less than 15 μm [82]. Dean flow-assisted sheath flow focusing of human red blood cells was demonstrated by Lee et al. in a microchannel comprised of an array of contraction and expansion regions (Fig. 3.12) [92].

In a 3D flow focusing method using grooved channels, two lateral sheath flows first forced a dye sample in the middle of the channel and then pairs of chevrons cut into the top and bottom walls of the channel directed the sheath fluid from the sides to the middle over and under the sample stream [94] (Fig. 3.13). Chevron-based 3D sheath flow focusing has also been demonstrated to focus 5.6 μm diameter polystyrene beads in a microflow cytometer In another design, combination of sheath flows and a
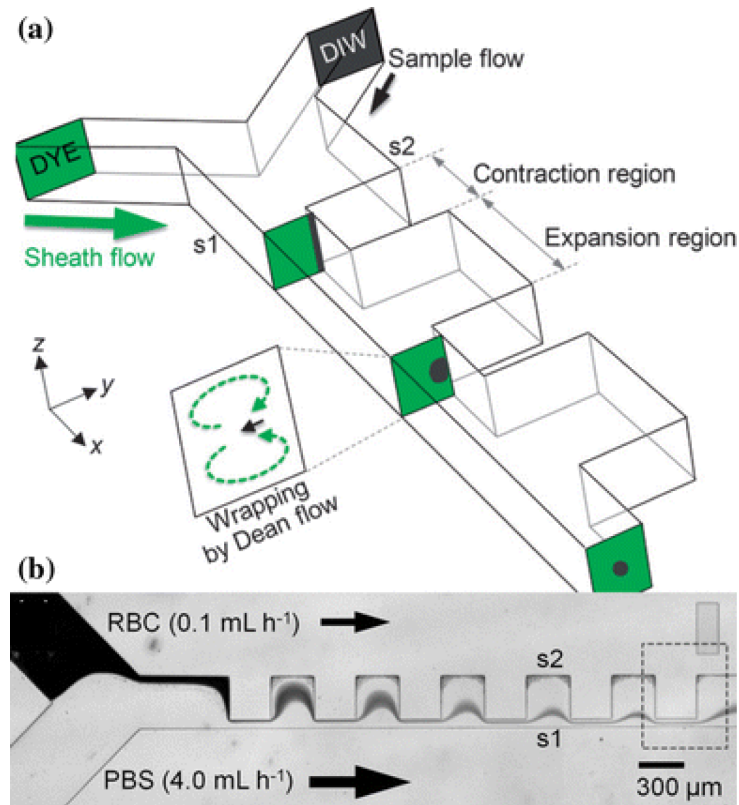
Figure 3.12: *a) Schematic of the contraction-expansion array microchannel for 3D hydrodynamic focusing. b) Image of red blood cells focused by a phosphate buffered saline flow in the xy plane [92].*
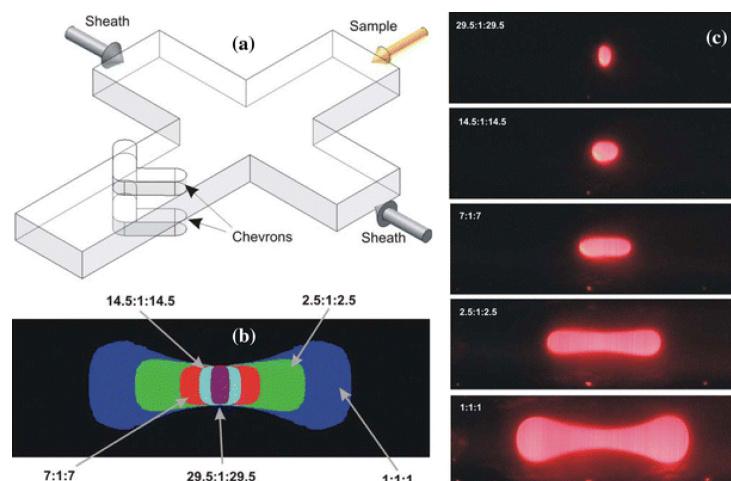
Figure 3.13: *a) Isometric schematic of the chevron-based sheath flow design. b) Numerically predicted size and shape of the sample cross-section at different sheath-to-sample flow-rate ratios for a design of four pair of chevrons. c) Experimentally observed sample cross-sections [94].*

micro-weir positioned right beneath the optical detection system was used to perform focusing of 5 μm and 10 μm polystyrene beads.

3.4.2 Sheathless focusing

Sheathless particle focusers rely on a force to manipulate the suspended particles laterally with respect to the main stream to their equilibrium positions. This force can be of an external origin or can be internally induced by channel topology.

Inertial focusing

Sheathless inertial focusing of 7 μm polymer beads has been achieved in straight microfluidic channels comprising regular alternating geometrical structures [95, 96]. Di Carlo et al. performed very detailed studies of Dean flows and inertial focusing in microfluidic systems, which were characterized by robust and high-rate functioning [97, 98]. The same group proposed a device exploiting lift forces in a serpentine channel for continuous focusing, self-ordering and separation of particles and red blood cells [99, 100].

Acoustic focusing

Acoustic focusing arises from the lateral action of acoustic wave-induced radiation pressure on particles, which forces particles toward either the pressure nodes or antinodes depending on the density and compressibility of the particle and the medium. The ultrasonic field was generated with different means, like a piezoceramic crystal attached to the external surface of a glass capillary tube [101] or a piezoceramic plate integrated into a silicon chip [102, 103], or by deposition a pair of interdigitated transducers onto a piezoelectric substrate, between which a PDMS-based microfluidic channel was bonded to the substrate (Fig. 3.14).

Dielectrophoretic focusing

(Di-)electrophoretic force is another interesting option for focusing particles, cells or single molecules [104–106]. Kim et al. performed axisymmetric flow focusing in a

circular microcapillary of 5 μm diameter polystyrene beads that were lagging behind the flow of a suspending fluid (a solution of water-glycerol mixture with the same density as the particle) due to application of a negative electrophoresis-force. The same principle has also been used to focus red blood cells [107].
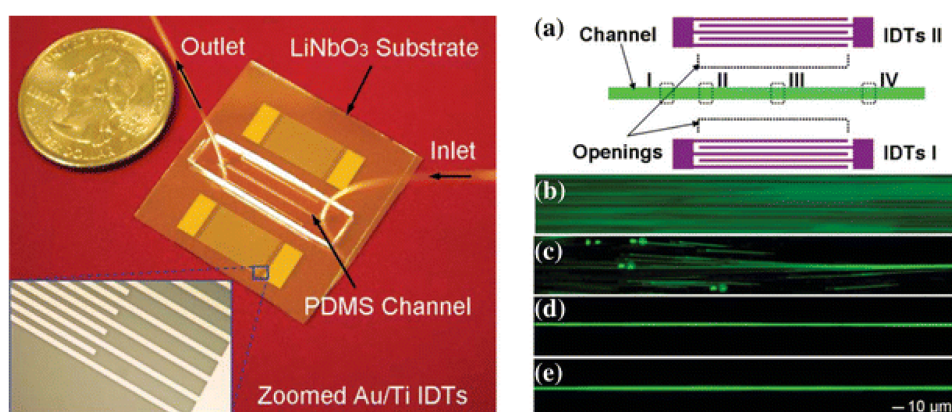
Figure 3.14: *(Left) Photograph of the bonded standing surface acoustic waves focusing device consisting of a $LiNbO_3$ substrate with two parallel interdigitated transducers and a PDMS channel; (right) recorded fluorescent images of 1.9 μm polystyrene beads at sites (I-IV) of the microchannel [105].*

Insulator-based DEP was first demonstrated by Cummings et al [108] in trapping particles through the use of a fabricated array of circular posts. As these posts are electrically insulating, electrical field gradients are formed around them. The induced dielectrophoretic motion overcomes the electrokinetic and Brownian motions, particles are stagnated and concentrated between the posts.

Hydrodynamic filtration-based focusing

The concept of 'hydrodynamic filtration' has been applied to focus 5 μm fluorescent beads into a stream along the centerline of a planar microchannel [109]. In this method, multiple 1 μm wide side channels first split the carrier fluid flows from the main channel, while leaving the beads in the main stream. Then, these split flows were re-injected into the main channel from both sides simultaneously focusing the beads to the center. Using the narrow microfluidic side channels required sophisticated microfabrication techniques and sufficiently clean flow solutions during operation to prevent clogging.
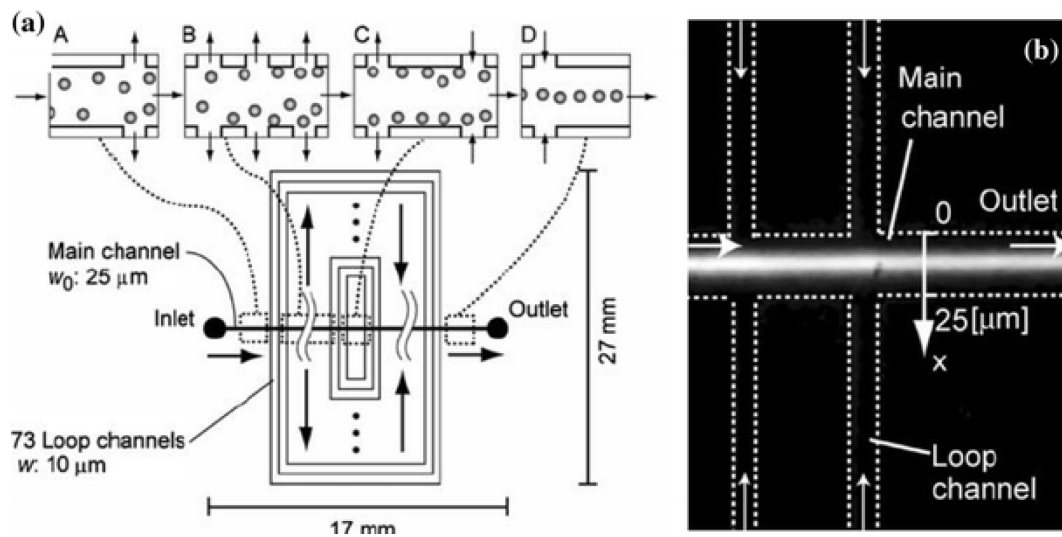
Figure 3.15: *a) Principle and microchannel design for hydrodynamic filtration-based focusing of particles; b) Image of 5 μm fluorescent beads flowing near the outlet of the main channel as indicated in a) [109].*

3.5 Immunoassays

3.5.1 General remarks

One of the main applications of lab-on-a-chip systems is that of biological assays. In particular, the microfluidic devices described in this thesis will be used for detection of antigens using immuno-agglutination techniques. An immunoassay is a test to measure the presence or concentration of an antigen in biological liquids such as serum, blood or urine. Such assays are based on the unique ability of an antibody to bind with high specificity to an antigen [110]. An immunoassay represents an analytical concept that has been widely used for diagnosis, chemical analysis, and screening [111]. In order to measure the amount of antigen present in a solution, an immunoassay often requires the use of a marker, or a labeled material. This label will react as part of the assay, provoking a change in signal that can be measured. Since its origin around 1960 with the introduction of the first generation of radio-immunoassays until now, research efforts have been directed toward increasing the sensitivity, decreasing the processing time, and reducing the amount of reagents and sample required. Depending on the technology used to detect the concentration of the antigen in the sample, and on the immunoassay structure, different types of tests can be identified as described in the following [112].
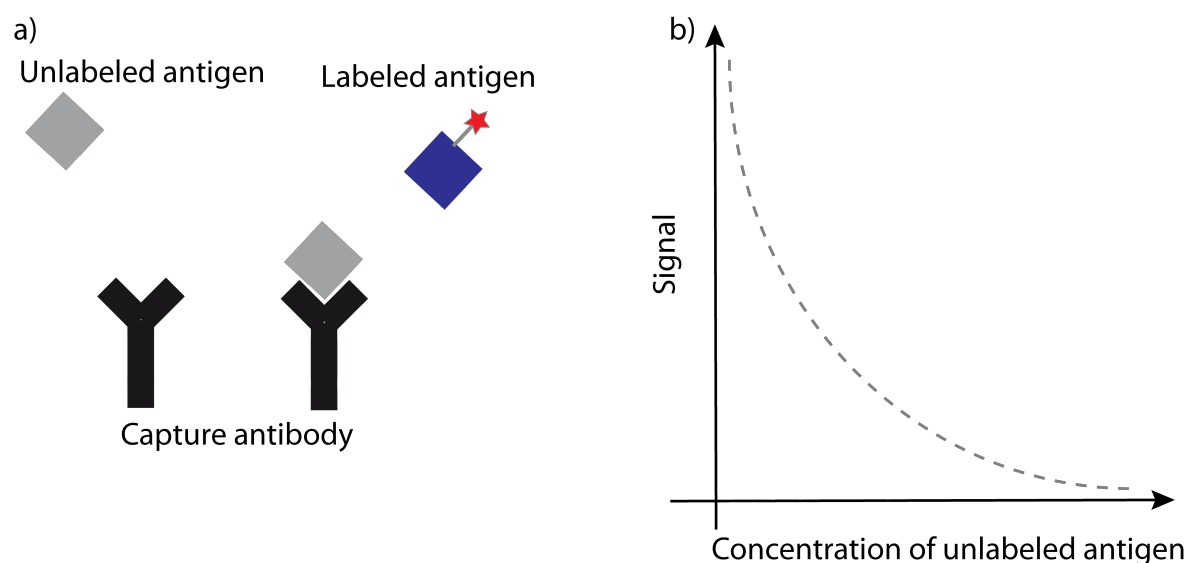
Figure 3.16: *a) Schematic representation of a competitive immunoassay, where the labeled antigen (Ag) is in competition with the unlabeled Ag. b) Typical competitive assay response.*

3.5.2 Competitive and non-competitive immunoassay

The principle behind a competitive immunoassay is that the target antigen in the sample solution competes with another labeled antigen (Ag) to bind with a capture antibody. The amount of labeled Ag or analyte bound is finally measured. When the unlabeled Ag binds to the capture antibody, it occupies and blocks that binding site, preventing the bonding of the labeled Ag. The response of a competitive immunoassay is inversely proportional to the Ag concentration in the sample solution (Fig. 3.16).

In non-competitive immunoassays, the Ag or analyte in the sample solution is bound to the capture antibody and detected using a labeled detection antibody (sandwich immunoassay). In this case, the amount of measured labeled antibody is directly proportional to the Ag concentration in the sample solution. A non-competitive immunoassay usually provides the highest level of sensitivity and specificity (Fig. 3.17) [113].

a)

b)

Detecting antibody

Antigen

Capture antibody

Signal

Concentration of antigen
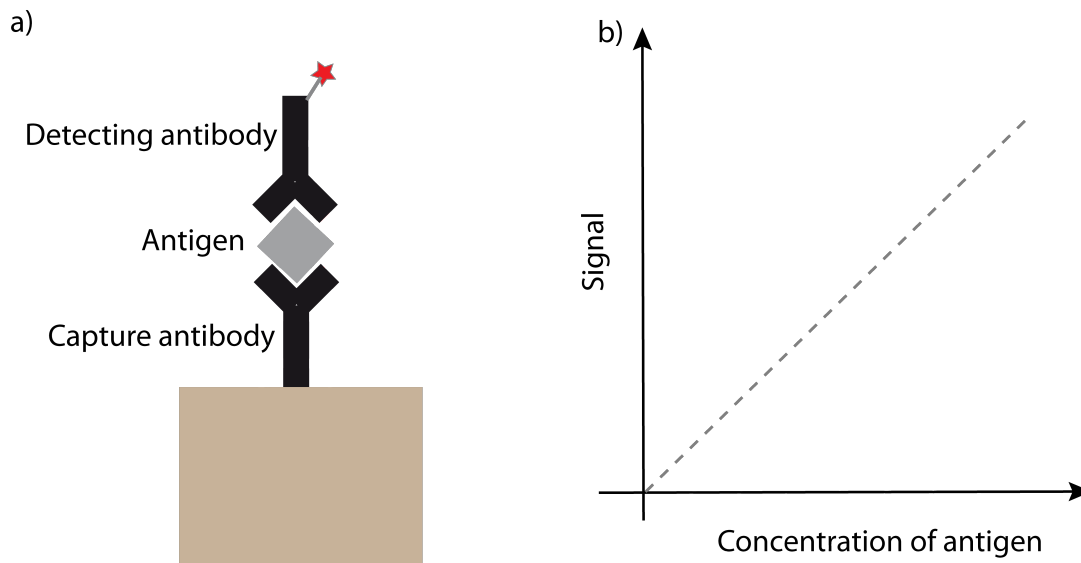
Figure 3.17: *Schematic representation of a sandwich immunoassay: the target Ag is sandwiched in between the capture and the labeled detection Ab.*

In this kind of assay, the measurement of labeled material is directly proportional to the concentration of the Ag or analyte in the sample, as schematically shown in 3.17b. This is in contrast with the indirect proportionality of a competitive immunoassay discussed earlier.

3.5.3 Homogeneous and heterogeneous methods

Immunoassays can be divided into heterogeneous and homogeneous methods. Heterogeneous formats require separation of surface-bound and free labels before quantifying the assay signal. Homogeneous assays do not require this separation step and therefore are faster, simpler, and more suitable for automation. The examples in the literature vary from assays within a single liquid phase, followed by turbidimetric [114], colorimetric [115], fluorometric [116], and luminescent [117] detection schemes, to the use of solid phases in a liquid, which includes beads [118], colloidal gold and latex particles [119], membranes [120], and cells [121].

A homogeneous immunoassay requires less manipulation steps compared to a heterogeneous assay. Consequently very small Ag concentrations can be measured

with homogeneous assays, provided pure samples are used. The performance of immunoassays is mainly limited by diffusion of the Ag to the bonding site. Moreover, in classical immunoassays, an elevated consumption of reagents and washing buffers adds additional costs to the tests. These disadvantages can be overcome with a microfluidic-based immunoassay. In microscopic analytical systems and lab-on-a-chip devices, the small dimensions help reducing the time needed for the reactions, and the low quantities of reagents can result in a cutdown of costs of the immunoassay.

3.5.4   Enzyme-linked immunoassays (ELISA)

One of the first types of immunoassays was the radioimmunoassay (radioactive isotopes are used as labels). The amount of radioactivity indicates the amount of Ag in the sample. Depending on the format (competitive or non-competitive), the relationship between radioactivity signal and amount of Ag could be directly or inversely correlated to the concentration of the Ag [122].

An ELISA is an important method which has been introduced in 1971 [123, 124]. The first step of the ELISA is the immobilization of a capture antibody on the surface. The second step is the introduction of the sample with an antigen or analyte of unknown concentration. If the Ag is present in the sample solution, a complex of capture Ab-Ag forms. After a washing step, the detection antibody solution is introduced. The latter is chosen in a way to bind specifically to the Ag. It is called detection antibody because it is labeled with an enzyme, that allows sensing its presence via an enzymatic reaction. The last step is the introduction of a "substrate" solution that changes colour or becomes fluorescent through the action of the enzyme.

3.5.5   Agglutination assay

The agglutination test is a homogeneous assay introduced by Singer and Plot in 1950 [125]. In an agglutination assay, dispersed particles which are functionalized with capture antibodies are mixed with an Ag sample solution. The concentration of the aggregates is proportional to the concentration of the Ag that may bind two particles by antigen-antibody complex formation (Ab-Ag-Ab). This reduces the requirements of rinsing steps (Fig. 3.18).
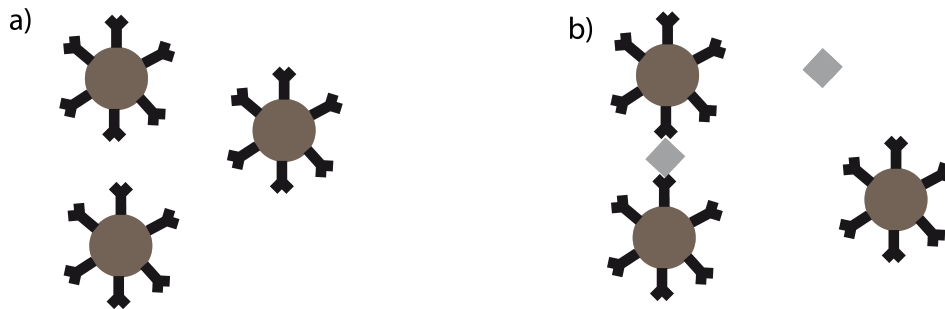
Figure 3.18: *Schematic representation of an agglutination assay: a) beads are grafted with capture antibody on the surface. b) The antigen binds to capture antibodies forming aggregates.*

Latex particle-based agglutination tests are used for the diagnosis of diseases in humans and animals [126]. They are generally simple, cheap, and do not require sophisticated equipment, nor highly specialized skills. These types of assay are mainly used for infectious disease detection and protein quantification, as long as the Ag concentration to be detected is larger than 1 nM. Different methods are used to detect the presence of the agglutinated clusters.

3.6 Magnetic bead-based immunoassays

3.6.1 Heterogeneous magnetic beads based bioassays

The majority of immunoassays on-chip based on magnetic beads are heterogeneous sandwich-type assays. Heterogenous assay protocols need several timed washing steps and separation of magnetic beads from the solution. These steps are accelerated and easier to perform on-chip using microfluidics. Fluorescent detetcion is a standard method of detection which can be perfomed on-chip under a microscope. The chemistry of labeling with different dyes and enzymes is well known.
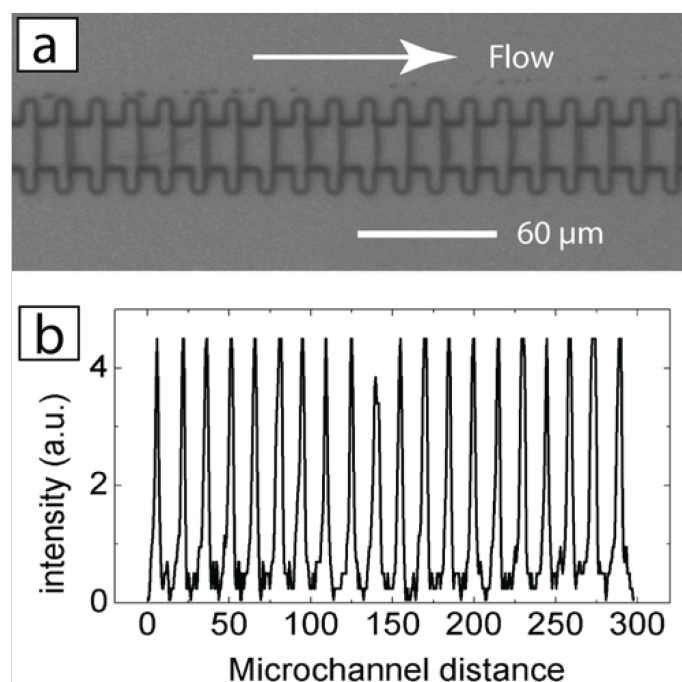
Figure 3.19: *a) Optical image of a microchannel showing the retention of 20 self-assembled nanoparticle magnetic chains that are perfectly positioned in geometrical traps, while applying a flow from the left to the right. b) Gray scale intensity profile, derived from an optical photograph like shown in part a, of 20 magnetic structures self-assembled in the microchannel [127].*

Complete on-chip sandwich immunoassays have been performed using geometrically trapped self-assembled magnetic nanoparticle chains. The immunoassay is based on the retention of magnetic nanoparticle chains in a microfluidic channel with periodically varying cross-section (Fig. 3.19). The nanoparticles specifically capture and detect a low number of target Ag molecules (down to 105) in a very small sample volume (down to 4.1 nL) in a matter of minutes and in a simple setup. Murine monoclonal Abs have been detected down to a concentration of 1 ng/mL. It has been demonstrated that the magnetic chains gradually deplete the Ab concentration from the flow, i.e., chains that are positioned more upstream in the flow capture more Ab. This shows that positioning the magnetic nanoparticles in chains across the microchannel strongly enhances the fluid perfusion through the magnetic structures, resulting in a very strong particle-liquid interaction. This method permits one to position a well-controlled and small amount of nanoparticles in the microfluidic system, which is essential for quantitative analysis.
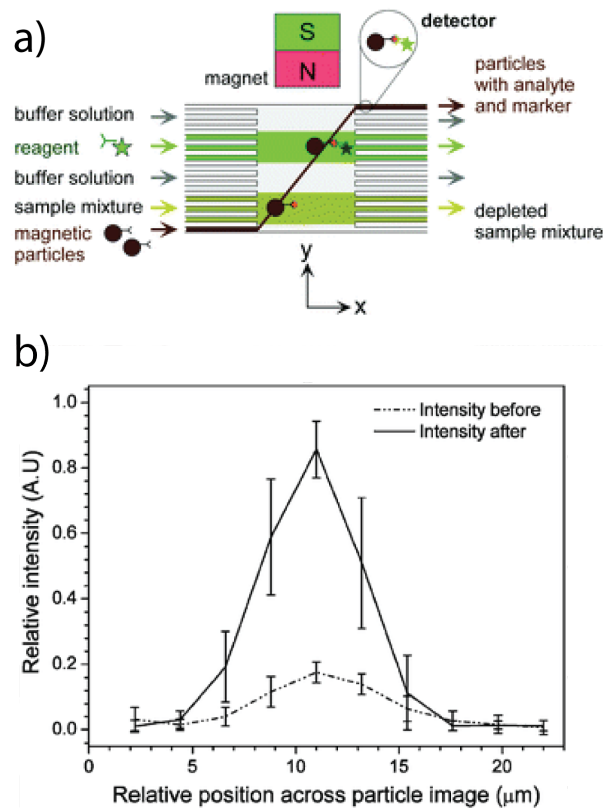
Figure 3.20: *a) The magnetic setup to pull magnetic particles continuously through reagent streams. A sandwich assay is shown schemtically. b) Fluorescence intensity of particles before entering the biotin flow stream and after leaving the biotin flow stream [79].*

Peyman et al. have demonstrated a dynamic concept for performing reactions on the surface of magnetic particles, while they are transported through different reagent streams (Fig. 3.20a). The flow stays laminar in the microfluidic device, i.e. different reagents do not mix in the chamber and magnetic particles are deflected (due to a magnetic gradient produced by the permanet magnet) through these reagents. This permits multiple steps of reaction, washing, and detection in the same chamber. To show the feasibility of the concept, a streptavidinbiotin binding assay has been performed on-chip [79]. The fluorescence intensity of the particles prior to entering the biotin stream and after leaving the biotin stream was compared. The relative intensities of 12 particles before and after passing through the biotin stream were averaged and plotted against distance across the particle image (Fig. 3.20b).

3.6.2 Homogeneous magnetic beads based bioassays

Bulk format

Latex particle-based homogeneous assays have relatively poor detection limits, despite the fact that many diagnostic assays require high sensitivity. They are generally performed by using the ELISA principle. In the range of low concentrations ($\approx$ pM), the reaction time of an agglutination assay naturally increases. By enhacing interactions between the beads, the time of the assay as well as the detection limit can be reduced. This can be achieved, for example by introducing magnetic beads. The rate of antibody-antigen-antibody complex formation in an agglutination assay depends on many parameters. Decreasing the number of antigens to be detected implies also decreasing the number of particles. As a direct result, the frequency of particle collisions decreases. At low concentration of Ag, one of the limiting parameters becomes therefore the encounter frequency between two particles.

Therefore, conditions and protocols that accelerate the specific recognition between grafted ligands and receptors have been investigated [10]. Under a homogeneous magnetic field, Brownian magnetic particles can capture and transport the Ag. As the particles are superparamagnetic with high susceptibility, the resulting magnetic colloidal forces induce a fast chaining process, that considerably increases the colliding frequency. These chains persist as long as the field is maintained and allows for rapid formation of ligand-receptor-ligand links between pairs of particles within the chain. In low Ag concentrations, the number of particle is large compared to the Ag molecules, so only doublets of particles can form (instead of bigger clusters). This requires a detection method which can distinguish between doublets and singlets.

To quantify the influence of this one-dimensional confinement on the recognition rate, Baudry et al. have detected the amount of doublets that remain after the field is switched off [10] (Fig. 3.21). This method provides the basis for a rapid, homogeneous, and highly sensitive bioanalytical method. This method was carried out in the microtitre plate format.

The magnetic agglutination assay developed by Baudry et al. consists of three steps:

- Step 1: Magnetic particles grafted with polyclonal antibodies (or two different monoclonal antibodies) are mixed with the sample, which contains the antigens. Antigens are captured by grafted beads.

- Step 2: The application of a magnetic field induces a magnetic dipole in each bead, allowing an almost instantaneous formation of chains. Essentially all particles that have captured an Ag will form a link with their neighbor.

- Step 3: After only a few minutes, the magnetic field is switched off, and, because of Brownian motion, only doublets that are linked remain. Doublets are detected by a turbidimetric measurement [10].
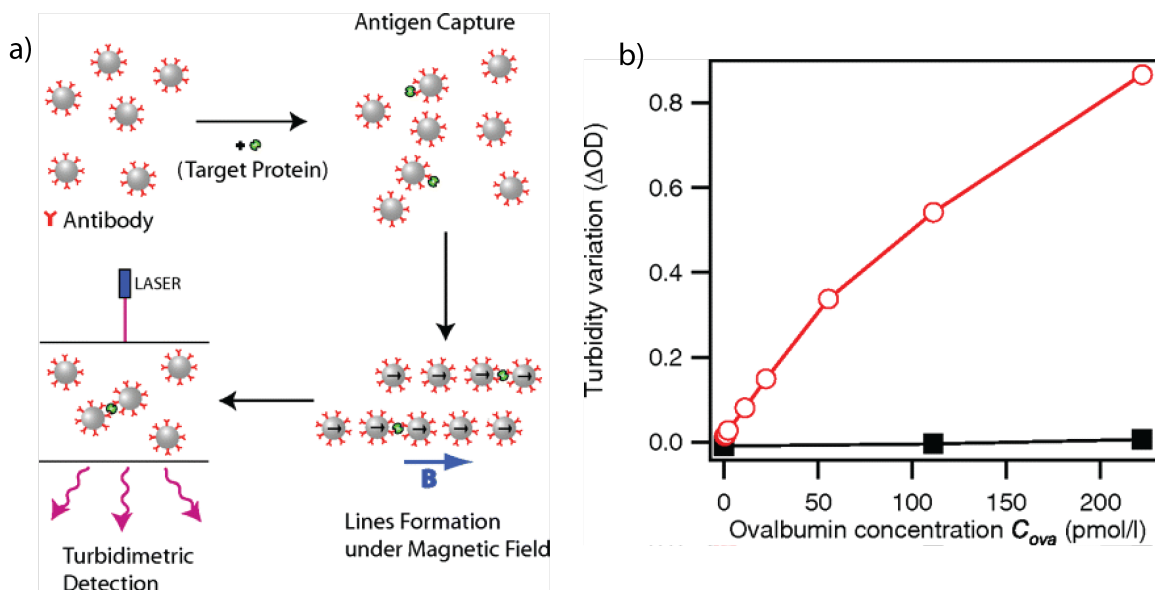
Figure 3.21: *a)Principle of a magnetic agglutination assay. b) Validation of the optical density difference measured with a UV/vis spectrophotometer before and after the application of the magnetic field B, vs. ovalbumin concentration [10].*

Magneto-microfluidic agglutination assay

A first microfluidic approach for an agglutination assay was presented by Degré et al [128]. In their system two permanent magnets were used to concentrate magnetic beads in a microchannel. The experiments were performed in PDMS microchannels, using streptavidin-coated superparamagnetic beads and two external magnets (Fig. 3.22). The target molecule is biotinylated protein A. By taking full advantage of the microfluidic conditions (scaling down of the detection volume and controlled action of the shear flow), in this method, the Ag was forced to pass through a limited number of magnetic beads using a microfluidic channel. This system is therefore more promising compared to the batch format.

When biotinylated protein is present in the sample, the target molecules may cross-link the beads, forming sandwich-type molecular assemblies. Fig. 3.22.ii(a)(c) displays, for different biotin concentrations, the state of the system well after the magnets have been taken away. For the highest concentration, most chains break into one or two long fragments after the magnets are removed (Fig. 3.22.ii(c)). By decreasing the concentration, the fragments become, shorter and their number increases (see Fig. 3.22.ii(b)). However, their length distributions are broad and there still exist, even at extremely low concentrations, a few long-lived filaments in the system, showing the presence of the target molecule. An example is shown in Fig. 3.22.iid) for a concentration of 10^{-14} mol/l biotinylated protein A.
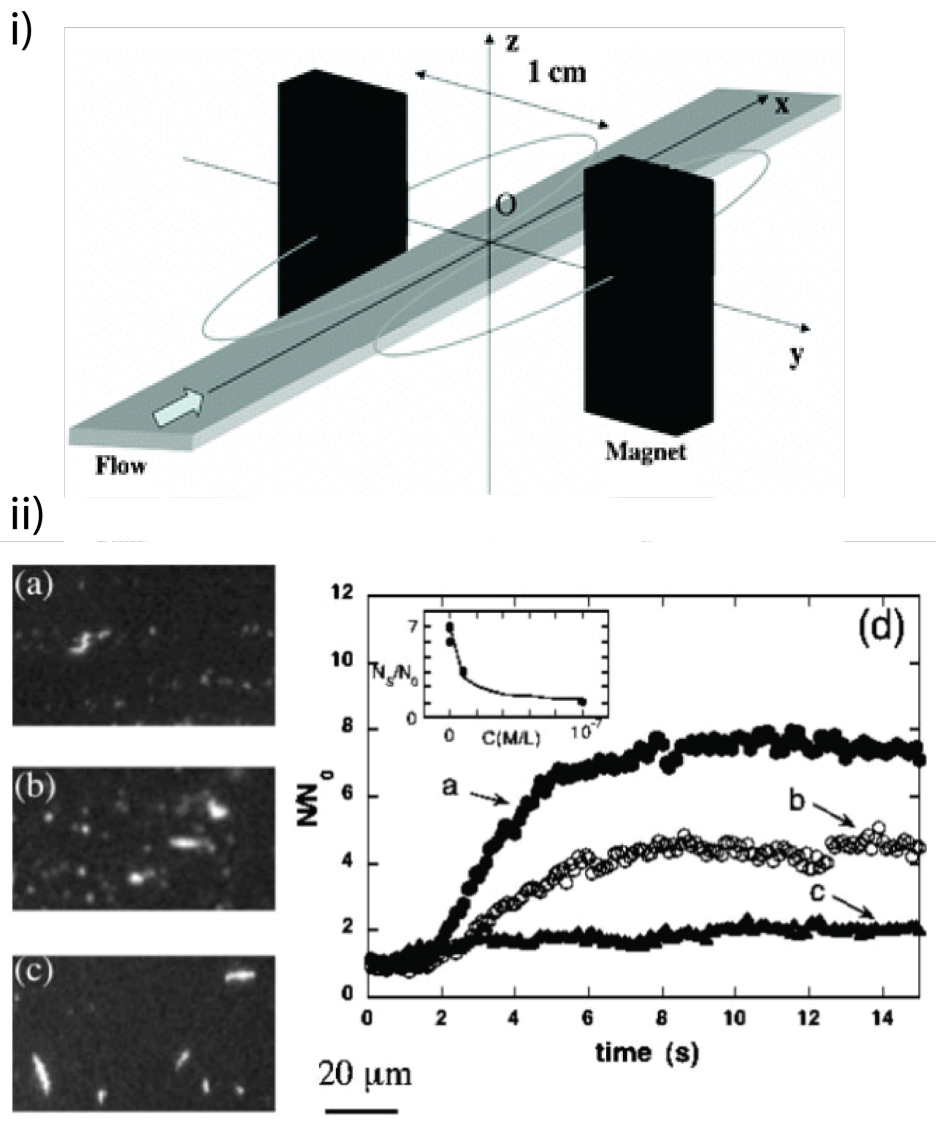
Figure 3.22: *i) Sketch of a magneto-microfluidic agglutination experiment. ii) Images (a) to (c) show the system, long after the magnets have been taken away, for different concentrations of biotinylated protein (d) shows the evolution of the quantity $N_s//N(0)$ as a function of time for different target molecule concentrations (where N_s is the number of objets (particles or chains) present in the system). Beads are visualized by dark field microscopy.*

In other work, the dynamic actuation of a confined plug of functionalized magnetic beads in a microchannel has been presented [129]. This system allows for Ag capture with improved efficiency. The system is shown and explained in Fig. 3.23.i. It is an integrated device comprising a quadrupolar magnetic set-up and a microfluidic chip

with a single channel. The magnetic field is generated by an external coil and guided through a magnetic core towards two magnetic micropoles on-chip (Fig. 3.23.ia). Two small removable permanent magnets (NdFeB) are positioned on top of the microchannel (Fig. 3.23.ia). They have high field strength and may be placed about 3 to 5 mm away from the active region in order to generate a field strength comparable to the AC field. A photograph of the assembled device is shown in Fig. 3.23.ib. Fig. 3.23.ic shows a schematic view of the magnetic particles moving across the channel (dynamic plug) in the Ag solution flow. Bead actuation in the microchannel is based on the forces exerted simultaneously by a time-varying field generated by the external electromagnet and the constant field of the two permanent magnets on top of the microchannel (Fig. 3.23.ia). The sinusoidal AC field is focused across the microchannel using two magnetic microtips that define the active volume. This combination makes the field in the active region between the poles, asymmetric with respect to the channel axis. Field maxima and minima are on opposing pole sides, and inverting the pole magnetization (coil current) shifts the field maxima to the opposite side. Consequently, the magnetic force acting on a particle will be changed likewise. As a consequence, in this quadrupolar magnetic actuation system, superparamagnetic beads can move across the channel by applying an alternating field to the poles.

In this method, the number of aggregated particles has been estimated by a diffusion-based detection method of the aggregated particles. The feasibility of an on-chip agglutination assay was demonstrated by means of the streptavidin/biotinylated-BSA model system. A detection limit of 200 pg/mL($\approx$ 3 pM) confirms the high potential of this approach. The principle of the method is schematically shown in Fig. 3.23.ii:

- (a) Functionalized magnetic particles are injected and magnetically trapped in a microchannel.

- (b) The confined dynamic bead plug is perfused with the Ag solution.

- (c) After Ag capture, beads are immobilized on one side of the channel to allow formation of aggregates.

- (d) The magnetic field is switched off and the beads are released. The area of the released plug is a measure of the amount of agglutination and the size of the aggregates.
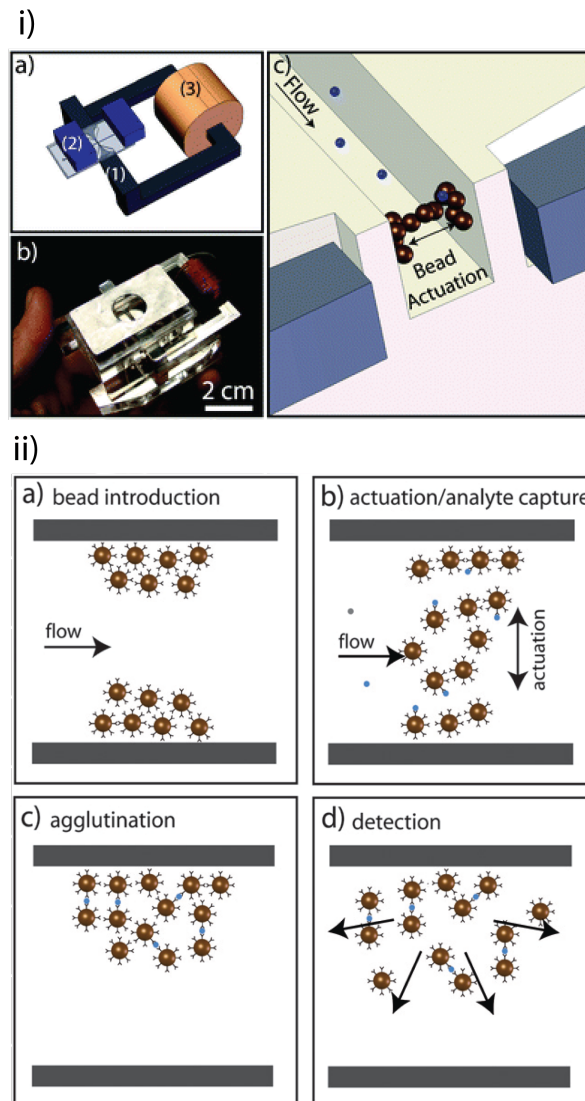
Figure 3.23: *i) a) Schematic view of the microfluidic chip and the magnetic actuation system comprising two soft magnetic microtips (1), two small permanent magnets (2) and a coil (3). (b) Photograph of the whole system. (c) 3-Dimensional schematic view of the particles moving across the microchannel in between the magnetic poles and perfusion with the antigen solution. ii)Principle of a microfluidic agglutination immunoassay. Detection is based on the measurement of the area of the released plug.*

4

The magneto-microfluidic platform

4.1 Concept of the platform

In this chapter, the microfluidic and magnetic platform we have developed is presented. The setup consists of three main parts: the PMMA platform, the microfluidic chip and the magnetic setup. A schematic view of the whole system is shown in Fig. 4.1. The PMMA platform comprises the fluidic connections from the microchip to the external fluidic pumps, and it provides the space for the magnetic setup consisting of a magnetic core and the coil. The chip is fabricated in PDMS and its channels are sealed by a glass substrate, being clamped together in the PMMA setup. The magnetic soft tips are inserted into both recesses of the PDMS chip. A similar platform has been used previously for the actuation of magnetic beads [20] and for the development of an agglutination test on-chip [129]. In the present thesis, the platform has been developed further to perform separation of magnetic beads and 3D focusing of beads on-chip [130].

4.2 The microfluidic chip

A standard molding process is used for the fabrication of the chip in PDMS (Sylgard 184, Dow Corning Inc. Midland, MI). PDMS is a silicon-based soft polymer that is commonly used for the fabrication of microfluidic systems. It can be poured on SU-8 mold for the formation of the desired structures.
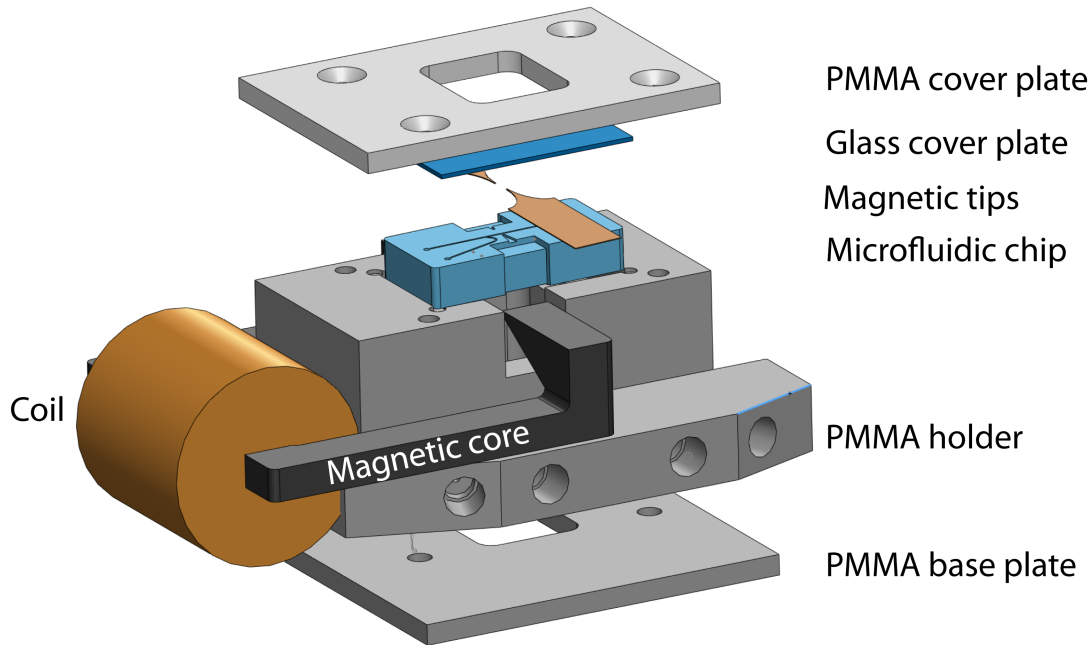
Figure 4.1: *Exploded view of the magneto-microfluidic platform. The holder is made of three PMMA parts: the PMMA cover plate, PMMA holder and the PMMA base part. The magnetic system is made of a coil, a magnetic core and the soft magnetic tips. The microchip consists of the microfluidic chip in PDMS and a glass slide.*

4.2.1 SU-8 molds for PDMS chips

A microstructured SU-8 mold is used for replica molding. SU-8 is an epoxy-based negative photoresist. Negative resist means that exposed parts will remain on the substrate, whereas unexposed areas are removed. It is well suited to realize different types of molds (e.g. micromolds for electroplating and molds for elastomeric replication) [131]. The different steps of a typical process for SU-8 photolithography are described here (Fig. 4.2):

- Substrate preparation

   Glass or silicon substrates can be used, the latter having better adhesion properties with respect to SU-8. In this project, silicon substrates were used. To ensure good
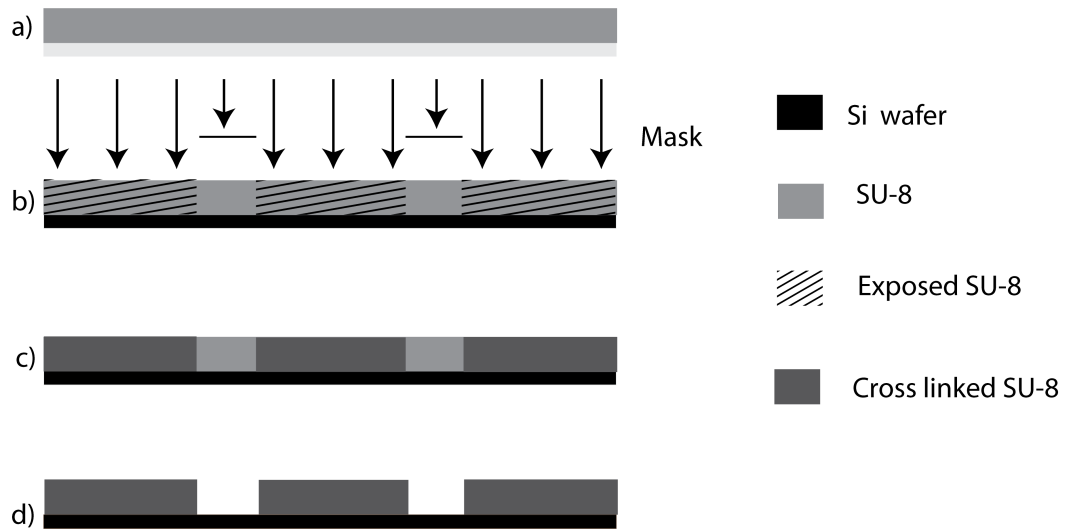
Figure 4.2: *Different steps for the photolithographic patterning of SU-8 resist: a) Spin-coating of SU-8 on a Si wafer and soft bake. b) Exposure with UV light through a photomask. c) Post exposure bake leading to cross-linking of the exposed parts. d) Final structure after development and removal of unexposed resist.*

adhesion, the substrate must be cleaned and dried prior to applying the SU-8 resist. To remove adsorbed water, the substrate is put in an oven at 130°C during 20 min or is exposed to an oxygen plasma.

- Spin-coating

  The resist is spread on the wafer by spin-coating at a certain speed to obtain the desired thickness (Fig. 4.2 a). Different types of resists with different viscosities are available. The viscosity depends on the amount of solvent in the SU-8. According to its viscosity, each resist can cover a certain thickness range. We used GM 1070 (Gersteltec) which is suitable for thicknesses between 15 and 200 μm.

- Soft Bake

  The resist is then prebaked at 130 °C to evaporate the solvent. Ramping and stepping of the soft bake temperature is recommended for a more controlled evaporation rate.

- Exposure

  The SU-8 contains acid-labile groups and a photoacid generator. Exposure to UV light (Fig. 4.2 b) generates a low concentration of acid which will act as a catalyst
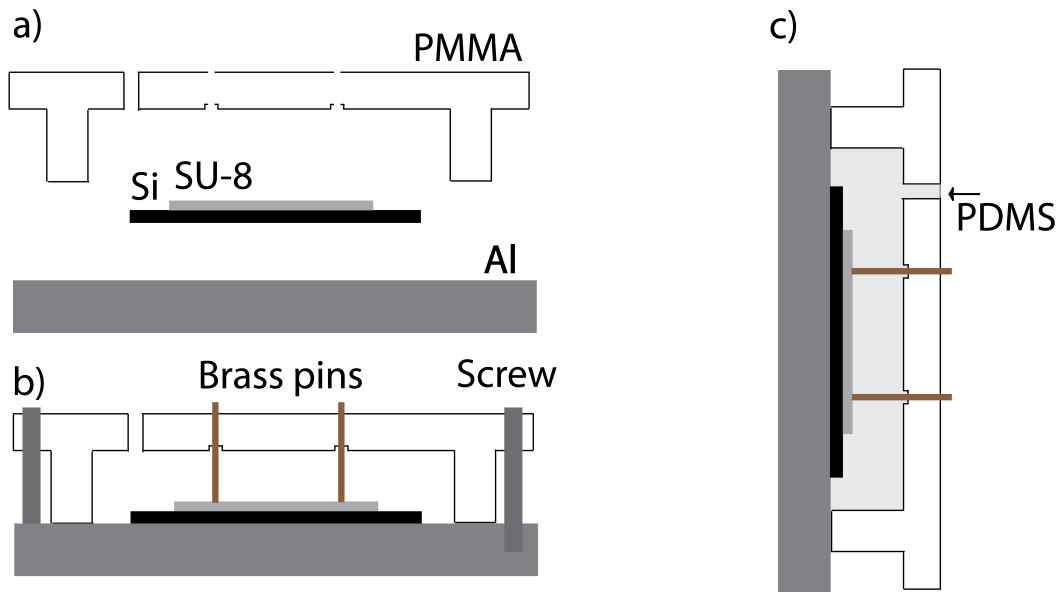
Figure 4.3: *PDMS chip molding a) SU-8/Si mold and Al support with PMMA case. b) Inserting brass pins and fixing of the mold using screws. c) Injection of PDMS in the mold.*

of the cross-linking process. However, cross-linking does not take place at room temperature. The exposure dose is proportional to the film thickness.

- Post Exposure Bake

  The SU-8 is heated on a hotplate up to a temperature of $95\,^{\circ}\mathrm{C}$ to cross-link the exposed parts (Fig. 4.2 c). Slow ramps of temperature for heating ($+2\,^{\circ}\mathrm{C}/\mathrm{min}$) and cooling ($-2\,^{\circ}\mathrm{C}/\mathrm{min}$) are essential to minimize internal stress, which could lead to adhesion problems of the cross-linked structures.

- Development

  The exposed SU-8 layers are developed in a solution of propylene glycol methyl ether acetate (PGMEA) (Fig. 4.2 d) to reveal the desired microstructures. Ultimately, the structures are rinsed with isopropanol.

4.2.2 PDMS chip fabrication

PDMS can seal to PDMS and other flat surfaces reversibly by conformal contact (via van der Waals forces), or irreversibly, if both surfaces are Si-based materials and have
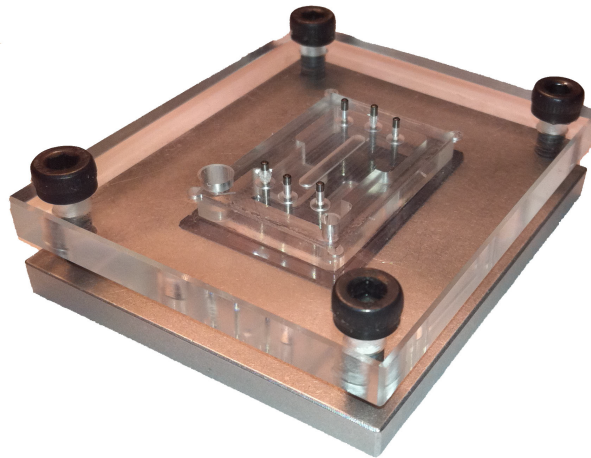
Figure 4.4: *A picture of the mold for PDMS consiting of the Al support, the SU-8/Si master, the PMMA parts and the brass pins.*

been oxidized by plasma before contact (a process that forms covalent O-Si-O bonds). Seals are watertight and can be formed under ambient conditions (unlike silicon and glass, for which bonding requires high temperatures or adhesives). If desired, many PDMS replicas can be made from a single SU-8 master. This way of producing the PDMS structure from the SU-8 master is called replica molding.

To create the PDMS mold, a liquid PDMS prepolymer (in a mixture of 10:1, base polymer: curing agent) is poured on the Si/SU-8 layer, the SU-8 structures on the Si wafer will form the microchannel in the PDMS chip.

For molding the PDMS chips SU-8 master is placed on an aluminum support plate (Fig. 4.3 a). A PMMA frame defines the PDMS chip outer dimensions. Brass pins are inserted in the top plate to form the fluidic access point (Fig. 4.3 b). The PMMA part is fixed using screws on the aluminum part. Finally PDMS is injected manually using a disposable syringe through a hole in the PMMA plate (Fig. 4.3 c). The vertical positioning of the frame during filling, allows the air getting out from another hole on the opposite position. After removing trapped bubbles in the mold, the PDMS is cured at 65 °C for 12 hours. A photograph of the mold is shown in Fig. 4.4.

4.2.3   Fluidic chip design

In order to assemble the whole system, the PDMS microchip is placed in the PMMA holder (Fig. 4.5). Fluidic connections are self aligned. Integrated PDMS O-rings assure
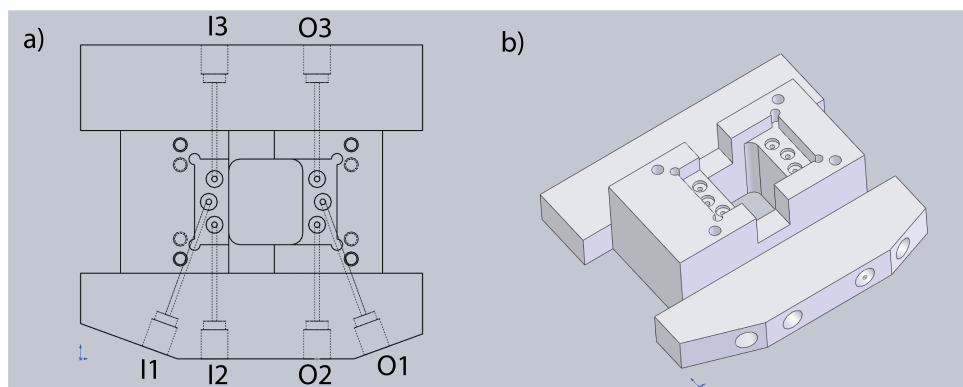
Figure 4.5: *a) The view of the chip holder (from the top) showing inlets and outlets. b) Place of the PDMS chip in the PMMA holder.*

tight fluidic connections between PDMS and PMMA. The microchannels in PDMS are ealed with the help of a glass slide and fixed by mechanical clamping. After that the magnetic tips (two pairs for the separation chip or one pair for focusing chip) are inserted.

In the PMMA case, six fluidic inlets and outlets have been incorporated in order to keep some flexibility for different applications. The outlets may be connected to syringe pumps (using Upchurch connectors) or are accessible (if left open) by using a micro loader, which is thin enough to introduce or extract solutions.

For the separation experiment, the chip had only a single straight channel (see Fig. 4.6 a and b). Outlet (O1) of the chip holder is connected to the syringe pump and inlet (I1) is used to introduce different samples and liquids (Fig. 4.5). A precise glass syringe is used for flow control in the microchannel. Before starting the experiments, the whole system can be purged with buffer solution by means of a plastic syringe. It is particularly important to remove all bubbles from the system to allow controlled operation at very low flow rates (typically at 1 nl/s).

For focusing, agglutination and in-line separation experiments, inlets I1 and I2 have been used as fluidic inlets and O1 as the outlet. The focusing chip has a principal straight microfluidic channel (10 mm long, 200 μm wide, 100 μm high) and a secondary microchannel (200 μm wide, 100 μm high). The fluidic junction is located 0.5 mm downstream the magnetic tip location (Fig. 4.6 c and d). Fig. 4.6 d is an enlarged schematic view of the region of interest. A single precision syringe pump is connected simultaneously to both fluidic inlets of the chip for fluidic control. Both channel portions
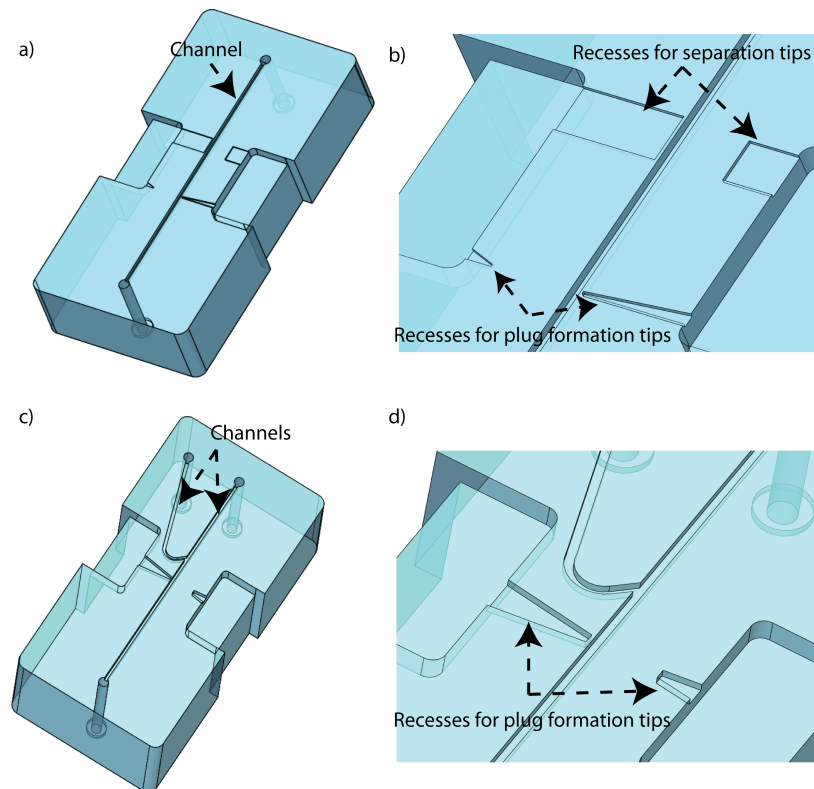
Figure 4.6: *Schematic view of the PDMS chips for separation and focusing: a) and b) Separation chip with a single microchannel and recesses for the tips. c) and d)Focusing chip with a main and a secondary channel.*

before the fluidic junction have equal hydraulic resistance, thus the flow rates in both sections are equal.

4.3 Magnetic actuation system

4.3.1 Magnetic core and coil

The magnetic actuation system consists of three different parts: external coil, magnetic core and magnetic soft tips. The external coil is connected to a power supply (KEPCO, BOP 50-2M) which is addressed by a function generator (Tektronix, AFG3021B) in order to create the current necessary in the coil for creating the magnetic flux. The field is guided through the yoke and is focused in the microfluidic channel area with the help of soft magnetic tips to manipulate the magnetic beads (Fig. 4.7). The magnetic system is designed to be positioned around the PMMA platform, which enables observation
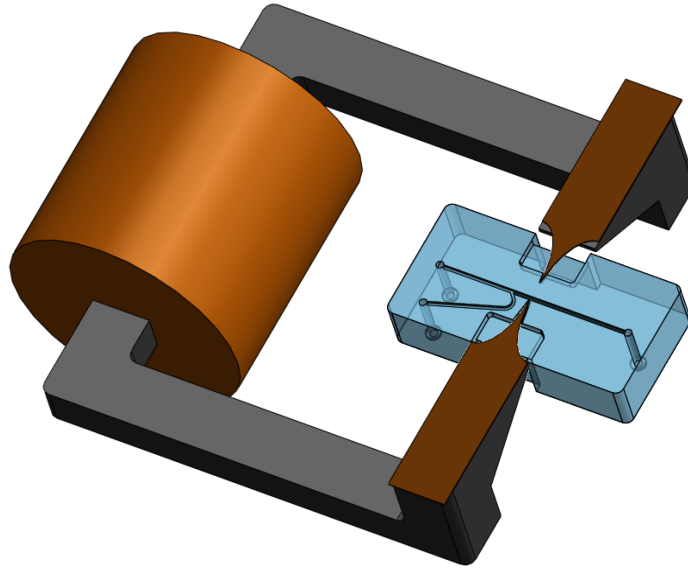
Figure 4.7: *Magnetic system consisting of a coil, a yoke and magnetic tips. Positioning of the microfluidic chip is shown.*

of the microchannel under an upright or an inverted microscope. We have used the system with an inverted microscope in order to have easy access to fluidic reservoirs in the PMMA holder. Beads were observed in transmission mode.

As the role of the core is to guide the magnetic flux from the coil to the microtips for focusing across the microchannel, its relative permeability should be high. Another parameter to choose the material was the ease machinability. Reliable machining of pure iron and soft ferrite is not easy, therefore the alloy PERMENORM (nickel-iron alloy) presented the best option. The satuartion induction of PERMENORM is 1.55 T and its coercivity is 0.08 A/cm. The core was fabricated using Computerized Numerical Control (CNC).

The magnetic potential produced by a coil is given by [132]:

$$\theta = N \cdot I = S \cdot J \tag{4.1}$$

where N is number of windings, I is the current, S is the cross section of the coil (horizontal plane through the windings), and J is the current density. The PMMA holderpart determines the maximum volume for the magnetic coil and of the whole system. It can be assembled under a standard optical microscope (coil section of 20×10 mm^2 and the Cu-filling factor was 50%). The maximim current density in a copper wire
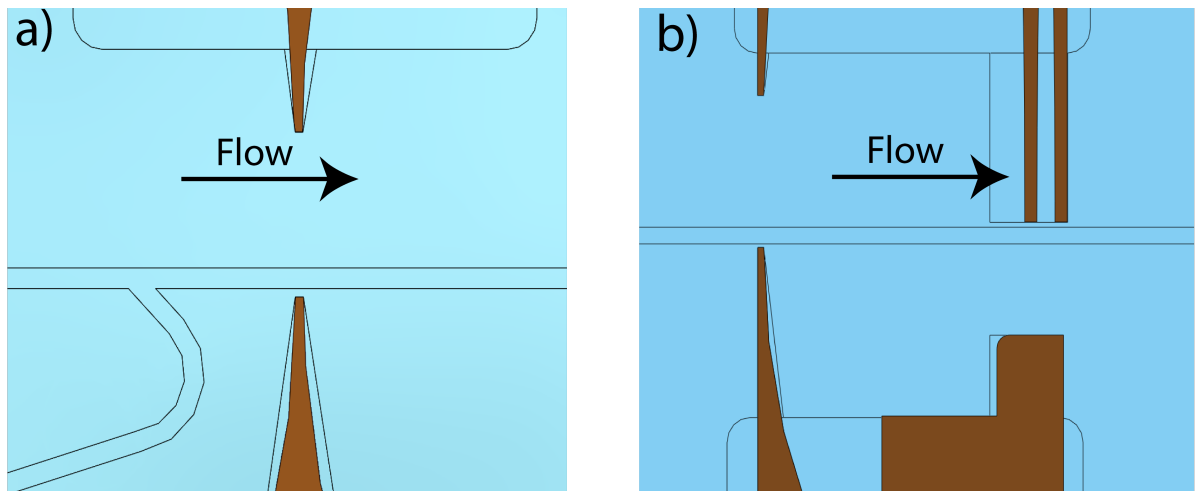
Figure 4.8: *Magnetic tip configurations: a) For the focusing system, one single soft-magnetic tip is positioned close to microchannel and the other one further away from the opposite channel wall. b) For the separation system, a second pair of tips is used consisting of one narrow double tip and a flat tip on the other side of the channel.*

(avoiding overheating) is estimated to be about 7 A/mm^2. Knowing the coil dimensions, the maximum magnetic potential produced by the coil is calculated as 700 A, using equation 4.1.

In order to have a good control over the magnetic field, the maximum current of 0.5 A could be applied to the wire. The number of windings was calculated to be 1400 and corresponded o the wire diameter of 0.3 mm. To avoid damaging the system caused by heating the limit of the current in the system was set to 0.3 A which heated the system till 40 °C. For focusing and separation application more than 0.2 A was not needed.

4.3.2 Magnetic tips

The magnetic tips are focusing the magnetic flux, which is generated by the coil and guided through the magnetic core. Different forms of magnetic tips had been used to create the magnetic field and the gradients in the microchannel for the two different applications, i.e. separation or focusing of beads. The material used for the tips need to have low coercivity to lose its magnetization while the external is switched off. The magnetic microtips are cut by laser out of a 100 μm thick magnetic foil (Vacoflux® 50, Vacuumschmelze, Germany). The width of the narrow tip end is 50 μm.

Fig. 4.8 shows schematically the two different configurations for the focusing and the separation chip respectively. In the focusing chip (Fig. 4.8 a), one single soft-magnetic

tip is placed in close proximity (40 μm distance) of the microchannel wall to focus there the external magnetic field generated by the coil. The other tip is positioned 500 μm away from the other channel side wall for closing flux loop. This arrangement leads to a strong magnetic gradient and force on only one side of the microchannel. In the separation chip (Fig. 4.8 b), the first pair of magnetic poles serves for the formation of a static bead plug and for subsequent controlled release of the particles. The two opposing tips are positioned asymmetrically with respect to the channel center axis (at a distance of 40 μm and 500 μm from the channel side wall, respectively). In this way, a single dense plug is formed in the channel by attracting beads from a suspension. Subsequent demagnetization of the tips releases the plug in a narrow stream adjacent to the channel side wall. The second pair of magnetic poles is situated in the separation zone. This arrangement consists of a broader part on one side of the channel (700 μm wide, at a distance of 500 μm from the channel wall) and a narrow double tip on the opposite side of the channel (100 μm wide each, spacing 200 μm, distance of 40 μm from the channel wall). The distance between retention and separation zone as chosen to 9 mm to minimize magnetic interference. Details will be discussed further in chapter 5 and 6. The complete setup for the separation application is shown in Fig. 4.9.
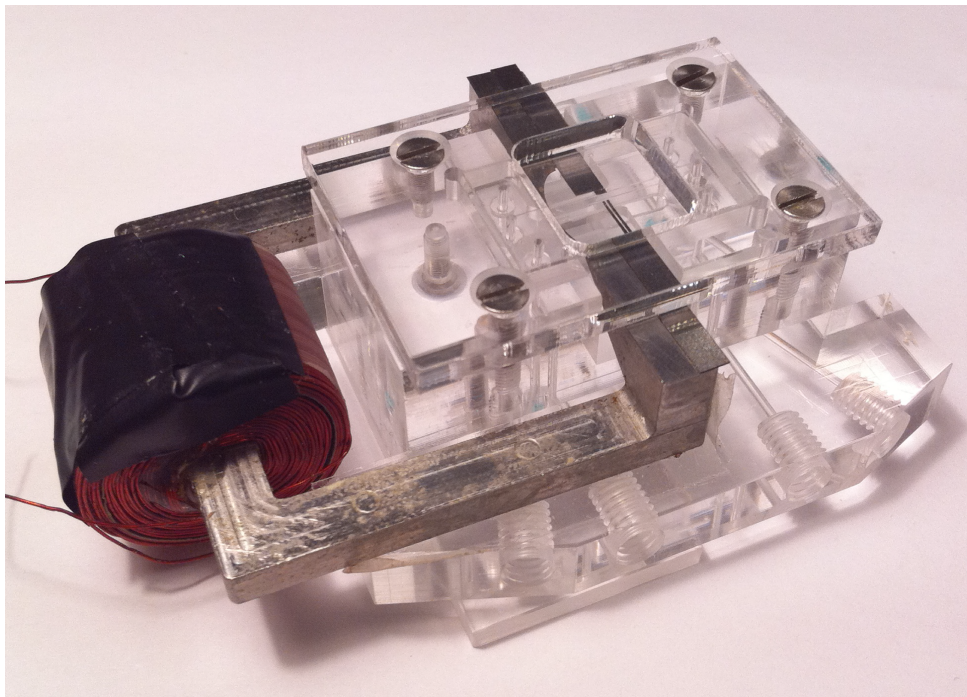
Figure 4.9: *Photograph of the magneto-microfluidic setup showing the inserted holder with the magnetic cicuit and the inserted PMMA platform. The presented magnetic tip configuration corresponds to the separation chip and system*

5

Magnetic particle dosing and size separation

5.1 Introduction

Separation of functional magnetic particles or magnetically labeled objects is a key feature for bioanalytical or biomedical applications and therefore also an important component of lab-on-a-chip devices for biological applications. In this chapter, we present a novel integrated microfluidic magnetic bead manipulation device, comprising the functions of dosing of magnetic particles, controlled release and subsequent magnetophoretic size separation with high resolution. The system is designed to meet the requirements of specific bioassays, in particular of on-chip agglutination assays for the detection of rare analytes by particle coupling as doublets. Integrated soft-magnetic microtips with different shapes provide the magnetic driving force of the bead manipulation protocol. The magnetic tips that serve as field concentrators of an external electromagnetic field, are positioned in close contact to a microfluidic channel in order to

generate high magnetic actuation forces. Mixtures of 1.0 μm and 2.8 μm superparamagnetic beads have been used to characterize the system. Magnetophoretic size separation with high resolution was performed in static conditions and in continuous flow mode. We could demonstrate the separation of 1.0 μm single beads, doublets and clusters in a sample flow.

5.2   Working principle

The experimental protocol comprises three subsequent steps in three corresponding subsections of the microfluidic channel:

1. Capture of a well-defined amount of magnetic beads in a localized area on the channel side wall (dosing).

2. Controlled release of the plug forming a confined stream of individual particles (magnetic focusing).

3. Continuous magnetophoretic separation by deviating the particles as a function of size in an inhomogeneous magnetic field perpendicular to the flow direction.

Fig. 5.1a is a schematic diagram on the microchip with the fluidic channel and integrated soft-magnetic parts. Two distinct configurations of these magnetic poles with different shapes are placed close to the sidewalls of the fluidic channel. They are magnetized via a magnetic yoke by an external electromagnet. The function of these passive magnetic poles is to concentrate the external field and to generate high field gradients across the microchannel, i.e. high magnetic actuation forces. This concept is based on a system developed previously by our group that allowed the formation of a dynamic bead plug in between a single pair of magnetic poles [20, 129].

In the present system, the first pair of magnetic poles serves for the formation of a static bead plug and for subsequent controlled release of the particles. For this reason, sharp magnetic tips are required (50 μm width at the end) in order to focus the magnetic field across the microchannel in a highly confined area. The two opposing tips are positioned asymmetrically with respect to the channel center axis (at a distance of 40 μm and 500 μm from the channel side wall, respectively) resulting in higher field
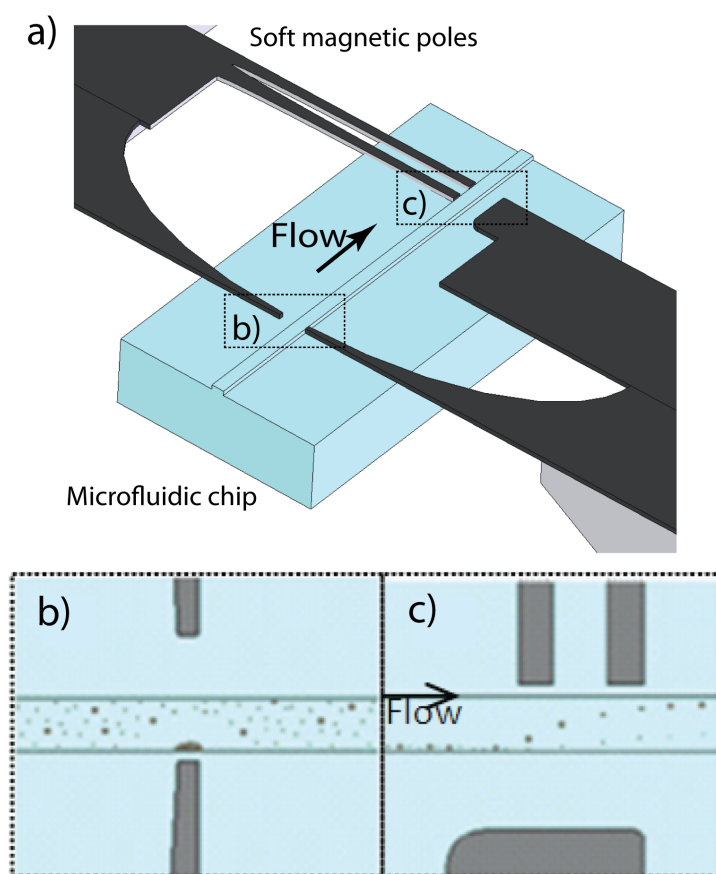
Figure 5.1: *a) View of the separation microchip showing the magnetic pole arrangement and the microfluidic channel. b) Schematic view of the magnetic plug formation/release section for particle dosing and focusing. c) Schematic view of the separation zone with two sharp and one broad tip. Beads in the flow are deviated in the field gradient towards the narrow tips.*

strength and stronger magnetic gradients on one side of the channel. In this way, a single dense plug is formed in the channel by attracting beads from a suspension. This situation is schematically shown in Fig. 5.1b. Magnetization of the tips through an external electromagnet allows controlling the amount of captured beads by simply adjusting the field strength. Subsequent demagnetization of the tips releases the plug in a narrow stream adjacent to the channel side wall. This is a prerequisite for efficient bead separation further downstream.

The second pair of magnetic poles is situated in the separation zone. This arrangement, as is schematically shown in Fig. 5.1c, consists of a broader part on one side of the channel (700 μm wide, at a distance of 500 μm from the channel wall) and a narrow double tip on the opposite side of the channel (100 μm wide each, spacing 200 μm,
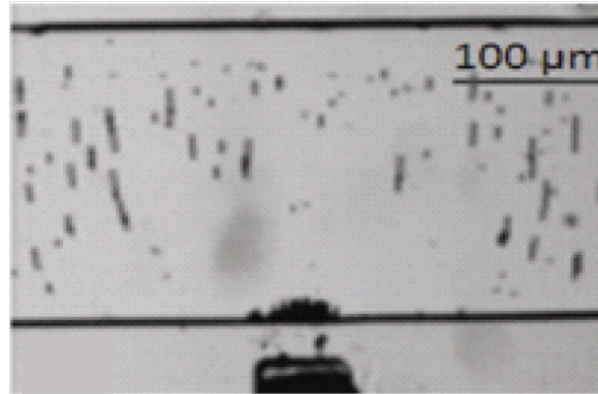
Figure 5.2: *Photograph of the plug formation in the microchannel. After having filled the microchannel with a homogeneous bead suspension, superparamagnetic beads were attracted towards the tip under the effect of the applied magnetic field forming a depleted zone within the microchannel.*

distance of 40 μmm from the channel wall). The combination of a broad and sharp tips generates magnetic gradients that are favorable for separation. Duplication of the sharp tip extends the effective separation zone to a total width of about 500 μm. The tip configuration and shape have been optimized using two-dimensional finite element simulations (FEM, see further). The distance between retention and separation zone was chosen to 9 mm to minimize magnetic interference.

5.3 Experimental procedure

In our experiments, we use two different types of superparamagnetic magnetic beads (Dynabeads®) with a mean diameter of 1.05 μm (MyOne™) and 2.83 μm (M-270), respectively. Bead suspensions as delivered are diluted and suspended in 15 mM phosphate buffer saline (PBS) suspensions with 0.5% surfactant (Tween 20) to reduce non-specific agglutination. A concentration of 5×10^8 beads/mL is used throughout the presented experiments. According to the definition in Eq. (2.12), we calculate a magnetophoretic mobility ξ_m of 7.6×10^{-2} mm^3(TAs)$^{-1}$ for the MyOne beads and 3.6×10^{-1} mm^3(TAs)$^{-1}$ for the 2.8 μm M-270 beads (using the magnetic susceptibilities $\Delta\chi = 1.38$ for MyOne beads and $\Delta\chi = 0.84$ for M-270 beads).

Flow control in the microchannel is achieved by means of a high precision syringe pump (neMESYS, Cetoni) in suction mode connected to the channel outlet. Observation is done under an inverted optical microscope (Zeiss Axiovert S100). Operation in
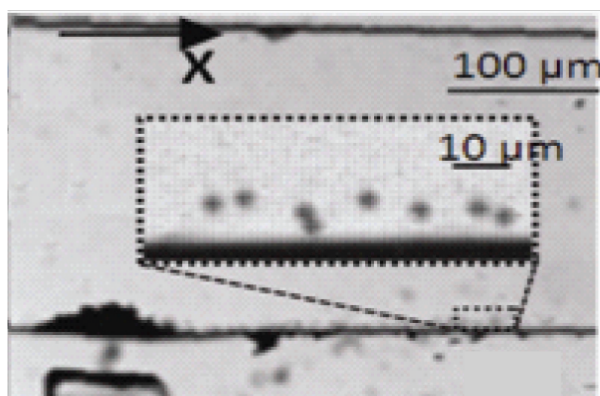
Figure 5.3: *Beads are progressively released from the plug into the flow by controlled attenuation of the sinusoidal coil current. The inset shows an enlarged view of the highly focused bead stream along the channel side wall. The bead size is 2.8 μm.*

suction mode allows introducing the particle suspension by simple pipetting into the inlet reservoir of the microfluidic chip holder.

Capture and dosing of the particles is initiated once the corresponding section in the microchannel is homogeneously filled (i.e. the area between the first pair of magnetic poles). At that point, the flow is stopped and a current is applied in the coil to generate the local magnetic field gradient between the tips required for plug formation.

The field strength may be adjusted through the current in the external coil. An AC current and field is used throughout the experiments (50 Hz or 100 Hz). This has no impact on the magnetophoretic properties of the superparamagnetic beads, as their magnetic moment instantaneously aligns with the external field. Applying an AC field, however, allows efficient demagnetization of the tips by gradual damping of the signal for subsequent release of the beads in the flow (see Fig. 5.3).

Once the particle batch enters the separation zone (i.e. the second pair of magnetic poles) the magnetic field is applied again. Particles entering the zone are deviated perpendicular to the flow direction. A fast monochrome digital camera (PixeLINK PL-B741 with StreamPix video recording software) and an image processing program (ImageJ), are used for analyzing the bead trajectories in the microchannel. In order to characterize the present device, separation of mixtures of single particles with different size and clusters was investigated either in a static mode (i.e. flow in the channel stopped prior to separation) or in continuous flow mode.

5.4 Particle dosing and release

Bead capture from the suspension and formation of the plug was characterized according to the experimental procedure described above. Fig. 5.2 shows a photograph of a plug formed by 2.8 μm beads on the side wall of the microchannel close to the magnetic tip. The magnetic field had been applied once the channel was filled homogenously with the colloidal suspension. The depleted area from which they have been attracted towards the tip is clearly visible. Magnetic bead chains are formed under the influence of the magnetic field. After plug formation, the microchannel may be flushed with buffer solution to remove the remaining suspended beads.

For a given bead concentration of 5×10^8 beads/mL in the channel and by measuring the depleted volume close to the tip, we can estimate the number of captured beads in the plug. The coil current has been varied from 0 mA to 120 mA. Based on FEM simulations, we estimate the maximum field strength near the tip to about 80 mT (for 120 mA).

As is reported in Fig. 5.4, the amount of captured particles is proportional to the applied field (i.e. the coil current). The experiments have been carried out separately for 1.0 μm and 2.8 μm beads. For the same field parameters, the number of beads forming a plug strongly depends on their size, as is expected from Eq. (2.9). Larger beads are attracted to the tip from a longer distance compared to smaller ones, i.e. the depleted area is larger. The number of captured beads in a plug is increasing linearly with the coil current amplitude, i.e. the magnetic field strength near the tip in the channel. 2.8 μm beads (solid line) are more strongly attracted from the suspension than 1.0 μm beads (dashed line) and form larger plugs. Both experiments have been carried out at two different frequencies.

From the graph in Fig. 5.4, we find, for instance, that a plug formed with a coil current of 80 mA using 1.0 μm beads contains about 400 beads, whereas a plug with 2.8 μm beads contains about 1000 beads. A more thorough quantitative analysis, however, is not appropriate because several parameters, like friction forces with the channel wall, are subject to high uncertainty. It is interesting to mention that a plug formed with a mixture of beads tends to contain a higher amount of larger beads.

Experiments have been carried out at two different frequencies (50 Hz and 100 Hz) of the applied magnetic field. Due to the superparamagnetic character of the beads, this has no impact on the plug formation (see Fig. 5.4).
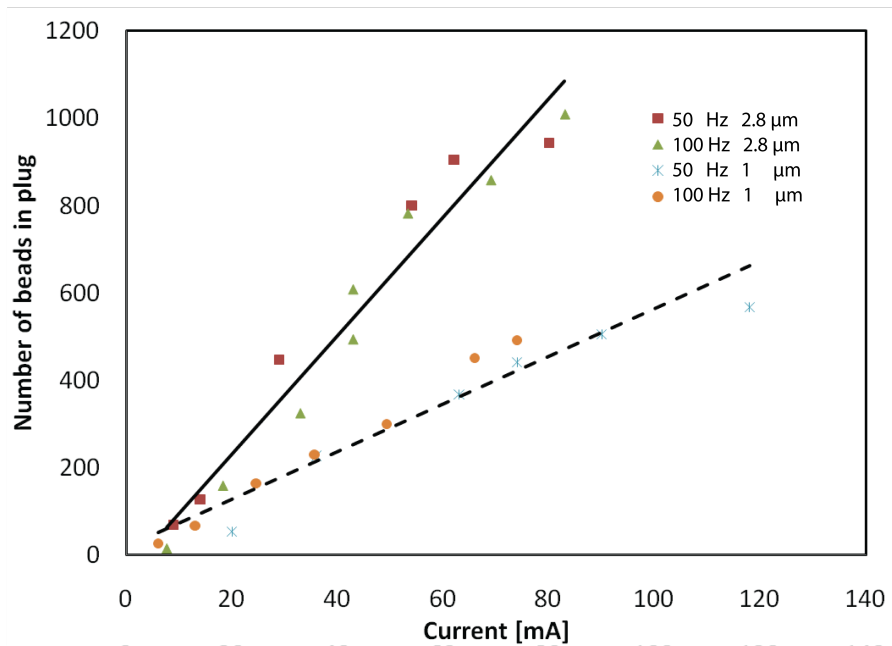
Figure 5.4: *Dosing of magnetic particles. The number of captured beads in a plug is increasing linearly with the coil current amplitude, i.e. the magnetic field strength near the tip in the channel. 2.8 μm beads (solid line) are more attracted from the suspension than 1.0 μm beads (dashed line) and form larger plugs. Both experiments have been carried out at two different frequencies.*

Fig. 5.3 demonstrates controlled and progressive release of 2.8 μm beads from the plug. Bead release is obtained by demagnetization of the magnetic poles and circuit through attenuation of the sinusoidal coil current. Released particles are confined in a narrow stream adjacent to the channel wall within a width of less than 20 μm (see inset of Fig. 5.3).

The rate of release can be controlled by adjusting the damping constant of the coil current or the laminar flow rate in the channel. With a flow speed of 0.3 $\mathrm{mm/s}$, the linear bead density along the channel is typically in the range of 250 $\mathrm{beads/mm}$. A low linear particle density is advantageous for preventing clustering or chain formation prior to separation. The velociy of the beads near the side of the channel is about 0.03 $\mathrm{mm/s}$.

5.5   Separation of magnetic particles in a stationary fluid

Size separation of the magnetic beads in the microchannel was first analyzed in static conditions, i.e. without applying a flow. After release of the plug, the particle stream enters the separation zone on the chip. When the flow is stopped, all particles are aligned on one channel wall. A mixture of 1.0 μm and 2.8 μm beads was used for these experiments. At this point, the magnetic separation field is applied through the dedicated magnetic poles (see Fig. 5.1c), resulting in a force that attracts the beads to the opposite side of the channel.

Fig. 5.5a shows a two-dimensional FEM simulation (COMSOL MultiphysicsR 3.5, COMSOL Inc.) of the magnetic field (external coil current of 80 mA) and the resulting force field $\mathbf{F}_{mag}$ (based on Eq. (2.7)) exerted on the beads in the microchannel portion in between the two sharp tips. The broad magnetic pole is situated on the channel side situated towards the lower part of the pictures in Fig. 5.5, and the two sharp tips are on the upper side. The simulation shows that the field lines are nearly perpendicular to the flow direction in this part of the separation zone. A magnetic particle experiences only a very weak gradient in the lateral direction (x-direction) ($\nabla B_x \approx 5$ mT/mm). However, the density of the field lines increases in the direction perpendicular to the channel (y-direction). From the simulations, we estimate a gradient $\nabla B_y \approx 90$ mT/mm) near the start position of the beads (lower side wall of the channel in Fig. 5.5).

The resulting magnetic force field attracts the beads towards the sharp tips. Experimentally recorded trajectories of 1.0 μm and 2.8 μm beads are shown in Fig. 5.5b. The photo is a superposition of six images of a time-lapsed sequence taken with an interval of 2 ms after application of the magnetic field. Bead motion starts from the lower channel side wall. As expected, the beads move towards the region of higher field gradients, i.e. towards the narrow tips. Larger beads are clearly moving faster than smaller ones, thus size separation can be achieved with this system. The trajectories are nearly perpendicular to the channel axis (except in the region close to the starting position) and correspond well to the simulated force field (Fig. 5.5a).

A quantitative analysis of the bead displacement versus time with respect to the channel side wall is shown in Fig. 5.6. Within the time lapse recorded in Fig. 5.5b (i.e. 10 ms), small beads cover a distance of about 15 μm, whereas the larger ones move up to 90 μm. Mean displacement distances are well reproducible for both types of beads.
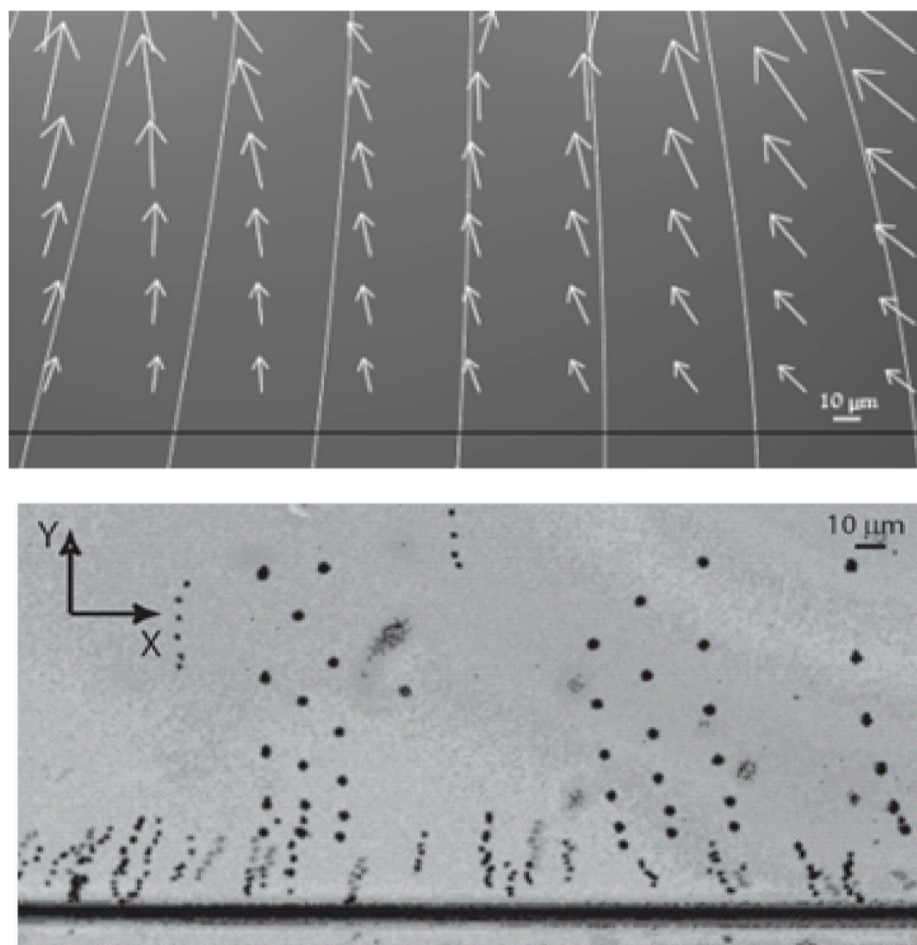
Figure 5.5: *a) 2D FEM simulation of the magnetic field lines and the magnetic force field exerted on a bead in the separation region (corresponding to the channel portion in between the two sharp tips of Fig. 1c). b) Static separation without sample flow. Experimental observation of the separation of 1.0 μm and 2.8 μm beads. The figure shows a superposition of a time sequence of photographs (t=Δ2 ms) taken in the separation section of the chip. Beads have been aligned on the lower channel side wall before applying the separation field. Larger beads clearly cover a larger distance, thus size separation occurs (the window does not show the full channel width).*

The velocity $\mathbf{v}_m$ of 1.0 μm beads within the small distance, from the channel wall can be considered as constant within the error of measurement (approximately 1.2 mm/s). The increase of the velocity $\mathbf{v}_m$ of the 2.8 μm beads was measured in a wider region (up to 60 μm from the wall) for a representative number of beads. According to Eq. (2.12), measuring $\mathbf{v}_m$ as a function of the y-position in the channel gives an indication on the magnetic field properties and the resulting magnetic force in the region of interest. These
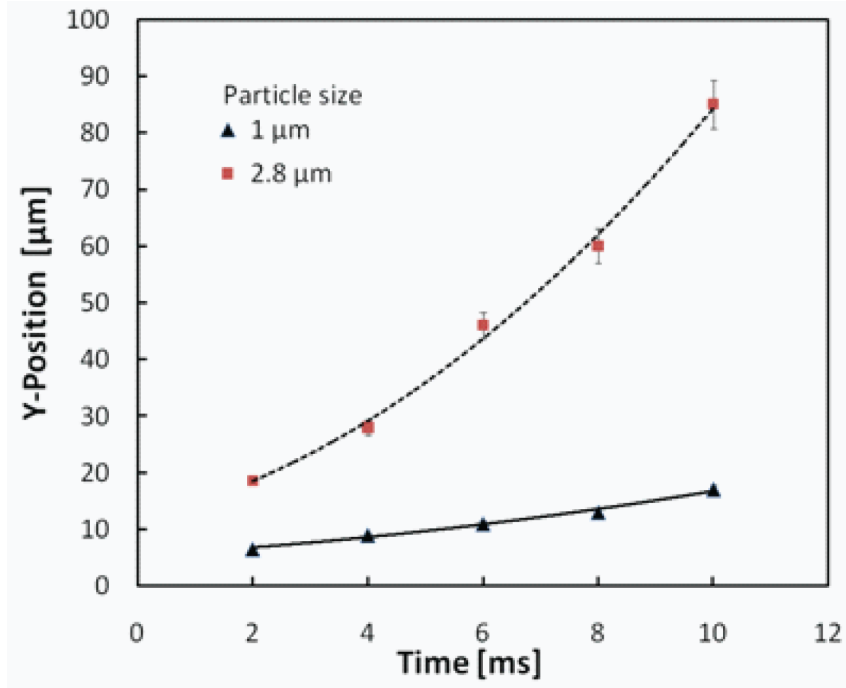
Figure 5.6: *Size separation of 2.8 μm and 1.0 μm beads. The graphs show the representative values for measured bead positions versus time in the channel during separation (y is the distance from the channel wall, as derived from Fig. 5.5).*

results are plotted in Fig. 5.7, where $\delta\mathbf{B}^2/\delta y$ has been calculated from the measured $\mathbf{v}_m$ values using Eq. (2.12) (with ξ_m =3.6×10^{-1} mm^3(TAs)$^{-1}$)).

We observe an approximately linear increase of $(\delta\mathbf{B}^2/\delta y)\mathbf{e}_y \approx \nabla\mathbf{B}^2$, i.e. the magnetic force, as the beads cross the channel (dashed line in Fig. 5.7). From this graph and Eq. (2.9), we estimate the range of the magnetic force $\mathbf{F}_{mag}$ on the 2.8 μm particles from 75 pN to 225 pN (for y = 20-60 μm).

The corresponding velocity $\mathbf{v}_m$ values are 2.8 mm/s (at y=20 μm) and 8.5 mm/s (at y=60 μm). Using this "calibration curve" for the magnetic force field in the present system, the magnetophoretic behavior of different types of beads can, in principle, be predicted (provided ξ_m is known). On the other hand, this method could also be used to derive the magnetic properties of unknown particles. An accurate quantitative evaluation of the force by FEM simulations (as shown in Fig. 5.5a) is difficult. As was outlined previously, force or velocity values derived in this way are generally overestimated [20]. Nevertheless, the simulated force field in Fig.5.5 a provides a good indication of the relative variation across the channel.

5.6   Separation of magnetic particles under fluidic conditions

In order to characterize the separation of a released plug during flow, a flow of 6 nL/s (22 μL/h) was applied in the microchannel, thus the magnetic particles were travelling with a lateral speed (x-direction) of 0.3 mm/s through the separation section. The typical throughput can be estimated to 50-100 beads/s (depending on the release parameters). A magnetic field was applied simultaneously to the magnetic poles resulting in a magnetophoretic deviation towards the sharp tips perpendicular to the flow direction (coil current of 80 mA).

Due to the controlled release from the plug, magnetic particles were confined in a narrow stream with a width of less than 20 μm adjacent to the lower side wall before separation. To provide a more versatile characterization of the size separation, we prepared a test suspension comprising a mixture of 1.0 μm and 2.8 μm beads but also a certain amount of aspecifically agglutinated particles, i.e. doublets or larger clusters. Clustering was obtained by non-specific agglutination of beads stored under non-optimum conditions.

Fig. 5.8 shows a superposition of several individual photographs that reveals the trajectories of single magnetic particles and clusters as a function of their size. As predicted by Eq. (2.12), the magnetophoretic drift velocity perpendicular to the channel increases with the particle size. Clusters are therefore deviated stronger than individual particles. Interestingly, doublets of 1.0 μm beads can be observed in Fig. 5.8. These doublets are deviated more than single 1.0 μm beads, but less than 2.8 μm beads.

In order to get a more quantitative idea of the efficiency of the separation system in dynamic mode, virtual exits have been arbitrarily defined in the channel at the end of the separation zone. These zones correspond to 20 μm subsections of the channel cross-section, as indicated in Fig. 5.9.

The presence of particles with different size in the virtual exits was counted to evaluate the statistical distribution. Fig. 5.9 shows a statistical analysis for 1.0 μm single beads, doublets of 1.0 μm beads and 2.8 μm beads that are predominantly deviated to exit 1, 2 or 3, respectively. This result shows that about 70 - 80% of a certain particle or cluster type can be found at the location of a corresponding 20 μm wide virtual outlet
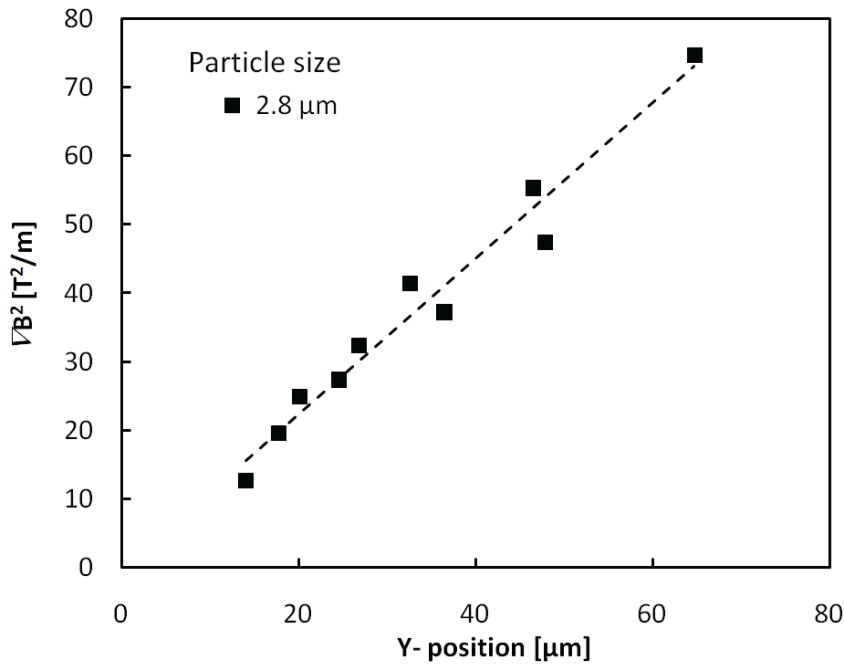
Figure 5.7: ∇B^2 *in the separation region versus y-position in the channel.* ∇B^2 *has been derived for 2.8* μm *beads from the magnetophoretic particle velocity perpendicular to the channel. This "calibration curve" of the magnetic system indicates a linear increase of the magnetic force. Values observed for 1.0* μm *beads confirm this tendency.*

channel. This size distribution is relatively narrow, indicating that reliable separation of particles in this size range is feasible. Larger clusters move to higher positioned vitual exits. We noted that some of the biggest clusters are strongly attracted to the opposite channel side wall and will not be able to leave the separation zone.

5.7 Discussion

The present system comprises three distinct steps of magnetic bead manipulation on-chip, i.e. bead retention with plug formation of defined size (dosing), spatially confined release with controlled density (magnetic focusing) and continuous in-flow size separation with high resolution. In principle, all three parts could be operated separately, however, combining the different functionalities on a single microfluidic chip improves the performance of the separation system, thus allowing to meet the requirements of specific bioassays. The use of an external electromagnet instead of a permanent magnet to magnetize the soft-magnetic parts offers additional flexibility.
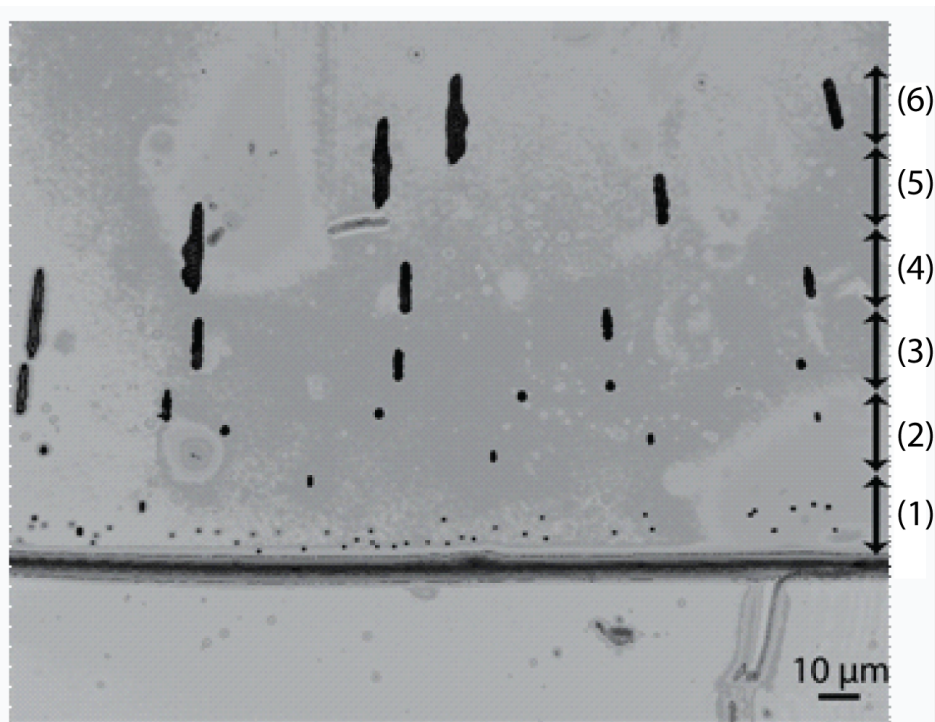
Figure 5.8: *Dynamic size separation during application of a sample flow. The figure is a superposition of photos taken in a portion of the separation section in the channel. The trajectories of 1.0 μm single beads, 1.0 μm bead doublets, 2.8 μm beads and larger clusters can be observed (from the bottom to the top). All particles have been aligned close to the lower side wall before entering the separation zone. On the right, virtual exits have been marked for statistical analysis (see Fig. 5.9).*

In our device, we optimized the resolution in terms of size separation by two means. First, the system allows for precise control of the force on the magnetic carriers, due to the positioning of the magnetic microtips in immediate proximity of the microfluidic channel with a spatial precision of about ± 5 μm. Second, magnetic focusing of the particle mixture on a channel side wall within a stream width of less than 20 μm provides an optimum precondition for subsequent separation based on the deviation from the initial trajectory. Dispersion of the bead mixture over a wider cross section at the inlet would necessarily result in a larger distribution at the outlet of the active zone of a separation system [76, 77]. Magnetic focusing of magnetic particles or magnetically labeled cells may be an interesting alternative to three-dimensional hydrodynamic focusing in microdevices, that require more complex fluidic arrangements [92].

In particular, the system could be used for high-resolution size separation of small magnetic particles, i.e. with a typical size down to 1 μm or even below. We could demonstrate, for instance, a clear separation of 1 μm single particles and 1 μm bead
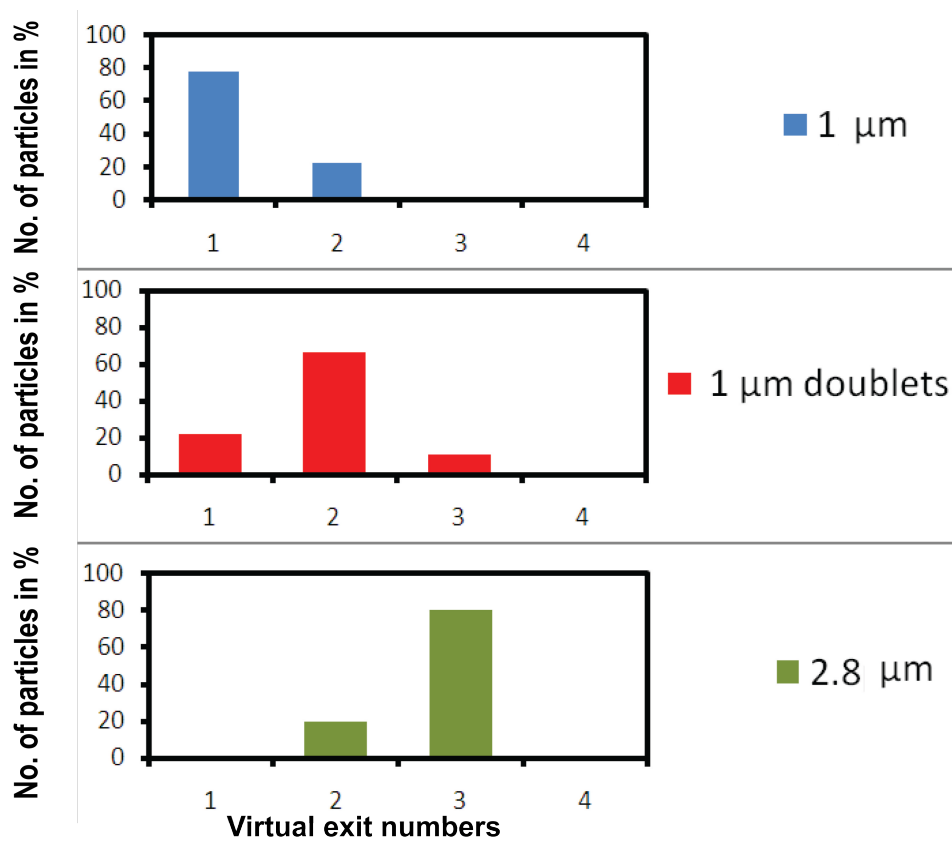
Figure 5.9: *Statistical distribution of the deflection of 1.0 μm beads, 1.0 μm bead doublets and 2.8 μm beads in the separation zone after dynamic size dependent separation. The corresponding virtual exits are defined in Fig. 5.8*

doublets (Figs. 5.8 and 5.9). Differentiation of this type of particles is of interest for the development of a high-sensitivity magnetic agglutination bioassay on-chip [10, 128] . In this assay type, agglutination between functionalized beads occurs in the presence of a specific target protein. Incubation of a representative and limited amount of beads for agglutination can be performed in the first part of the system, i.e. during plug formation [20]. A washing step can also be introduced at this stage of the protocol. At low analyte concentrations, only doublets will form and their number is a direct measure for the analyte concentration. Subsequent separation of singlets and doublets prior to detection, i.e. counting of doublets, significantly simplifies data recording and thus may improve the performance of such a system (for instance, by reducing the assay time).

6

3-dimensional focusing and in-flow size separation of magnetic beads

6.1   Introduction

Magnetic micro- and nanoparticles (beads) are versatile mobile carriers in microfluidic lab-on-a-chip systems, in particular for bio-analytical and diagnostic applications. It is particularly attractive to implement an individual bead analysis approach on-chip, like used in a cytometer, for the accurate discrimination, counting or quantitative immunofluorescent detection, instead of analyzing the average signal from larger particle or cell populations. Such approach, however, requires three-dimensional (3D)

focusing of the particle suspension into a single focused stream for reliable detection. Particles should indeed pass one-by-one, in-line and with a constant speed through the illumination spot of a laser or sensitive zone of an optical or impedimetric detector that is directly interfacing with the microchannel. The requirement of a very narrow focused particle stream is particularly important for detecting small cells or micrometer-size beads.

In this chapter magneto-microfluidic three-dimensional focusing is presented. In this system magnetic microparticles from a dense plug are released into a single streamline with longitudinal inter-particle spacing. Plug formation is induced by a high-gradient magnetic field generated at the sidewall of a microchannel by a micromachined magnetic tip that is connected to an electromagnet. Controlled release of the microparticles is achieved using an exponential damping protocol of the magnetic retention force in the presence of an applied flow. Carefully balancing the relative strengths of the drag force imposed by the flow and the magnetic retention force moreover allows in-flow size separation of the microparticles. Adding subsequently a lateral sheath flow focuses the microparticles into a single stream situated within $\pm\ 5\ \mu$m from the channel center axis. Separation of the magnetic beads with respect to size was observed in-line with the particle stream during release and 3D focusing. Size separation is achieved by careful adjustment of the protocol for the release of the bead plug, without the need of additional magnetic or fluidic structures. The separation is happening by balancing the relative strength of magnetic and viscous drag forces.

6.2   Microfluidic set-up

The same magneto-microfluidic set-up as before has been used for this application, however, the magnetic microtips and the microfluidic chip have modified. Fig. 6.1a, shows a zoom on the microfluidic chip. The chip has a principal straight microfluidic channel (10 mm long, 200 μm wide, 100 μm high), and a secondary microchannel (200 μm wide, 100 μm high). The fluidic junction is located 0.5 mm downstream the magnetic tip location. Fig. 6.1b is an enlarged schematic view of the region of interest, illustrating the release of a magnetically retained bead plug into a 3D-focused stream. Only a single precision syringe pump is connected simultaneously to both fluidic inlets of the chip for fluidic control. As both channel portions before the fluidic junction have

equal hydraulic resistance, the flow rates in both sections are equal. Consequently, the secondary flow focuses the released magnetic bead stream exactly towards the middle of the main channel.
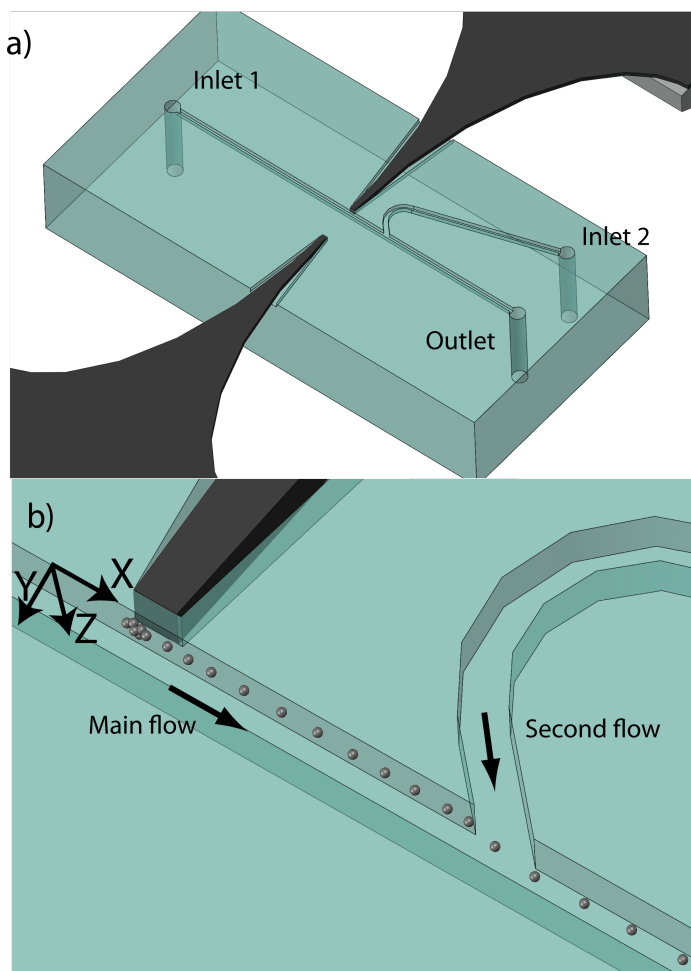
Figure 6.1: *a) Zoom on the microchip comprising a first microfluidic channel (inlet 1), a secondary channel (inlet 2), the main channel (outlet) and the asymmetric arrangement of two magnetic poles. b) Enlarged view of the zone of interest on the chip, showing schematically the release of a magnetic bead plug and the deviation of a 3D focused stream of individual beads towards the middle of the main channel.*

The microfluidic chips are cast in a single piece of poly-dimethylsiloxane (PDMS) at standard 10:1 PDMS base-to-catalyst ratio (Sylgard 184, Dow Corning Inc. Midland, MI) using a standard SU-8/Si mold. Sealing of the channels is achieved by mechanically clamping the PDMS part onto a glass slide by means of a PMMA chip holder with suitable fluidic connections.

6.3   Magnetic set-up and field simulation

We use magnetophoretic force to attract the magnetic beads towards the tip. The magnetic force F_m on the beads in an induction field B was calculated in Eq 2.9. F_m is proportional to the magnetically active volume of the bead V_m.

In the present device, only a single soft-magnetic tip is placed in close proximity (40 μm distance) of the microchannel wall to focus there the external magnetic field generated by the coil (Fig. 6.1b). The other tip is positioned 500 μm away from the other channel side wall for flux closure. This arrangement leads to a strong magnetic gradient and force on only one side of the microchannel. The magnetic microtips are cut by laser out of a 100 μm thick magnetic foil (Vacoflux$^{\circledR}$ 50, Vacuumschmelze, Germany). The width of the narrow tip end is 50 μm. The PDMS part of the chip comprises recesses to receive the pair of magnetic poles in a reliable manner.

Fig. 6.2a shows a two-dimensional (2D) Finite Element Method (FEM) simulation of the magnetic field lines in the channel plane (x-y plane) and the magnetic force field close to the tip that is adjacent to the microchannel(COMSOL MULTIPHYSICS 3.4). The resulting force field is asymmetric with respect to the channel middle axis. Beads will therefore be attracted towards this tip and form a plug on the channel sidewall. Due to the rectangular cross section of the tip end, the force field distribution has a similar symmetry in the channel cross section (y-z plane) as in the channel plane (x-y plane). Fig. 6.2b shows the result of a 3D FEM simulation of the magnetic flux density in the x-z plane. The strong flux gradient in the channel is illustrated by three plots taken at different distances in the y direction from the tip adjacent to the channel. The flux density obviously is highest at the channel wall near the tip (i.e. at a distance of 40 μm from the tip) and becomes very low close to the opposite sidewall of the channel (i.e. at a distance of 120 μm from the tip).

When connected to a bipolar operational power supply (KEPCO, BOP 50-2M) which is addressed by a function generator (Tektronix, AFG3021B) , the external coil is fed by a 50 Hz damped sinusoidal current in order to facilitate controlled demagnetization of the magnetic tip for release of the beads. Due to the low coercivity of the used superparamagnetic beads (see further), their kinetic behavior depends only on the absolute effective value of the field intensity. This means that a static plug forms on the channel wall, even if a dynamic AC field is applied [20].
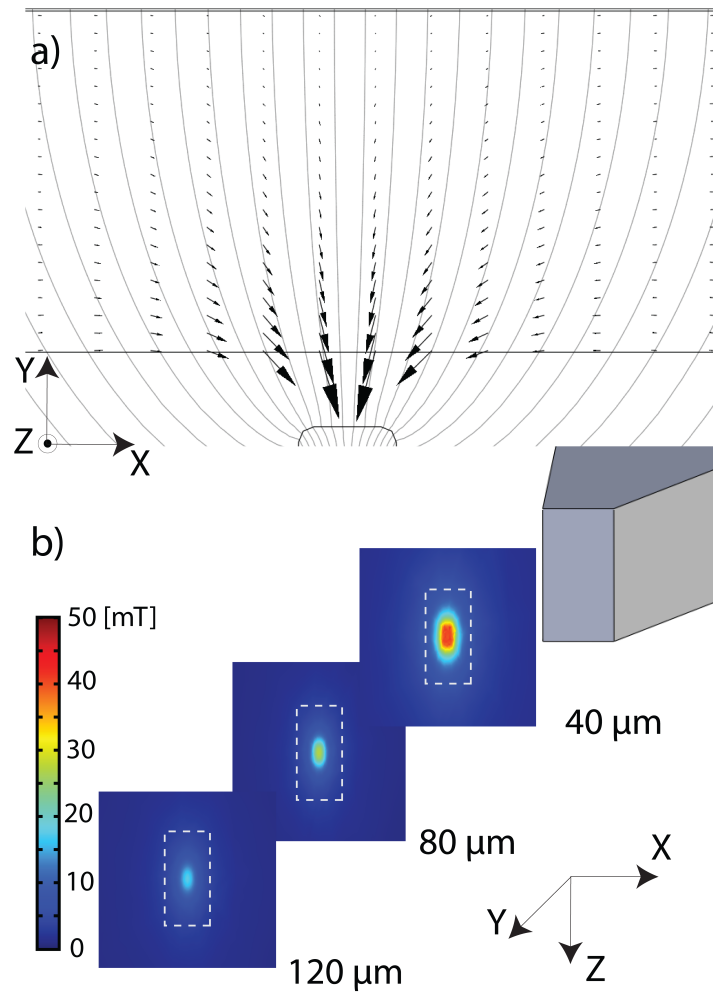
Figure 6.2: *a) 2D FEM simulation of the magnetic field lines in the channel close to the adjacent tip. The resulting magnetic force field exerted on a magnetic particle is represented by arrows of different size. Significant field concentration, thus attractive force, is observed only on one channel side wall due to the asymmetric positioning of the two tips. b) 3D FEM simulation of the magnetic field flux density in the channel. Images represent calculations of the magnetic flux density in the x-z plane at different distances y from the adjacent tip (positioned at y=0 μm). The first image (at y=40 μm) corresponds to the field distribution at the channel sidewall. The two other images correspond to the middle and the opposite side of the channel.*

6.4 Protocols for bead capture and release

Two types of superparamagnetic beads with $\Delta\chi$=1.38 and 0.84 with a diameter of 1.05 μm (Dynabeads $^{\circledR}$ MyOne$^{\text{TM}}$) and 2.83 μm(Dynabeads$^{\circledR}$ M-270), respectively, are used in the experiments. Bead solutions are diluted and suspended in 15 mM phosphate

buffer saline (PBS) solution with 0.5% surfactant (Tween 20) to improve the colloidal stability.

The experimental procedure starts by sucking 2 μL of bead solution with a concentration of 5×10^8 beads/mL from the outlet into the main channel at a flow rate of 20 nL/s. The flow is stopped and the tip is magnetized, once the particle suspension fills uniformly the channel portion close to the tip. The amount of captured particles forming the plug is proportional to the coil current and can be estimated from the depleted area in the channel close to the tip [130]. The surplus of beads is flushed away by pumping buffer solution to the outlet (flow rate of 50 nL/s). Subsequently, a constant and equal flow rate of typically 6 nL/s is applied through inlet 1 and 2 of the microchip. For the 3D focusing experiments that do not involve separation, the 50 Hz sinusoidal coil current is exponentially attenuated to zero (with a damping constant 0.018 ms^{-1}) and controlled release of the bead plug is achieved by applying subsequently the flow. For the in-flow separation experiments of beads with different sizes, the 50 Hz sinusoidal coil current is exponentially attenuated to 40 mA, after which the flow is applied while the current is further decreasing to zero.

Observation of the particle trajectories is done using an inverted optical microscope (Zeiss Axiovert S100) equipped with a fast monochrome digital camera (PixeLINK PL-B741) and using video recording software (StreamPix$^{\text{TM}}$) and image processing for particle counting (ImageJ, open source). Reconstructed fluorescent images in the vertical (x-z) plane are obtained by recording the autofluorescent images of 2.8 μm beads with a Leica SP5 inverted confocal scanning microscope (due to their lower autofluorescence, the 1 μm beads could not be clearly visualized). The confocal microscope is equipped with a 488 nm Argon laser for fluorescent excitation. Autofluorescent images are first collected every 20 ms in the x-y plane, spanning a range of 100 μm in the z-direction at 3 μm per z-sectioning step. All images are analysed using LAS AF 9000 software to provide the reconstructed image in the x-z plane.

6.5 3D focusing of beads

6.5.1 Vertical positioning of the plug

Bead capture and plug formation near the magnetic tip on the channel wall, as well as subsequent release is demonstrated in the images shown in Fig. 6.3a and Fig. 6.3b. In the

present case, parameters have been chosen to form a plug that contains 400±20 beads of 1 μm diameter (using a coil actuation current of 80 mA) (Fig. 6.3a). Superparamagnetic beads progressively lose their magnetic moment during exponential attenuation of the magnetic field (Fig. 6.3b). The hydrodynamic shear force progressively overrules the decreasing magnetic retention force and tears off the beads from the plug. The released particles are confined in a narrow stream close to the channel wall.
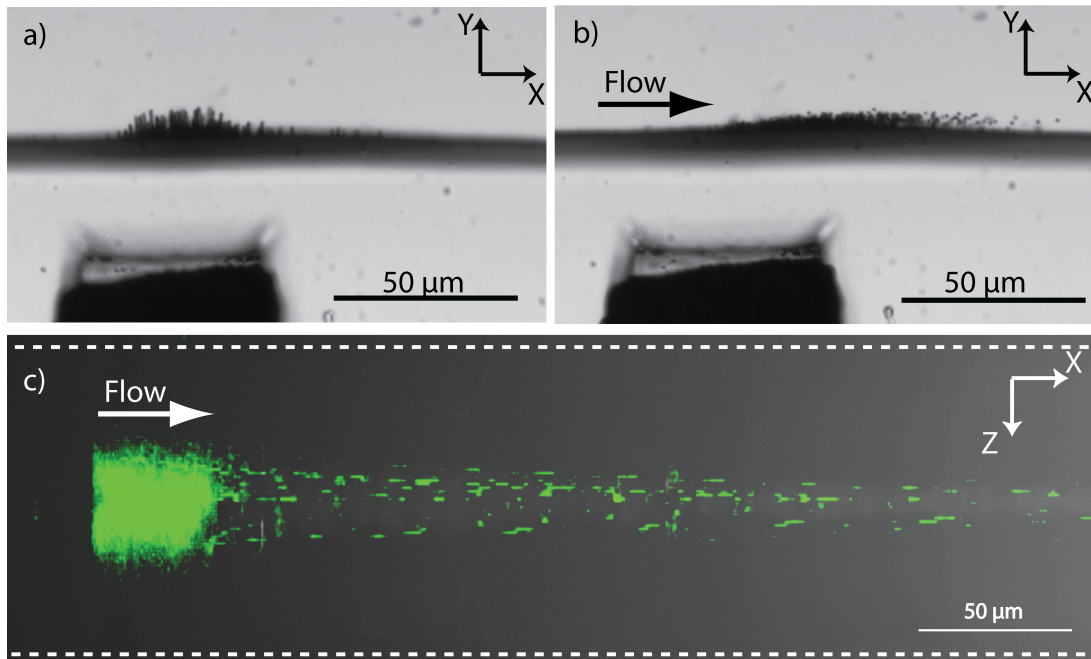
Figure 6.3: *a) Top view photograph of a magnetic plug immobilized on the sidewall of microchannel under the effect of the applied magnetic field (about 400 beads of diameter 1 μm are retained, t=0 s). b) After t≈1 s, beads are progressively released from the plug into the flow by controlled attenuation of the sinusoidal coil current. c) Reconstructed side view fluorescent image of the plug and the released particle stream in the x-z plane, by processing 40 confocal microscope images in the x-y plane. The autofluorescent signal (488 nm excitation from an argon laser) signal of 2.8 μm beads is detected at t≈3 s. The plug is magnetically positioned in the middle of the channel (the tip height is equal to channel height) and subsequent vertical flow-focusing of the stream at half-height of the channel is observed.*

Fig. 6.3c shows a fluorescent image of a plug of 2.8 μm beads with a total extension of less than 50 μm in the z-direction in the tip area and the stream of released particles in the x-z plane near the channel wall using a flow rate of 6 nL/s. This flow is characterized by a low Reynolds number $Re = 0.03$, where $v = 0.3$ mm/sec is the average flow speed, $h = 100\,\mu$m the channel height, and $\nu = 10^{-6}\,\mathrm{m^2/s}$ the kinematic viscosity of the fluid.

Fig. 6.3c has been obtained by reconstruction from a series of confocal images taken in the x-y plane with a sectioning in the z-direction of 3 μm. The extension of the released particle stream shrinks further down to about 10 μm at a distance of 300 μm from the plug location, probably related to either the laminar flow pattern that forms around the plug or to the interaction of the flow with a slightly expanding plug after removal of the field [129]. With the present chip design, focusing in the z-direction is easily achieved thanks to the magnetic field configuration. Experimental observation reveals that beads are first attracted towards the middle of the microtip area, where magnetophoretic forces are highest. The plug forms around this center position and is confined in a volume that is much smaller than the volume defined by the lateral and vertical dimensions of the tip, depending on the amount of retained beads.

6.5.2   3D focusing after the junction

At the fluidic junction, the released magnetic bead stream is deviated towards the center of the main channel where the flow rate and the maximum flow velocity are twice as high as in the upstream channel sections. Furthermore, beads are pushed from a region with very low flow velocity close to the channel wall towards the center of the parabolic flow profile. Particles in the released stream are therefore strongly accelerated. This simple fluidic arrangement allows stretching and one-by-one alignment of the released beads in the flow direction. Fig. 6.4a shows a simulation of the flow streamlines in the junction area. The simulated path and acceleration of a bead is also indicated.
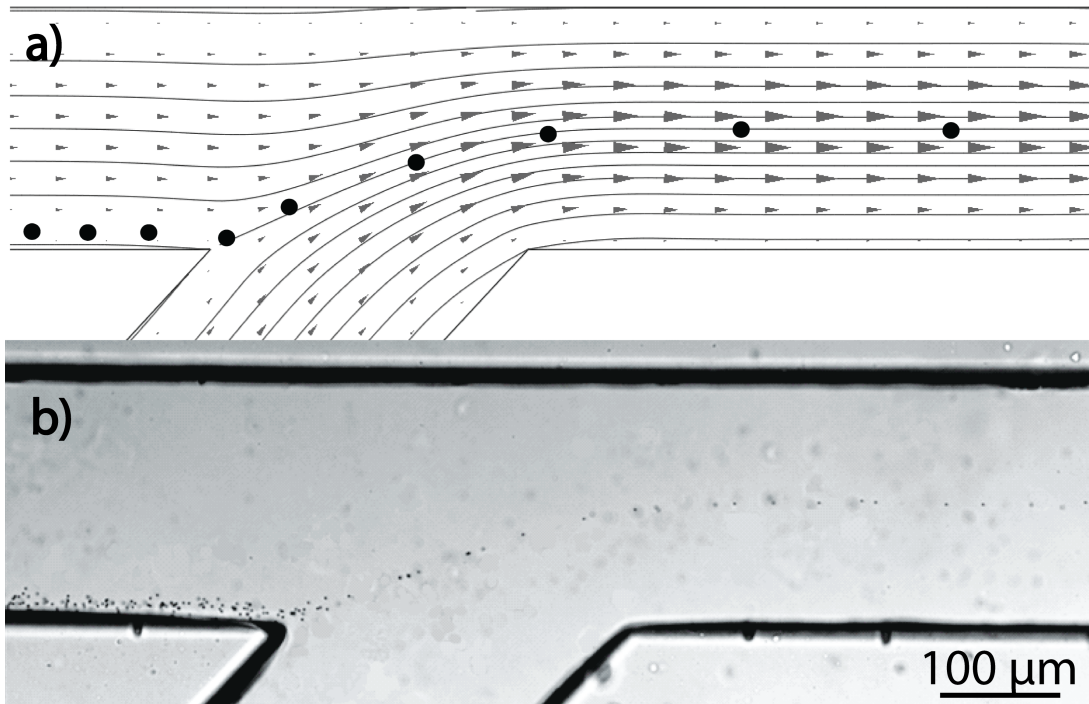
Figure 6.4: *a) 2D FEM simulation of the laminar flow streamlines at the fluidic junction of the main channel and the secondary channel. Arrows represent the velocity field. The black dots represent the simulated path and acceleration of a bead (i.e. increasing bead interspacing) that is placed in the flow. b) Photograph of the focused 1 μm bead stream at the channel junction. The final bead velocity is 0.6 mm/s.*

The corresponding experimental observation using 1 μm beads is shown in the photograph of Fig. 6.4b. For the flow parameters chosen in Fig. 6.4b, the particle speed after the junction is 0.6 mm/s and beads align in the middle of the flow channel with a maximum deviation of ± 5 μm in the lateral direction (y-direction) from the center position. The linear bead density in the released stream is about 20 beads/mm. The rate of release can be trivially tuned by varying the field damping constant and the flow rate. Also the lateral dimension of the focused stream is a function of flow speed. Reducing the maximum speed in the main channel from 0.6 mm/s to 0.3 mm/s, for instance, results in a 30 μm wide and focused particle stream with a dense and random distribution of particles. The reason for this increased width of the stream of released beads is the interaction of the flow with the slightly expanding plug after removal of the field [129].

3D focusing of a released stream of the 2.8 μm beads is demonstrated in Fig. 6.5a. The image shows a cross-section of the beam in the microchannel in the y-z plane taken

50 μm after the fluidic junction. The flow speed in the center of the main channel is 0.6 mm/s. The focused beam diameter is about 10 μm, i.e. 10% of the channel height and 5% of the channel width. Considering the parabolic flow profile, the maximum variation of the bead velocity in the focused stream can be estimated to be about 1%.
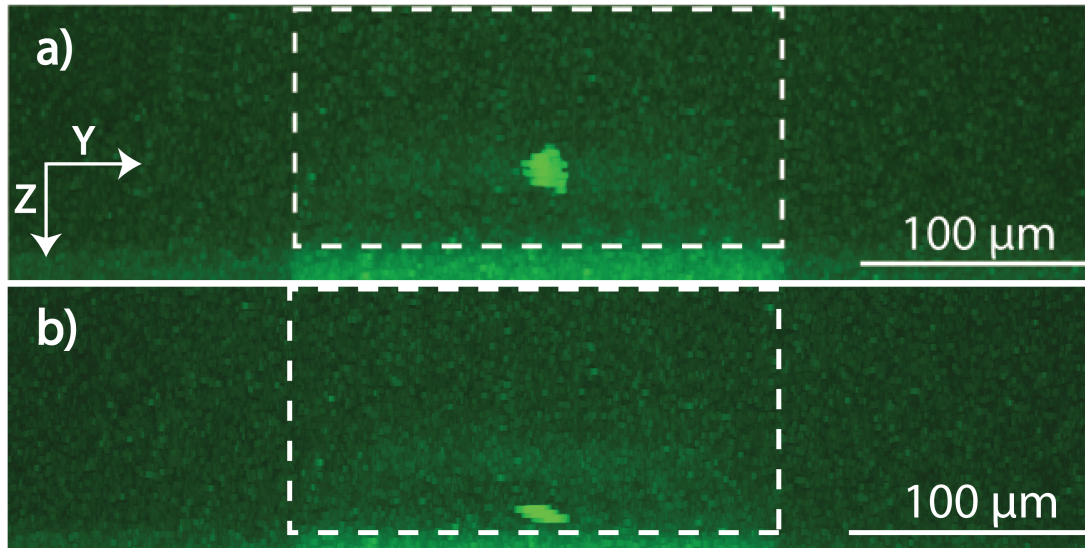
Figure 6.5: *Cross-section of the focused 2.8 μm bead stream in the main channel (dashed rectangle) taken 50 μm after the fluidic junction, reconstructed from a series of fluorescent confocal images taken in the x-y plane (vertical sectioning 3 μm). The bead stream diameter is about 10 μm. a) At a bead velocity of 0.6 mm/s, the stream is nearly in the middle of the channel. b) Reducing the bead velocity to 0.1 mm/s increases the impact of sedimentation and the stream of beads 'sinks' towards the bottom of the channel.*

At the location of the channel considered in Fig. 6.5a, the beads appear not to be exactly focused at half height, but the center of the beam is deviated by 10 μm from the middle of the channel towards the bottom. Fig. 6.5b shows an image of the bead stream taken at the same location using a lower flow rate, resulting in a bead velocity of 0.1 mm/s in the main channel. In Fig. 6.5b, the center beam is deviated by 45 μm and nearly reaches the bottom of the channel. The total travel time of the beads after release is about 4 times longer than for the situation of Fig. 6.5a (velocity is not constant in the channel junction), therefore the impact of sedimentation is expected to be significantly stronger. The deviation observed in both cases corresponds well to the speed of sedimentation that was calculated to 4.5 μm/s by equalizing the gravitational force F_g and the viscous force F_d in z-direction. For calculation of the gravitational force, we take the 'buoyant mass', $\mathbf{m}_b$ as defined in Eq. 2.14.

For example, 2.8 μm diameter M-280 Dynabeads $^{\circledR}$ have a volume of 11.48 μm^3, 12% iron content, and a bead density of 1.6 g/cm^3 resulting (using Eq. 2.13) in a gravitational force of 0.067 pN. As $F_g \sim d^3$ and $F_d \sim d$, where d is the particle diameter, sedimentation and beam deviation in the channel will be much less pronounced for 1 μm beads. Similar to the situation shown in Fig. 6.5b for 2.8 μm beads, the deviation of 1 μm beads at a flow speed of 0.1 mm/s can be estimated to be only 4 μm at the same location.

6.6 In-flow size separation

Instead of using suspensions of either 1.0 μm or 2.8 μm beads, respectively, the bead plug can also be formed from a mixture of both particle types. Interestingly, separation of the magnetic beads with respect to size was observed in-line with the particle stream during release and 3D focusing. Size separation could be achieved simply by careful adjustment of the protocol for the release of the bead plug, without the need of additional magnetic structures. Simply balancing the relative strength of the viscous drag and magnetic forces induced by the current enables separation.
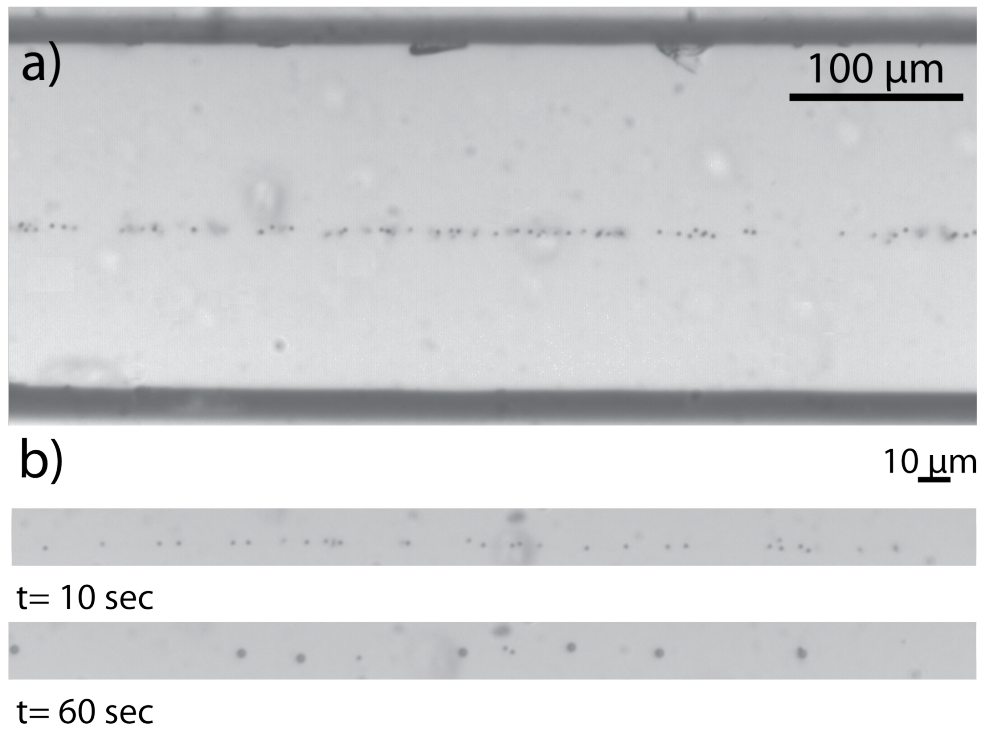
Figure 6.6: *In-flow separation of 1 μm and 2.8 μm particles: a) Photograph of the released stream at t = 40 s within the observation window, which comprises part of the main channel starting 50 μm behind the fluidic junction (bead velocity 0.6 mm/s; t=0 is defined as the time the first bead enters the observation window); b) Two zooms taken at t=10 s and 60 s, respectively, showing a majority of 1 μm or 2.8 μm beads, respectively.*

In order to determine the size distribution in the entire released stream as a function of time, an observation window of 230 μm $\times$ 600 μm and located 350 μm (center position) behind the fluidic junction has been defined. Fig. 6.6a shows a photograph of the focused stream in the observation window at a time t= 40 s, with t=0 defined as the time the first bead enters the observation window. The enhanced views in Fig. 6.6b, taken after 10 and 60 s, respectively, illustrate that the first portion of the released stream (up to 35 s after release) corresponds to an in-flow alignment of predominantly 1 μm beads, whereas the last portion (45 to 60 s after release) mainly contains 2.8 μm beads. A mixture of beads is found at intermediate observation times.
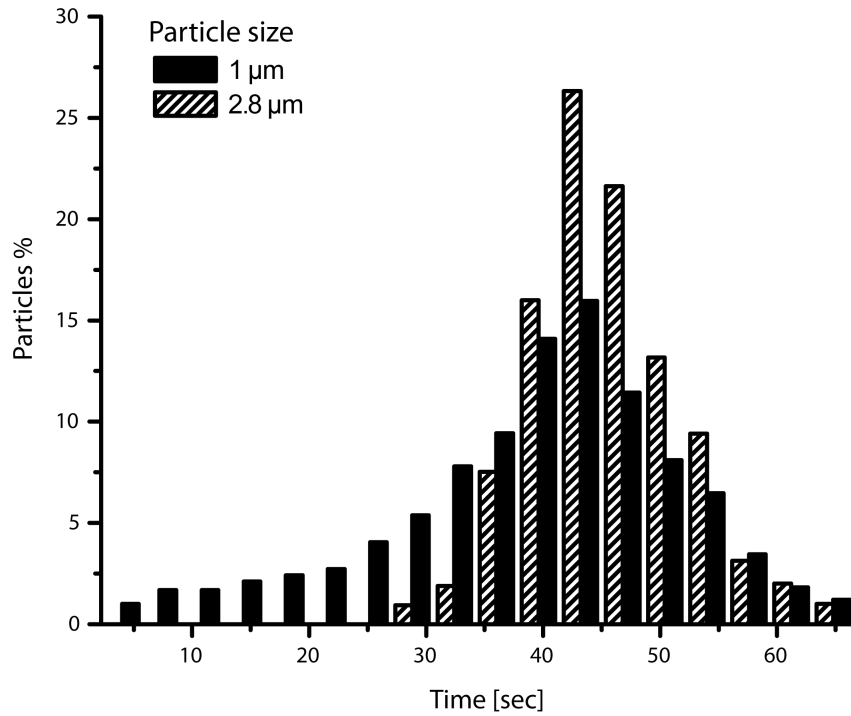
Figure 6.7: *Histogram showing the distribution of 1 μm and 2.8 μm particles in the observation window as a function of the time t following the normal protocol for 3D focusing.*

In order to have the in-line separation in the released bead stream, the protocol has to be adjusted carefully. If the flow has been applied after the full demagnetization (i.e. 60 sec), no in-line size separation has been observed. The corresponding distribution of 1 μm and 2.8 μm is uniform and shown in Fig. 6.7. If the flow was applied before the complete demagnetization (i.e. 40 sec), size separation occurs (Fig. 6.8).
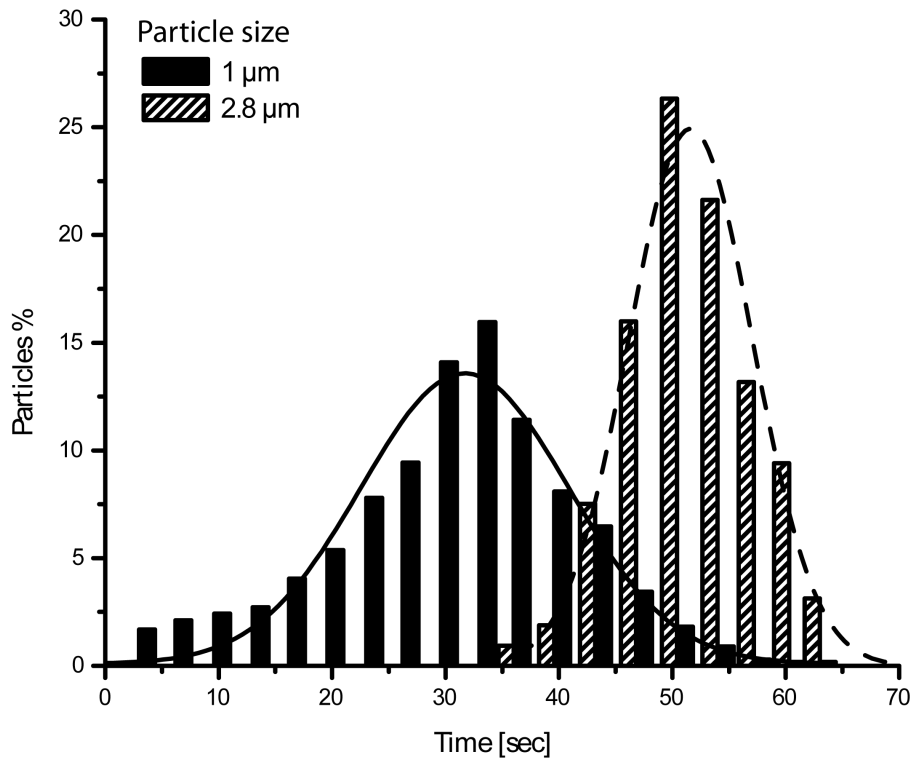
Figure 6.8: *Histogram showing the distribution of 1 μm and 2.8 μm particles in the observation window as a function of the time t. Gaussian curves have been used as an approximation for the distribution of both particle sizes in the released stream. This separation was performed by the protocol modified for in-line separation*

Fig. 6.8 shows a quantitative analysis of the particle size distribution in the stream as a function of time. Separation of the particles could be clearly and in a straightforward way demonstrated. While separation is quasi-perfect for times lower than 30 s and larger than 55 s, for intermediate times, both 1 μm and 2.8 μm beads are contained within the flow. This observation can be explained by the way the magnetic bead plug expands when decreasing the applied magnetic field. Indeed, first the smaller 1 μm beads are released from the plug and dragged away by the flow, as their magnetic volume V_m and magnetic retention force (eq. (2.9)) are typically an order of magnitude lower than those of the 2.8 μm beads.

6.7 Discussion

Most of the microfluidic 3D focusing systems proposed in literature target medium or high-throughput applications in order to meet specifications that are in line with the

performance of commercial cytometers [80]. Often a compromise between accuracy of focusing, throughput and complexity of the design has to be found [81]. As an example, on-chip hydrodynamic 3D focusing with a minimum beam diameter down to 0.2 μm has been achieved [91]. However, this device comprises several fluidic inlets (up to 5, including the sample inlet), necessitating sensitive fluidic protocols and accurate flow and pressure control to provide stable focused streams. On the other hand, simpler systems, such as hydrophoretic focusing systems, using no or only a single sheath flow, give less focused particle streams.

The 3D confinement of the particle stream demonstrated in the present work is extremely easy to achieve and compatible with on-chip flow cytometric approaches [81]; moreover, it has the potential to allow detection of single particles [84]. We want to stress that, unlike precedent approaches, the primary purpose of our system is to provide a concept that allows manipulating a small and well-defined amount of functionalized magnetic beads on-chip. In chapter 5, we already demonstrated the possibility of controlling precisely the amount of retained beads, i.e. dosing in the range of 10^2 to 10^3 beads, by adjusting the magnetic field strength induced by magnetic tips in the microchannel [130]. Reducing the number of beads in a bio-assay is interesting, especially in the range of very low analyte or antigen concentrations, as the amount of captured antigens per bead increases (provided the antigen capture efficiency can be kept constant). Consequently, the signal-to-noise ratio increases, due to an enhancement of the detection signal (e.g. the immunofluorescent signal per bead), pushing the detection limit to lower values.

Discussion

94

7

Magnetic agglutination assay on-chip

Parts of this chapter is adapted from the journal article:

7.1   Introduction

The high potential of the 3D focusing platform is demonstrated by performing an on-chip magnetic bead-based immuno-agglutination assay with accurate detection, taking advantage of the particle alignment in the 3D focused stream. The system allows 3D focusing with a maximum deviation of ± 5 μm from the center position, resulting in reliable counting of singlets and agglutinated doublets. It is shown that certain quantifiable parameters derived from in-line separation of aggregates and singlets can give an idea about the concentration of the analyte in the sample solution.

Magnetic actuation allows efficient analyte capture on the surface of the functionalized superparamagnetic particles. The amount of agglutinated particles and thereby the analyte concentration is determined by observation of the 3D focused stream of released particles. A biotin-streptavidin model assay was used to perform the assay. Using in-line separation in the magnetic 3D focusing device, we may take advantage

of the strong increase of the colliding frequency between the magnetic carriers in the presence of a magnetic field leading to the formation of magnetic chains.

We demonstrate the potential of the agglutination assay in a microfluidic format using a streptavidin/biotinylated-bovine serum albumin (bBSA) model system. A detection limit of about 400 pg/mL (6 pM) is achieved.

7.1.1 Protocol for on-chip immuno-agglutination and detection

We take advantage of the strong affinity of streptavidin for biotin to develop a model assay for agglutination on-chip. In our system, the analyte (or target Ag) is biotinylated-BSA (bBSA) (Sigma-Aldrich, Buchs, Switzerland) that may link to streptavidin-coated beads, thus forming doublets or larger aggregates. The analyte test solution is 15 mM PBS containing variable bBSA concentrations in the range of 10 pg/mL to 1 $\mu g/mL$ (0.15 pM to 0.15 μM). A surfactant (0.5%, Tween 20) was added to reduce non-specific agglutination.

The principle of the on-chip agglutination assay is illustrated in Fig. 7.1. First, a colloid of functionalized streptavidin-coated magnetic beads is injected into the microchannel and magnetically immobilized in the form of a dense plug on one of the sidewalls (Fig. 7.1 a). The side channel in closed in this step. In order to determine precisely the amount of specifically agglutinated particles (i.e. linked by bBSA), it is important to record accurately an in-situ reference signal prior to each measurement. For that the beads are simply released in the buffer solution and the focused stream is analyzed (side channel open) (Fig. 7.1 b). Beads are counted by automated image recording in an observation window in order to determine the amount of single beads and aggregates. The centre of this window is located 350 μm behind the fluidic junction on the chip (window size 230 μm × 600 μm). The bead stream (about 5 mm) passing the window is recorded and the video sequence is analyzed. Subsequently, the flow direction is inverted and the beads are captured again in a plug at the initial location as the side channel is closed again (Fig. 7.1 c). The majority of the initial amount of beads (more than 95%) is recovered at the end of this procedure.
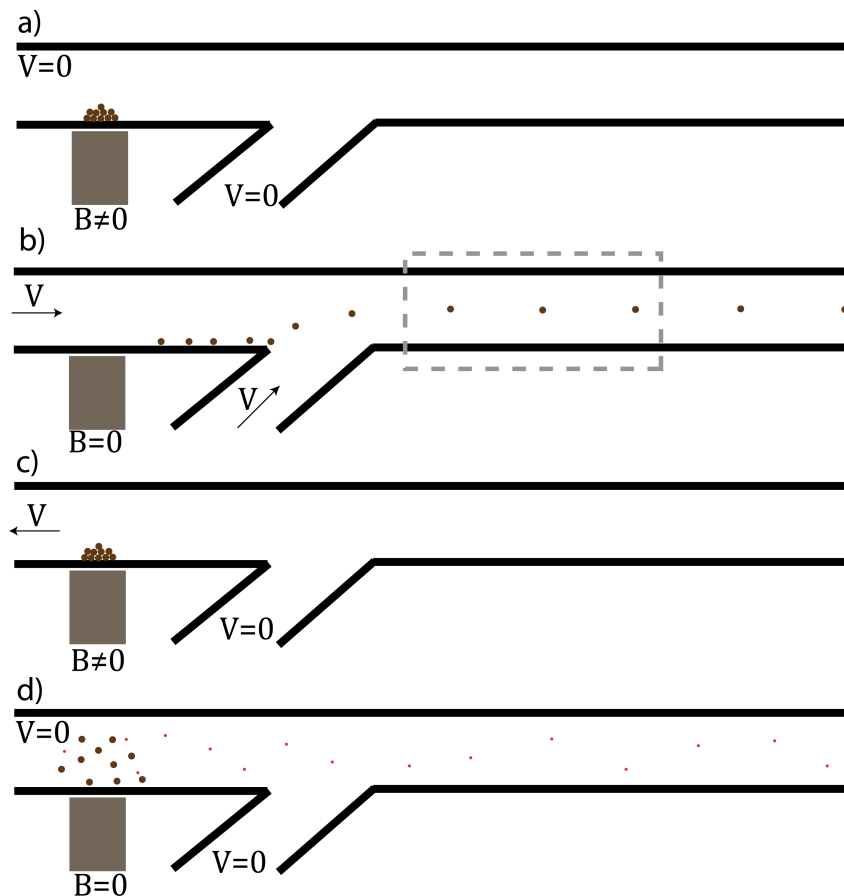
Figure 7.1: *Principle of the microfluidic agglutination immuno-assay. a) Formation of a dense magnetic bead plug at the channel sidewall. b) Release and 3D focusing of the beads in a solution flow by controlled attenuation of the field. A detection window is defined (dashed rectangle) for automated counting of the particles in the focused stream. c) Inverting the flow direction allows capturing again the whole amount of beads and the formation of a dense plug. Steps a) to c) are performed in buffer solution and serve as in situ reference experiment. d) The buffer solution is replaced by the analyte solution. Dissociation of the confined bead plug allows capturing the analyte (no flow is applied). Dense plug formation and dissociation may be repeated several times to increase the amount of antigens on the beads. Subsequently, beads are released for detection (step b).*

The agglutination protocol starts by introducing the analyte solution in the microchannel. Once the channel is filled, the flow is stopped and the field is removed (Fig. 7.1 d). The highly localized bead plug dissociates in the bBSA solution allowing capturing the analyte molecules on the beads. After this step, the magnetic field is applied and the beads form again a dense plug. This cycle may be repeated several times, replacing the bBSA solution after each cycle. The impact of repeated cycling

and a variable residence time of the beads in the dissociated state are studied in the following. Subsequently, the agglutinated colloid is released and focused for detection.
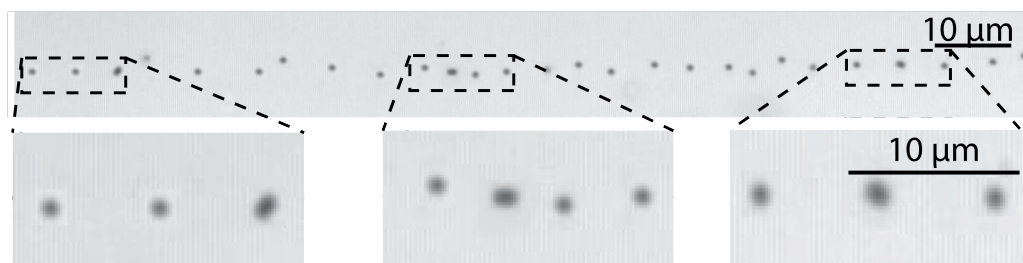
Figure 7.2: *The photograph shows a stream of released and focused particles. The insets show a zoom where single beads and doublets can be distinguished (bead diameter 1 μm).*

Analyte capture on functionalized beads is achieved by releasing the plug in the sample solution without applying a flow (see Fig. 7.1 d). The dissociated plug increases the bead/analyte encounter probability and thereby the capture efficiency [129]. Subsequent formation of aggregates is achieved under re-confinement of the beads in a dense plug. The analyte concentration is related to the number of aggregates formed.

Fig. 7.2 shows the alignment of single beads and doublets in a released and focused stream. For quantitative measurements, the number of aggregates/doublets and single beads in the stream may be counted by using standard image processing. In our case, the resulting decrease of the number of singlets was determined. The area of each particle is recorded (number of pixels) and, below a certain threshold, the particle is counted as singlet. In order to obtain the best signal possible, i.e. high specific agglutination for a given analyte concentration, while minimizing the amount of non-specific aggregates, the parameters for analyte capture have been optimized.

Two parameters have been investigated:

- The number of cycle repetitions

- The residence time of the beads in the dissociated state of the plug

One standard cycle consists of dissociating the plug during 1 min followed by the re-formation of a dense plug for 1 min.
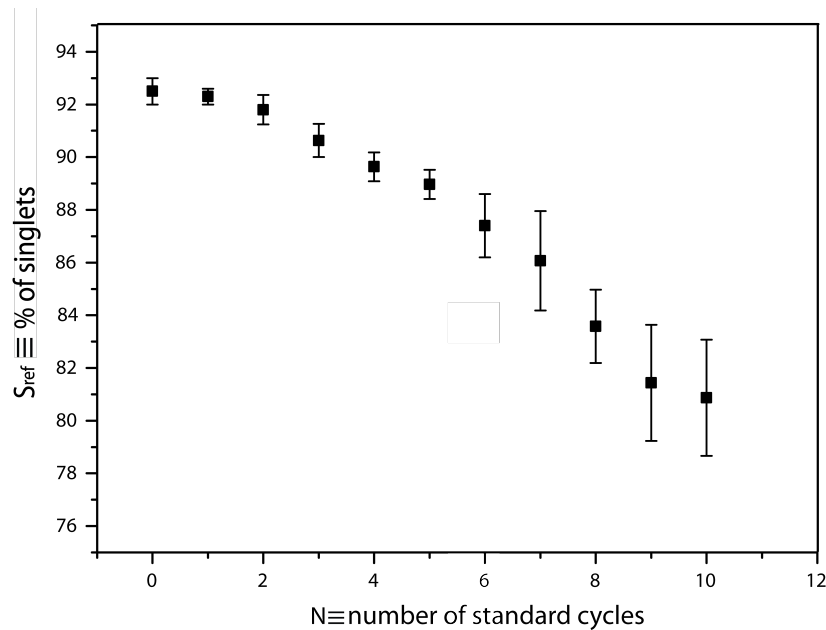
Figure 7.3: *Graph showing the impact of the number of standard cycles on non-specific agglutination in buffer solution, as monitored by the reduction of the number of singlets. One standard cycle consists of forming a dense plug for 1 min prior to plug dissociation during 1 min (no flow applied).*

7.2 In situ reference test

First, nonspecific agglutination was investigated. Fig. 7.3 demonstrates the impact of repeated cycling in buffer solution. The initial amount of singlets before cycling $S_{ref,N=0}$ was 92.5 %. The graph shows a decrease of the amount of singlets with the number of cycles N, i.e. an increase of non-specific agglutination (formation of doublets). Non-specific interaction and sticking of the beads to each other occurs during the formation of the dense plug. The cycles have been repeated up to 10 times, resulting in a decrease of the number of single beads to 80 %. For the proper agglutination assay, we use 3 cycles and the corresponding reference signal $S_{ref,N=3}$. A correction factor $F = (S_{ref,N=3}/S_{ref,N=0})$ was defined. Then $F = 1.02$, which corresponds to a 2% reduction of the initial number of singlets (formation of clusters) due to non-specific agglutination. This value is acceptable compared to the significant increase of specific agglutination after 3 cycles (see below).
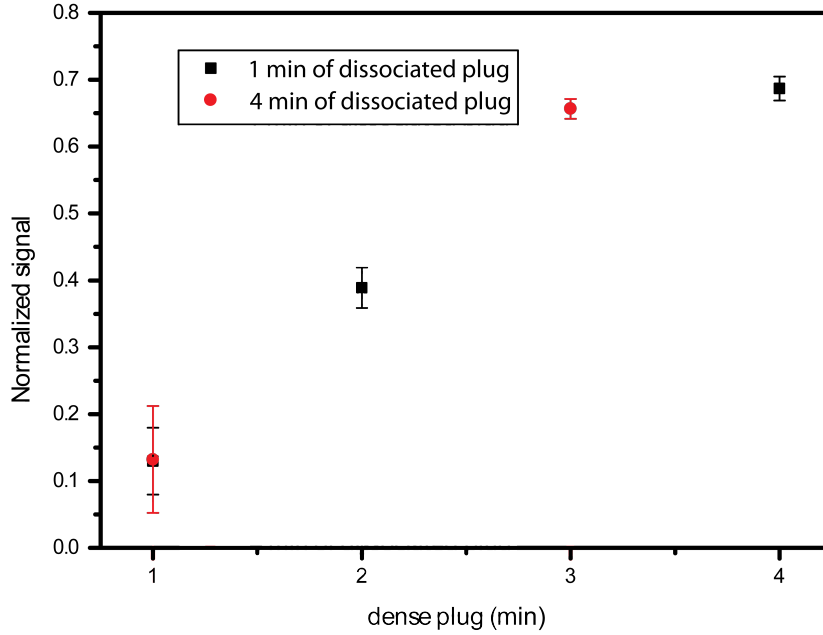
Figure 7.4: *Graph demonstrating the increase of specific agglutination with the number of cycles. Analyte capture was performed by dissociating the plug in a solution of 10 ng/mL bBSA. Two different times (1 and 4* min*), during which the beads are kept in the dissociated state have been tested.*

7.3 Analyte test

In a second step, the analyte capture was evaluated for different configurations. Fig. 7.4 compares the normalized signal for an increasing number of cycles and for two different dissociation times. The experiments have been carried out with a bBSA concentration of 10 ng/mL. The bBSA solution has been replaced after each cycle. An on-chip reference test (1 cycle taking buffer solution without analyte) was carried out before each measurement in order to determine the amount of non-specific agglutination (see Fig. 7.1). We consider the normalized signal

$$1 - \frac{S_{bBSA,N}}{S_{ref,N}} \tag{7.1}$$

defining the percentage of the single beads in the released stream after a number of cycles N, based on the signal $S_{ref,N}$ and $S_{bBSA,N}$, defined by the percentage of the number of singlets in the reference and the analyte measurement, respectively. Increasing the number of cycles form 1 to 3 resulted in an about 7 fold increase of the detection signal.

Squares in Fig. 7.4 correspond to a dissociation time of 1 min and circles to a time of 4 min. The incubation time, i.e. the formation of the dense plug, was 1 min in both cases. Only a very small change was found between cycle 3 and 4. We conclude that the optimum density of bead surface-bound antigens is obtained after 3 cycles. Furthermore, we may deduce from the curve in Fig. 7.4 that the plug dissociation time seems to have no significant impact on the capture efficiency. This result indicates that the analyte capture is not limited by diffusion under the present conditions.

Two methods were used for counting the agglutinated particles. The first one was to count all particles and to take the percentage of the agglomerates as the signal. The second method was to analyse the parameters of the Gaussian fits corresponding to the in-line separation of agglomerates and particles (explained below).

7.4   Analyte dose-response curve from in-line separation

Particles and aggregates were counted in time lapses, and the percentages of each group have been calculated according to the protocol described in chapter 6.6 "agglutination assay". For each concentration the in-line curve graph has been plotted and the Gaussian fits have been calculated.

Fig. 7.5 shows a quantitative analysis of the particle and agglomerates distribution in the stream as a function of time. Separation of the particles and agglomerates could be observed as for in-line size separation. First the 1 μm single beads are released from the plug and dragged away by the flow, as their magnetic volume V_m and magnetic retention force (eq. (2.9)) are typically lower than those for doublets or aggregates.

For each concentration two Gaussian curves have been fitted (one for the singlets and one for agglomerates). It can be observed from Fig. 7.5 that the difference of the peaks in time changes by changing the concentration. The separation is more pronounced when the concentration of the analyte, i.e. the amount of aggregates, is higher. The two peaks get closer with decreasing concentration until they are not distinguishable anymore. The time-shift between the two Gaussians correspond to the signal of our test, and is the main parameter to obtain the dose-response curve. The method of in-line separation was not successful for the reference signal because the number of aggregates was only about 2%. Separation with this low concentration was not reproducible.

Figure 7.5: *In-line separation of singlets and agglomerates and corresponding Gaussian fits for different concentrations: a)6* ng/mL *b) 20* ng/mL *and c) 200* ng/mL.

Figure 7.6: *Dose-response curve for a magnetic agglutination assay using a streptavidin-bBSA model system. A full on-chip assay (squares), where analyte capture was achieved by magnetic actuation on-chip, and a partially off-chip assay (circles) are compared. A detection limit of 10* ng/mL *was obtained for the on-chip assay.*

In the low concentration range, the in-line separation method is not precise. Low concentrations of bBSA give rarely rise to aggregates and the separation method is not successful. The dose-response curve is shown in Fig. 7.6 for both off-chip and on-chip agglutination protocols. For the off-chip assay, the beads are first mixed off-chip with solutions containing different analyte concentrations (incubation time of 6 min). Subsequently, the agglutinated colloid is introduced in the microfluidic chip and immobilized. The plug is released (no cycling) for counting in the 3D focused stream.

The limit of detection obtained from both on-chip or off-chip in-line separation is about 1 ng/mL, while the off-chip standard deviation is much larger comparing to on-chip protocol.This shows that the way of detecting is the weak point of this method.

103

7.5 Analyte dose-response curve from 3D focusing experiments

In the present case, a 3D focused stream of beads that contains a mixture of aggregates of different size as well as single beads was analysed. In the limit of low concentrations, mainly doublets will form aggregates [10]. We note that, without 3D focusing, it is extremely difficult to distinguish singlets and doublets of very small size (typical diameter 1 μm) in a stream with a normal microscope setup. As described above, we take here clear advantage of the 3D focused beam for accurate counting of the particles. All particles are well aligned and in the same focal plane, thus reliable detection of single beads and doublets can be made by using simple image processing software.

In order to demonstrate the feasibility of a sensitive agglutination assay, we established a dose-response curve for the bBSA-streptavidin model assay. Fig. 7.7 compares the dose-response curves for the on-chip assay (squares) and for an off-chip experiment (circles). An on-chip reference test (1 cycle, buffer solution without analyte) is carried out before each measurement in order to determine the amount of non-specific agglutination (see Fig. 7.1). As explained before, we consider the normalized signal

$$1 - \frac{S_{bBSA,N=3}}{S_{ref,N=0} \cdot F} \tag{7.2}$$

defining the percentage of the single beads in the released stream for the reference and the analyte measurement, respectively. The curve recorded in Fig. 7.3 in principle would allow determining a non-specific correction factor F as a function of cycle number N.

In this study, 3 standard cycles have been performed, resulting in a reduction of 2% of the amount of singlets, *i.e.* $F = 1.02$. This method results in a reliable read-out of the specific agglutination, even at very low bBSA concentrations. The reference test is very accurate as it is performed in situ, i.e. the same beads are used for the reference test and the assay.
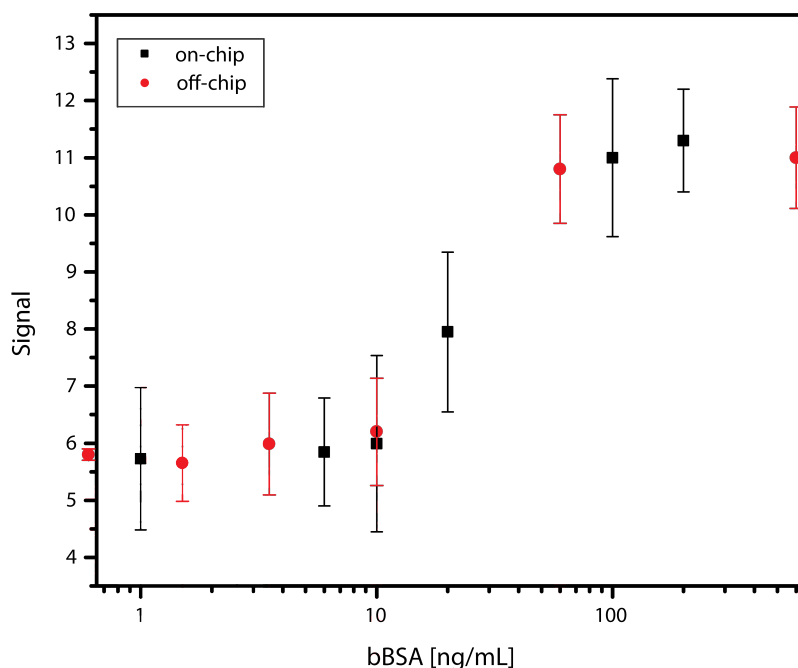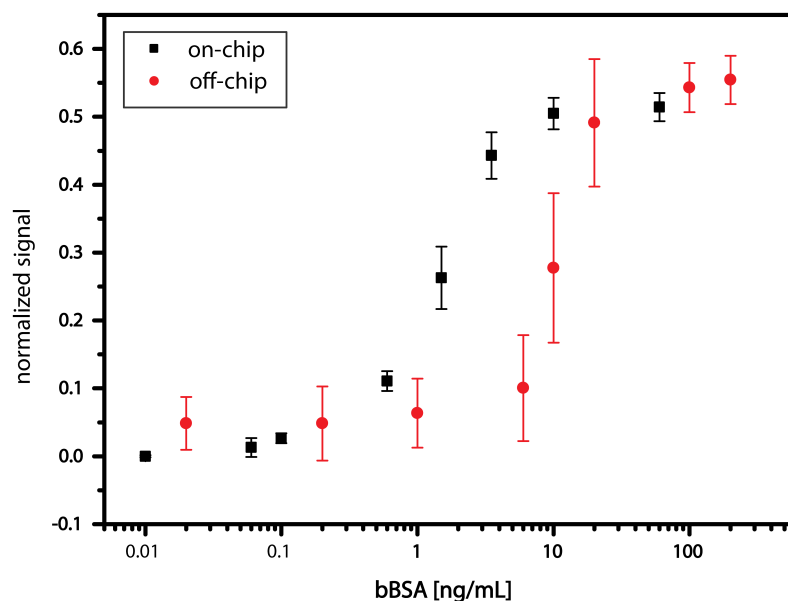
Figure 7.7: *Dose-response curve for a magnetic agglutination assay using a streptavidin-bBSA model system. A full on-chip assay (squares), where analyte capture was achieved by magnetic actuation on-chip, and a partially off-chip assay (circles) are compared. A detection limit of 400 pg/mL s obtained for the on-chip assay.*

The dose-response curve was recorded for bBSA concentrations in the range of 0.01 ng/mL (0.15 pM) to 1 μg/mL (15 nM). We can safely determine a detection limit of about 400 pg/mL ($\approx$6 pM). The signal for this concentration is more than three times the standard deviation above zero. Saturation occurs for concentrations above 10 ng/mL (150 pM), where most of the beads are agglomerated. As the total number of retained beads can be controlled during the formation of the plug [130] (see chapter 5.4), the nominal number of beads for each measurement was the same to ensure reproducibility and reliability of the assay.

The microfluidic agglutination protocol might seem complex due to the repetitive trapping and release of the particles. However, doing this permits us to explicitly take advantage of the control offered by the microfluidic format. Indeed, the possibility to manipulate essentially the same ensemble of beads under quasi-continuous observation allows us to determine the reference signal with the utmost accuracy. This is of particular interest for the lowest concentrations of bBSA (smaller than 1 ng/mL), where the specific agglutination signal (the number of doublets) is small. In principle, it would not have been necessary to consider such dynamic reference signal for the higher concentrations,

but we have always performed the same protocol. Also, the drawback of this apparently complex protocol is very relative, as the whole manipulation is done under computer control.

The results of the off-chip protocol have also been investigated with the 3D focusing method. It can be seen in Fig. 7.7, that the standard deviation for the off-chip experiment is much larger than for the on-chip experiment, as no accurate in situ reference signal can be recorded in this case. Also controlling the total number of beads is more complicated. As a consequence, the detection limit can be estimated to about 10 ng/mL, which is a factor of 25 higher than for the full on-chip assay.

8

Conclusion and outlook

Magnetic bead-based systems have high potential for various lab-on-a-chip applications. The objective of the DetectHIV project was to design a system transferable to market; as a result one of the design rules of the the microfuidic system of this project was simplicity compared to existing approaches. The magnetic actuation system had to be integrated with an optical detection unit to form a biosensor prototype. We therefore focused our efforts on providing simple design and fabrication rules as well as experimental protocols, for the magnetic actuation system.

8.1   Lateral magnetic separation

In the present work, we have presented a microfluidic magnetic bead manipulation device comprising three distinct functions:

1. Dosing and immobilization of a controlled amount of magnetic beads

2. Release of the beads in a highly confined particle stream

3. Continuous magnetophoretic size separation with high resolution

System characterization was carried out with 1.0 μm and 2.8 μm superparamagnetic beads. Integrated soft-magnetic micropoles adjacent to the PDMS microchannel served as field concentrators to generate high field gradients and high local field strength for efficient bead manipulation. The protocol combines a batch process (dosing) and

a continuous process (separation). In particular, we demonstrated the possibility to discriminate a defined amount of 1.0 μm single beads and 1.0 μm bead doublets by magnetophoretic separation. This feature is a requirement for the development of high-sensitivity magnetic agglutination assays on-chip. Based on the present development, several steps of an agglutination assay protocol, including incubation for doublet formation and subsequent deviation of the doublets into a dedicated outlet channel for optical detection, can be implemented on-chip. Versatility, ease-of-use and low-cost of the present approach provides a high potential for incorporating our device in a bioanalytical lab-on-a-chip platform for point-of care applications.

8.2   3-dimensional focusing and in-flow separation

We presented a new magneto-microfluidic method for 3D focusing and size separation of 1.0 μm and 2.8 μm magnetic beads in the flow direction. The particles are aligned one-by-one in a stream with a maximum deviation of ± 5 μm from the center position in the channel. Focusing in the vertical direction is achieved by taking advantage of the strongly focused magnetic field generated by a soft-magnetic microtip that is integrated on-chip. Accuracy and stability of focusing is suitable for combination with on-chip particle counting applications. Moreover, only a very simple and robust experimental protocol is needed. Size-separation in the flow direction opens the way towards simplified detection protocols, e.g. for multiplex bio-assays or agglutination assays, without losing the benefit of 3D focusing. In addition to 3D focusing, our set-up allows precise dosing, i.e. retention of a very accurate and small amount of beads in the sample flow. Moreover, it enables dynamic actuation of the beads in the flow, useful for antigen capture. The demonstrated in-flow separation may simplify and optimize detection protocols and, in particular, this method takes full advantage of 3D focusing. We think that the present device may play a future role in an integrated versatile platform for performing several magnetic manipulation steps on-chip, like required for magnetic bead-based bio-assays.

8.3   Agglutination on-chip

The magneto-microfluidic method for 3D focusing of magnetic beads is of particular interest for fully integrated on-chip immuno-agglutination assays, which are based on determining the ratio of single beads and aggregates. Capture of the analyte was achieved by repeated densification and dissociation of a plug of functionalized beads. Subsequent use of the 3D focusing effect allowed accurate counting of single or agglutinated particles.

In-flow separation has been used to perform an agglutination assay. A detection limit of about 400 pg/mL (6 pM) was found using a bBSA-streptavidin model assay. This is competitive with state-of-the-art microfluidics-based assays, several orders of magnitude lower than typical values obtained for standard (non-magnetic) bulk assays, and comparable to a previously reported magnetic assay in the bulk format.

Thereby our work demonstrated the high potential of 3D focusing of a magnetic bead stream for the automatic detection of low concentration target analytes. Indeed, positioning the beads exactly in focus of the optical observation plane using our extremely simple magnetic method, which avoids the application of complex multiple fluid focusing streams, allowed establishing an easy counting protocol, performing the in situ reference test, and the precise dosing of a low number of beads. The latter aspect could be of special interest in future experiments, where very dilute target analytes can be preconcentrated on a minimum number of beads for subsequent detection and analysis. Moreover, in future, the present system could be further exploited when combined with on-chip particle detectors [84], and may be developed into a fully integrated versatile platform for performing different types of magnetic bead-based bio-assays requiring several manipulation steps on-chip.

Real testing using p24 Ag's on-chip was not implemented. Experiments and evaluation of p24 agglutination assays in the microtitre plate format, carried out in parallel in the frame of the DetectHIV project, revealed some problems with the stability of anti-p24-coated beads. After solving this problem this system eventually could be used for the p24 on-chip assay.

8.4 The DetectHIV biosensors platform

8.4.1 General approach

One of the main goals of the European project DetectHIV was the design of a biosensor platform, which allows performing a magnetic agglutination test for the detection of the HIV virus capsid protein p24 on a disposable chip. 1.0 μm beads have been used in different modules of the project. Their size was chosen is a way to be observale via microscope, in the same time they needed to be uniform in size. During the project it has been decided to develop a first version of the integrated system which comprises a module for the retention of magnetic beads, and a module for the detection of doublets and singlets by light scattering. The module for enrichment of doublets prior to the detection planned to be integrated in the second generation of the platform once the feasibility of integration has been accomplished. Adding the separation module would add complexity to the system.

An integrated chip comprising the magnetic actuation part (developed at EPFL) and the optical detection system (developed at the Danmark Tekniske Universitet, DTU) was fabricated in the frame of the DetectHIV project. The challenge of the integration was to make the fabrication process of the two systems compatible.

8.4.2 Magnetic system

The microsystem for the magnetic retention of superparamagnetic beads on-chip was developed in parallel to this present thesis at EPFL [132]. A highly confined and dynamically actuated plug of biochemically functionalized beads is formed in a microchannel. This plug extends over the channel cross-section, thus allowing efficient analyte capture from the flow. Subsequent immobilization of the plug for incubation modifies the colloidal state (agglutination test). Dynamic actuation of beads is enabled by superposing a static magnetic field and a time-varyingmagnetic field. The latter field is highly focused and concentrated across the microchannel by means of soft magnetic microtips. The magnetic actuation system consists of a single channel with an open inlet reservoir and an outlet connected to a syringe pump. The liquids have to be driven in a pulling (suction) mode from the outlet to provide an open access for pipetting solutions and bead suspension into the inlet.
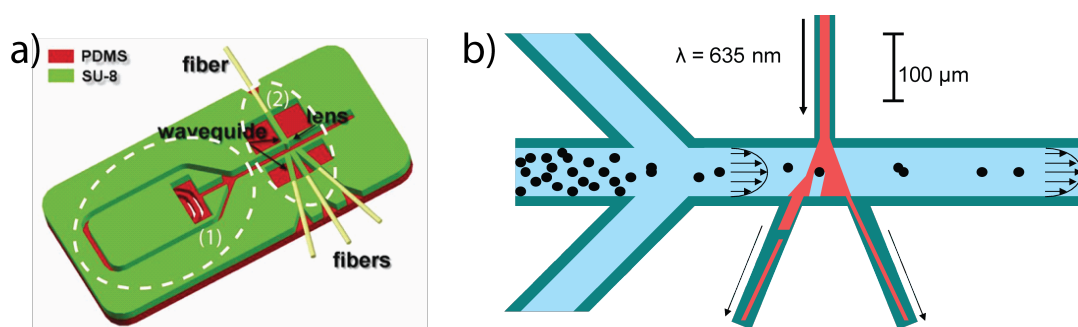
Figure 8.1: *Optical detection system developed at DTU: (a) The microchip comprises 3D hydrodynamic focusing (1) and an optical detection module (2). The setup employs a laser as incident light source. The incoming and outgoing optical fibers are aligned to the chip using structured grooves in the SU-8 layer. Scattered light is collected by on-chip waveguides and measured using a photo muliplier tube. (b) The hydrodynamically focused beads modify the intensity of the scattered light as they pass the laser beam (courtesy of G.S. Zhuang, T.G. Jensen)*

8.4.3 Optical detection system

The optical detection system developed at DTU is schematically presented in Fig. 8.1. The chip first comprises a part for 3D hydrodynamic focusing to concentrate the beads in the middle of the channel cross section prior to the detection (Fig. 8.1a). The right part of the chip is made for the detection of the beads by light scattering (Fig. 8.1b). The light of a laser is guided towards the chip using an integrated SU-8 waveguide. The beads crossing the laser beam modify the intensity of the scattered light. The scattered light is then measured using the two symmetric detection waveguides and a photo multiplier tube. Multiple fluidic connections make the fluidic control complex.

8.4.4 The integrated system

Fig. 8.2a shows the design of the integrated chip. The chip is made of a PDMS layer and a glass slide with patterned SU-8 on top. The main channel network is molded in the PDMS while the optical detection system is made from SU-8 (right-hand side of the chip).Two open reservoirs (R-1 and R-2) are used for the introduction of beads and sample. The six inlets (I-1 to 6) are needed to perform 3D focusing of the beads in the middle of the channel prior to the optical detection.
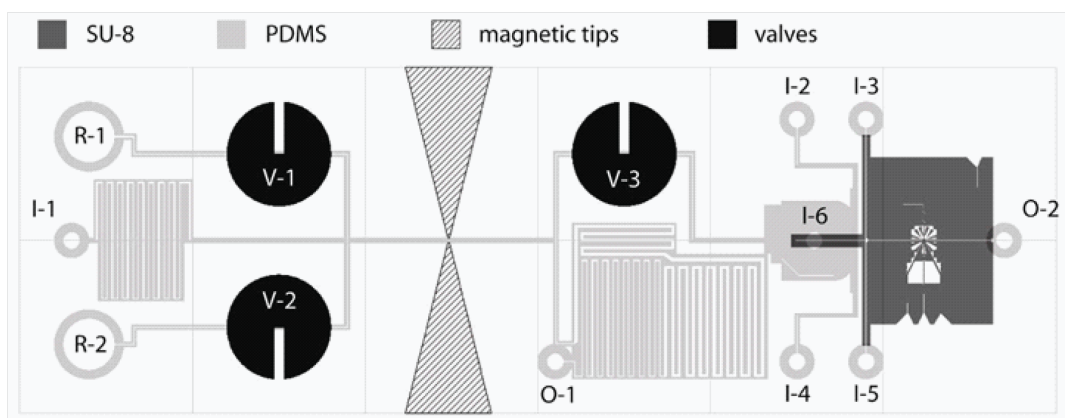
Figure 8.2: *Schematic view of the integrated chip. The main fluidic channel network is molded in the PDMS layer. Two open reservoirs (R-1 and R-2) serve to introduce beads and sample solutions. Six fluidic inlets (I-1 to 6) are used to focus the beads prior to the optical detection. Serpentine structures serve to avoid the contamination of the chip holder. The optical detection system is made from SU-8. Access for the valves (V-1 to 3) and the magnetic tips is also shown b=3D schematic view of the assembled chip. The PDMS/SU-8/glass chip is clamped in a PMMA case with the magnetic tips and optical fibers glued on the glass slide (courtesy of Julien Charpentier, Bertin Technologies)*

The fabrication of PDMS chip was carried out in PDMS using the same method explained in this thesis. It was sealed by clamping of the PDMS and the SU-8/glass slide in a PMMA case designed and fabricated by Bertin Technologies (Fig. 8.2b)

The demonstrator platform was designed and fabricated by Bertin Technologies. Fig. 8.3 shows a photograph of the final demonstrator with the integrated chip. A drawer serves to slide the disposable chip in the platform, three linear motors actuate the integrated valves and a permanent magnet may be manually positioned on top of the system. The demonstrator is ready to be tested and a model agglutination assay based on the streptavidin and biotin interaction will be first developed and tested.

After validation of the first generation DetectHIV platform comprising the basic functionalities of the device (mixing and detection), integration of 3D focusing and in-line separation, could be envisioned.

Magnetic retention and separation systems are based on a similar design and fabrication process. This makes a combination with the actual integrated chip layout straight forward.

In order to integrate the 3D magnetic fluidic focusing on chip, the same pair of tips as for the dynamic actuation can be used, no major changes are necessary for the
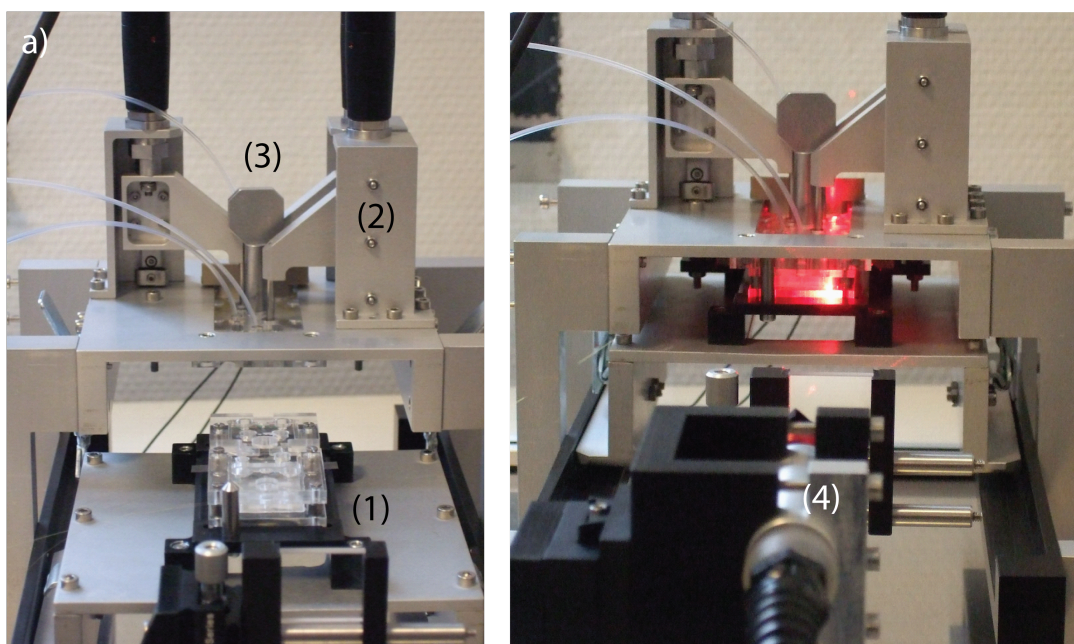
Figure 8.3: *Photographs of the DetectHIV biosensor platform:(a) The chip (1) on a drawer, before introduction in the platform(b) Chip inserted in the platform ready for an experiment. A red laser is used to perform the detection by light scattering (4) (courtesy of Julien Charpention, Bertin Technologies).*

magnetic system (core and coil). The fluidic design of the integrated chip, however, can be significally simplified. The 6 fluidic entrances for hydrodynamic focusing may be replaced with one inlet to push the beads to the middle of the channel. For that the SU-8 master to mold the PDMS should be changed. This will make the fluidic manipulations easier. The in-line separation which works with the 3D focusing system can be an option for enriching the sample for detection system, as the time of arrival of aggregates is predictable. For ultimate sensitivly the lateral separation system can be added to the integrated platform.

Bibliography

[1] A. Manz, N. Graber, and H. M. Widmer, "Miniaturized total chemical-analysis systems - a novel concept for chemical sensing," *Sensors and Actuators B-Chemical*, vol. 1, no. 1-6, pp. 244–248, 1990.

[2] D. R. Reyes, D. Iossifidis, P.-A. Auroux, and A. Manz, "Micro total analysis systems. 1. introduction, theory, and technology," *Analytical Chemistry*, vol. 74, no. 12, pp. 2623–2636, 2002.

[3] J. West, M. Becker, S. Tombrink, and A. Manz, "Micro total analysis systems: Latest achievements," *Analytical Chemistry*, vol. 80, no. 12, pp. 4403–4419, 2008.

[4] N. Constantine, "Enhanced chemiluminescence as a means of increasing the sensitivity of western blot assays for hiv antibody," *Journal of Virological Methods*, vol. 47, no. 1-2, pp. 153–164, 1994.

[5] E. M. Lackritz, G. A. Satten, J. Aberle-Grasse, R. Y. Dodd, V. P. Raimondi, R. S. Janssen, W. F. Lewis, E. P. Notari, and L. R. Petersen, "Estimated risk of transmission of the human immunodeficiency virus by screened blood in the united states," *New England Journal of Medicine*, vol. 333, no. 26, pp. 1721–1725, 1995.

[6] J.-A. Kwo, S.-Y. Yoon, C.-K. Lee, C. Lim, K. Lee, H. Sung, C. Brennan, and S. Devare, "Performance evaluation of three automated human immunodeficiency virus antigen-antibody combination immunoassays," *Journal of Virological Methods*, vol. 133, no. 1, pp. 20–26, 2006.

[7] D. Owens, M. Holodniy, A. Garber, J. Scott, S. Sonnad, L. Moses, B. Kinosian, and J. Schwartz, "Polymerase chain reaction for the diagnosis of hiv infection in adults: A meta-analysis with recommendations for clinical practice and study design," *Annals of Internal Medicine*, vol. 124, no. 9, pp. 803–815, 1996.

[8] J. Schupbach, J. Boni, M. Flepp, Z. Tomasik, H. Joller, and M. Opravil, "Antiretroviral treatment monitoring with an improved hiv-1 p24 antigen test: An inexpensive alternative to tests for viral rna," *Journal of Medical Virology*, vol. 65, no. 2, pp. 225–232, 2001.

[9] J. Baudry, E. Bertrand, N. Lequeux, and J. Bibette, "Bio-specific recognition and applications: from molecular to colloidal scales," *Journal of physics. Condensed matter*, vol. 16, no. 15, p. R469, 2004.

[10] J. Baudry, C. Rouzeau, C. Goubault, C. Robic, L. Cohen-Tannoudji, A. Koenig, E. Bertrand, and J. Bibette, "Acceleration of the recognition rate between grafted ligands and receptors with magnetic forces," *Proceedings of the National Academy of Sciences*, vol. 103, no. 44, pp. 16076–16078, 2006.

[11] M. A. M. Gijs, "Magnetic bead handling on-chip: New opportunities for analytical applications," *Microfluidics and Nanofluidics*, vol. 1, no. 1, pp. 22–40, 2004.

[12] "Ferromagnetic materials." http://www.doitpoms.ac.uk/tlplib/ferromagnetic/printall.php?question=1&type=4, 2010.

[13] S. Chikazumi, *Physics of magnetism*. Wiley series on the Science and Technology of Materials, Wiley, 1964.

[14] "Magnetic materials: Types." http://www.magnets.bham.ac.uk/magneticmaterials/types.shtml, 2010.

[15] W. F. Brown, "Thermal fluctuations of a single-domain particle," *Phys. Rev.*, vol. 130, pp. 1677–1686, Jun 1963.

[16] A. H. Morrish, *The Physical Principles of Magnetismm*. WileyNew York: IEEE Press, 2001.

[17] Q. A, J. Connolly, S. K. Jones, and J. Dobson, "Applications of magnetic nanoparticles in biomedicine," *Journal of Physics D: Applied Physics*, vol. 36, no. 13, p. R167, 2003.

[18] M. A. M. Gijs, F. Lacharme, and U. Lehmann, "Microfluidic applications of magnetic particles for biological analysis and catalysis," *Chemical Reviews*, vol. 110, no. 3, pp. 1518–1563, 2010. doi: 10.1021/cr9001929.

[19] D. Horak, M. Babic, H. Macková, and M. J. Bene, "Preparation and properties of magnetic nano- and microsized particles for biological and environmental separations," *Journal of Separation Science*, vol. 30, no. 11, pp. 1751–1772, 2007.

[20] Y. Moser, T. Lehnert, and M. A. M. Gijs, "Quadrupolar magnetic actuation of superparamagnetic particles for enhanced microfluidic perfusion," *Applied Physics Letters*, vol. 94, no. 2, p. 022505, 2009.

[21] R. Wirix-Speetjens, W. Fyen, K. Xu, J. De Boeck, and G. Borghs, "A force study of on-chip magnetic particle transport based on tapered conductors," *IEEE Transactions on Magnetics*, vol. 41, no. 10, pp. 4128–4133, 2005.

[22] D. J. Beebe, G. A. Mensing, and G. M. Walker, "Physics and applications of microfluidics in biology," *Annual Review of Biomedical Engineering*, vol. 4, pp. 261–286, 2002.

[23] E. M. Purcell, "Life at low reynolds-number," *American Journal of Physics*, vol. 45, no. 1, pp. 3–11, 1977.

[24] D. J. Harrison, A. Manz, Z. Fan, H. Ludi, and H. M. Widmer, "Capillary electrophoresis and sample injection systems integrated on a planar glass chip," *Analytical Chemistry*, vol. 64, no. 17, pp. 1926–1932, 1992.

[25] E. Verpoorte, "Beads and chips: New recipes for analysis," *Lab on a Chip*, vol. 3, no. 4, pp. 60N–68N, 2003.

[26] N. Pamme, "Magnetism and microfluidics," *Lab on a Chip*, vol. 6, no. 1, pp. 24–38, 2006.

[27] L. R. Huang, E. C. Cox, R. H. Austin, and J. C. Sturm, "Continuous particle separation through deterministic lateral displacement," *Science*, vol. 304, no. 5673, pp. 987–990, 2004.

[28] M. Yamada, M. Nakashima, and M. Seki, "Pinched flow fractionation:a continuous size separation of particles utilizing a laminar flow profile in a pinched microchannel," *Analytical Chemistry*, vol. 76, no. 18, pp. 5465–5471, 2004.

[29] B. S. Cho, T. G. Schuster, X. Zhu, D. Chang, G. D. Smith, and S. Takayama, "Passively driven integrated microfluidic system for separation of motile sperm," *Analytical Chemistry*, vol. 75, no. 7, pp. 1671–1675, 2003.

[30] H. Lu, S. Gaudet, M. Schmidt, and K. Jensen, "A microfabricated device for subcellular organelle sorting," *Analytical Chemistry*, vol. 76, no. 19, pp. 5705–5712, 2004.

[31] S. Fiedler, S. Shirley, T. Schnelle, and G. Fuhr, "Dielectrophoretic sorting of particles and cells in a microsystem," *Analytical Chemistry*, vol. 70, no. 9, pp. 1909–1915, 1998.

[32] T. Hunt, H. Lee, and R. Westervelt, "Addressable micropost array for the dielectrophoretic manipulation of particles in fluid," *Applied Physics Letters*, vol. 85, no. 26, pp. 6421–6423, 2004.

[33] A. Fu, C. Spence, A. Scherer, F. Arnold, and S. Quake, "A microfabricated fluorescence-activated cell sorter," *Nature Biotechnology*, vol. 17, no. 11, pp. 1109–1111, 1999.

[34] M. Wang, E. Tu, D. Raymond, J. Yang, H. Zhang, N. Hagen, B. Dees, E. Mercer, A. Forster, I. Kariv, P. Marchand, and W. Butler, "Microfluidic sorting of mammalian cells by optical force switching," *Nature Biotechnology*, vol. 23, no. 1, pp. 83–87, 2005.

[35] M. Yamada and M. Seki, "Microfluidic particle sorter employing flow splitting and recombining," *Analytical Chemistry*, vol. 78, no. 4, pp. 1357–1362, 2006.

[36] N. Pamme, "Continuous flow separations in microfluidic devices," *Lab on a Chip*, vol. 7, no. 12, pp. 1644–1659, 2007.

[37] C. H. Hsu, D. Di Carlo, C. Chen, D. Irimia, and M. Toner, "Microvortex for focusing, guiding and sorting of particles," *Lab on a Chip - Miniaturisation for Chemistry and Biology*, vol. 8, no. 12, pp. 2128–2134, 2008.

[38] L. R. Huang, J. O. Tegenfeldt, J. J. Kraeft, J. C. Sturm, R. H. Austin, and E. C. Cox, "A DNA prism for high-speed continuous fractionation of large dna molecules," *Nature Biotechnology*, vol. 20, no. 10, pp. 1048–1051, 2002.

[39] L. Krivankova and P. Bocek, "Continuous free-flow electrophoresis," *Electrophoresis*, vol. 19, no. 7, pp. 1064–1074, 1998.

[40] D. Raymond, A. Manz, and H. Widmer, "Continuous sample pretreatment using a free-flow electrophoresis device integrated onto a silicon chip," *Analytical Chemistry*, vol. 66, no. 18, pp. 2858–2865, 1994.

[41] D. Raymond, A. Manz, and H. Widmer, "Continuous separation of high molecular weight compounds using a microliter volume free-flow electrophoresis microstructure," *Analytical Chemistry*, vol. 68, no. 15, pp. 2515–2522, 1996.

[42] M. Mazereeuw, C. De Best, U. Tjaden, H. Irth, and J. Van Der Greef, "Free flow electrophoresis device for continuous on-line separation in analytical systems. an application in biochemical detection," *Analytical Chemistry*, vol. 72, no. 16, pp. 3881–3886, 2000.

[43] D. de Jesus, L. Bianes, and C. do Lago, "Microchip free-flow electrophoresis on glass substrate using laser-printing toner as structural material," *Electrophoresis*, vol. 27, no. 24, pp. 4935–4942, 2006.

[44] B. Fonslow, V. Barocas, and M. Bowser, "Using channel depth to isolate and control flow in a micro free-flow electrophoresis device," *Analytical Chemistry*, vol. 78, no. 15, pp. 5369–5374, 2006.

[45] W. Coakley, "Ultrasonic separations in analytical biotechnology," *Trends in Biotechnology*, vol. 15, no. 12, pp. 506–511, 1997.

[46] T. Laurell, F. Petersson, and A. Nilsson, "Chip integrated strategies for acoustic separation and manipulation of cells and particles," *Chemical Society Reviews*, vol. 36, no. 3, pp. 492–506, 2007.

[47] M. MacDonald, G. Spalding, and K. Dholakia, "Microfluidic sorting in an optical lattice," *Nature*, vol. 426, no. 6965, pp. 421–424, 2003.

[48] G. P. Hatch and R. E. Stelter, "Magnetic design considerations for devices and particles used for biological high-gradient magnetic separation (hgms) systems," *Journal of Magnetism and Magnetic Materials*, vol. 225, no. 1-2, pp. 262–276, 2001.

[49] I. Safarik and M. Safarikova, "Use of magnetic techniques for the isolation of cells," *Journal of Chromatography B: Biomedical Sciences and Applications*, vol. 722, no. 1-2, pp. 33–53, 1999.

[50] B. Hirschbein and G. Whitesides, "Affinity separation of enzymes from mixtures containing suspended solids - comparisons of magnetic and nonmagnetic techniques," *Applied Biochemistry and Biotechnology*, vol. 7, no. 3, pp. 157–176, 1982.

[51] K.-B. Lee, S. Park, and C. Mirkin, "Multicomponent magnetic nanorods for biomolecular separations," *Angewandte Chemie - International Edition*, vol. 43, no. 23, pp. 3048–3050, 2004.

[52] M. Zborowski, L. R. Moore, P. S. Williams, and J. J. Chalmers, "Separations based on magnetophoretic mobility," *Separation Science and Technology*, vol. 37, no. 16, pp. 3611 – 3633, 2002.

[53] M. Zborowski, L. Sun, L. R. Moore, P. Williams, and J. J. Chalmers, "Continuous cell separation using novel magnetic quadrupole flow sorter," *Journal of Magnetism and Magnetic Materials*, vol. 194, no. 1-3, pp. 224–230, 1999.

[54] L. R. Moore, A. R. Rodriguez, P. S. Williams, K. McCloskey, B. J. Bolwell, M. Nakamura, J. J. Chalmers, and M. Zborowski, "Progenitor cell isolation with a high-capacity quadrupole magnetic flow sorter," *Journal of Magnetism and Magnetic Materials*, vol. 225, no. 1-2, pp. 277–284, 2001.

[55] C. B. Fuh, H. Y. Tsai, and J. Z. Lai, "Development of magnetic split-flow thin fractionation for continuous particle separation," *Analytica Chimica Acta*, vol. 497, no. 1-2, pp. 115–122, 2003.

[56] F. Carpino, L. R. Moore, J. J. Chalmers, M. Zborowski, and P. S. Williams, "Quadrupole magnetic field-flow fractionation for the analysis of magnetic nanoparticles," *Fifth International Conference on Fine Particle Magnetism*, vol. 17, pp. 174–180, 2005.

[57] A. H. Latham, R. S. Freitas, P. Schiffer, and M. E. Williams, "Capillary magnetic field flow fractionation and analysis of magnetic nanoparticles," *Analytical Chemistry*, vol. 77, no. 15, pp. 5055–5062, 2005.

[58] C. H. Ahn, M. G. Allen, W. Trimmer, Y. N. Jun, and S. Erramilli, "A fully integrated micromachined magnetic particle separator," *Microelectromechanical Systems, Journal of*, vol. 5, no. 3, pp. 151–158, 1996.

[59] J.-W. Choi, T. M. Liakopoulos, and C. H. Ahn, "An on-chip magnetic bead separator using spiral electromagnets with semi-encapsulated permalloy," *Biosensors and Bioelectronics*, vol. 16, no. 6, pp. 409–416, 2001.

[60] T. Deng, M. Prentiss, and G. Whitesides, "Fabrication of magnetic microfiltration systems using soft lithography," *Applied Physics Letters*, vol. 80, no. 3, pp. 461–463, 2002.

[61] J. Do, J.-W. Choi, and C. H. Ahn, "Low-cost magnetic interdigitated array on a plastic wafer," *Magnetics, IEEE Transactions on*, vol. 40, no. 4, pp. 3009–3011, 2004.

[62] K. Smistrup, B. G. Kjeldsen, J. L. Reimers, M. Dufva, J. Petersen, and M. F. Hansen, "On-chip magnetic bead microarray using hydrodynamic focusing in a passive magnetic separator," *Lab on a Chip*, vol. 5, no. 11, pp. 1315–1319, 2005.

[63] K.-Y. Lien, J.-L. Lin, C.-Y. Liu, H.-Y. Lei, and G.-B. Lee, "Purification and enrichment of virus samples utilizing magnetic beads on a microfluidic system," *Lab on a Chip*, vol. 7, no. 7, pp. 868–875, 2007.

[64] K. Smistrup, O. Hansen, H. Bruus, and M. F. Hansen, "Magnetic separation in microfluidic systems using microfabricated electromagnets–experiments and simulations," *Journal of Magnetism and Magnetic Materials*, vol. 293, no. 1, pp. 597–604, 2005.

[65] K. S. Kim and J.-K. Park, "Magnetic force-based multiplexed immunoassay using superparamagnetic nanoparticles in microfluidic channel," *Lab on a Chip*, vol. 5, no. 6, pp. 657–664, 2005.

[66] M. Berger, J. Castelino, R. Huang, M. Shah, and R. H. Austin, "Design of a microfabricated magnetic cell separator," *Electrophoresis*, vol. 22, no. 18, pp. 3883–3892, 2001.

[67] W. Inglis, David, R. Riehn, R. Austin, and J. Sturm, "Continuous microfluidic immunomagnetic cell separation," *Applied Physics Letters*, vol. 85, no. 21, pp. 5093–5095, 2004.

[68] A. C. Siegel, S. Shevkoplyas, D. Weibel, D. Bruzewicz, A. Martinez, and G. Whitesides, "Cofabrication of electromagnets and microfluidic systems in

poly(dimethylsiloxane)," *Angewandte Chemie (International ed.)*, vol. 45, no. 41, pp. 6877–6882, 2006.

[69] N. Pekas, M. Granger, M. Tondra, A. Popple, and M. D. Porter, "Magnetic particle diverter in an integrated microfluidic format," *Journal of Magnetism and Magnetic Materials*, vol. 293, no. 1, pp. 584–588, 2005.

[70] R. Rong, J.-W. Choi, and C. H. Ahn, "An on-chip magnetic bead separator for biocell sorting," *Journal of Micromechanics and Microengineering*, no. 12, p. 2783, 2006.

[71] K.-H. Han and A. B. Frazier, "Continuous magnetophoretic separation of blood cells in microdevice format," *Journal of Applied Physics*, vol. 96, no. 10, pp. 5797–5802, 2004.

[72] K.-H. Han and A. B. Frazier, "Paramagnetic capture mode magnetophoretic microseparator for high efficiency blood cell separations," *Lab on a Chip*, vol. 6, no. 2, pp. 265–273, 2006. 10.1039/b514539b.

[73] E. P. Furlani, "Magnetophoretic separation of blood cells at the microscale," *Journal of Physics. D, Applied Physics*, vol. 40, no. 5, pp. 1313–1319, 2007. 0022-3727.

[74] K.-H. Han, A. Han, and A. B. Frazier, "Microsystems for isolation and electrophysiological analysis of breast cancer cells from blood," *Biosensors and Bioelectronics*, vol. 21, no. 10, pp. 1907–1914, 2006.

[75] N. Xia, T. Hunt, B. Mayers, E. Alsberg, G. Whitesides, R. Westervelt, and D. Ingber, "Combined microfluidic-micromagnetic separation of living cells in continuous flow," *Biomedical Microdevices*, vol. 8, no. 4, pp. 299–308, 2006.

[76] N. Pamme and A. Manz, "On-chip free-flow magnetophoresis: Continuous flow separation of magnetic particles and agglomerates," *Analytical Chemistry*, vol. 76, no. 24, pp. 7250–7256, 2004.

[77] N. Pamme, J. C. T. Eijkel, and A. Manz, "On-chip free-flow magnetophoresis: Separation and detection of mixtures of magnetic particles in continuous flow," *Journal of Magnetism and Magnetic Materials*, vol. 307, no. 2, pp. 237–244, 2006.

[78] N. Pamme and C. Wilhelm, "Continuous sorting of magnetic cells via on-chip free-flow magnetophoresis," *Lab on a Chip*, vol. 6, no. 8, pp. 974–980, 2006.

[79] S. A. Peyman, A. Iles, and N. Pamme, "Rapid on-chip multi-step (bio)chemical procedures in continuous flow - manoeuvring particles through co-laminar reagent streams," *Chemical Communications*, no. 10, pp. 1220–1222, 2008.

[80] J. P. Nolan and L. A. Sklar, "Suspension array technology: evolution of the flat-array paradigm," *Trends in Biotechnology*, vol. 20, no. 1, pp. 9–12, 2002.

[81] C. Simonnet and A. Groisman, "High-throughput and high-resolution flow cytometry in molded microfluidic devices," *Analytical Chemistry*, vol. 78, no. 16, pp. 5653–5663, 2006.

[82] X. Mao, S. C. S. Lin, C. Dong, and T. J. Huang, "Single-layer planar on-chip flow cytometer using microfluidic drifting based three-dimensional (3d) hydrodynamic focusing," *Lab on a Chip*, vol. 9, no. 11, pp. 1583–1589, 2009.

[83] N. Watkins, B. M. Venkatesan, M. Toner, W. Rodriguez, and R. Bashir, "A robust electrical microcytometer with 3-dimensional hydrofocusing," *Lab on a Chip*, vol. 9, no. 22, pp. 3177–3184, 2009.

[84] E. P. Dupont, E. Labonne, C. Vandevyver, U. Lehmann, E. Charbon, and M. A. M. Gijs, "Monolithic silicon chip for immunofluorescence detection on single magnetic beads," *Analytical Chemistry*, vol. 82, no. 1, pp. 49–52, 2010.

[85] X. Xuan, J. Zhu, and C. Church, "Particle focusing in microfluidic devices," *Microfluidics and Nanofluidics*, vol. 9, no. 1, pp. 1–16, 2010.

[86] N. Sundararajan, M. S. Pio, L. P. Lee, and A. A. Berlin, "Three-dimensional hydrodynamic focusing in polydimethylsiloxane (pdms) microchannels," *Journal of Microelectromechanical Systems*, vol. 13, no. 4, pp. 559–567, 2004.

[87] C. C. Chang, Z. X. Huang, and R. J. Yang, "Three-dimensional hydrodynamic focusing in two-layer polydimethylsiloxane (pdms) microchannels," *Journal of Micromechanics and Microengineering*, vol. 17, no. 8, pp. 1479–1486, 2007. Cited By (since 1996): 22 Export Date: 9 December 2009 Art. No.: 009.

[88] R. Scott, P. Sethu, and C. K. Harnett, "Three-dimensional hydrodynamic focusing in a microfluidic coulter counter," *Review of Scientific Instruments*, vol. 79, no. 4, p. 046104, 2008.

[89] C. H. Tsai, H. H. Hou, and L. M. Fu, "An optimal three-dimensional focusing technique for micro-flow cytometers," *Microfluidics and Nanofluidics*, vol. 5, no. 6, pp. 827–836, 2008.

[90] R. Yang, D. L. Feeback, and W. Wang, "Microfabrication and test of a three-dimensional polymer hydro-focusing unit for flow cytometry applications," *Sensors and Actuators, A: Physical*, vol. 118, no. 2, pp. 259–267, 2005.

[91] Y. Gambin, C. Simonnet, V. VanDelinder, A. Deniz, and A. Groisman, "Ultrafast microfluidic mixer with three-dimensional flow focusing for studies of biochemical kinetics," *Lab on a Chip*, pp. 598–609, 2010.

[92] M. G. Lee, S. Choi, and J.-K. Park, "Three-dimensional hydrodynamic focusing with a single sheath flow in a single-layer microfluidic device," *Lab on a Chip*, vol. 9, no. 21, pp. 3155–3160, 2009.

[93] X. Mao, J. R. Waldeisen, and T. J. Huang, ""microfluidic drifting" - implementing three-dimensional hydrodynamic focusing with a single-layer planar microfluidic device," *Lab on a Chip*, vol. 7, no. 10, pp. 1260–1262, 2007.

[94] P. Howell Jr., J. Golden, L. Hilliard, J. Erickson, D. Mott, and F. Ligler, "Two simple and rugged designs for creating microfluidic sheath flow," *Lab on a Chip - Miniaturisation for Chemistry and Biology*, vol. 8, no. 7, pp. 1097–1103, 2008.

[95] H. Sato, Y. Sasamoto, D. Yagyu, T. Sekiguchi, and S. Shoji, "3d sheath flow using hydrodynamic position control of the sample flow," *Journal of Micromechanics and Microengineering*, vol. 17, no. 11, pp. 2211–2216, 2007.

[96] S. Choi, S. Song, C. Choi, and J. K. Park, "Sheathless focusing of microbeads and blood cells based on hydrophoresis," *Small*, vol. 4, no. 5, pp. 634–641, 2008.

[97] D. Di Carlo, "Inertial microfluidics," *Lab on a Chip*, vol. 9, no. 21, pp. 3038–3046, 2009.

[98] S. C. Hur, H. T. K. Tse, and D. D. Carlo, "Sheathless inertial cell ordering for extreme throughput flow cytometry," *Lab on a Chip*, vol. 10, no. 3, pp. 274–280, 2010.

[99] D. Di Carlo, D. Irimia, R. G. Tompkins, and M. Toner, "Continuous inertial focusing, ordering, and separation of particles in microchannels," *Proceedings of the National Academy of Sciences of the United States of America*, vol. 104, no. 48, pp. 18892–18897, 2007.

[100] D. Di Carlo, J. F. Edd, D. Irimia, R. G. Tompkins, and M. Toner, "Equilibrium separation and filtration of particles using differential inertial focusing," *Analytical Chemistry*, vol. 80, no. 6, pp. 2204–2211, 2008.

[101] G. Goddard, J. Martin, S. Graves, and G. Kaduchak, "Ultrasonic particle-concentration for sheathless focusing of particles for analysis in a flow cytometer," *Cytometry Part A*, vol. 69, no. 2, pp. 66–74, 2006.

[102] T. Laurell, F. Petersson, and A. Nilsson, "Chip integrated strategies for acoustic separation and manipulation of cells and particles," *Chemical Society Reviews*, vol. 36, no. 3, pp. 492–506, 2007.

[103] F. Petersson, A. Nilsson, C. Holm, H. Jonsson, and T. Laurell, "Continuous separation of lipid particles from erythrocytes by means of laminar flow and acoustic standing wave forces," *Lab on a Chip - Miniaturisation for Chemistry and Biology*, vol. 5, no. 1, pp. 20–22, 2005.

[104] T. H. Wang, Y. Peng, C. Zhang, K. W. Pak, and C. M. Ho, "Single-molecule tracing on a fluidic microchip for quantitative detection of low-abundance nucleic acids," *Journal of the American Chemical Society*, vol. 127, no. 15, pp. 5354–5359, 2005.

[105] J. Shi, X. Mao, D. Ahmed, A. Colletti, and T. J. Huang, "Focusing microparticles in a microfluidic channel with standing surface acoustic waves (ssaw)," *Lab on a Chip*, vol. 8, no. 2, pp. 221–223, 2008.

[106] Y. W. Kim and J. Y. Yoo, "Axisymmetric flow focusing of particles in a single microchannel," *Lab on a Chip*, vol. 9, no. 8, pp. 1043–1045, 2009.

[107] Y. W. Kim and J. Y. Yoo, "Three-dimensional focusing of red blood cells in microchannel flows for bio-sensing applications," *Biosensors and Bioelectronics*, vol. 24, no. 12, pp. 3677–3682, 2009.

[108] E. Cummings and A. Singh, "Dielectrophoresis in microchips containing arrays of insulating posts: Theoretical and experimental results," *Analytical Chemistry*, vol. 75, no. 18, pp. 4724–4731, 2003.

[109] R. Aoki, M. Yamada, M. Yasuda, and M. Seki, "In-channel focusing of flowing microparticles utilizing hydrodynamic filtration," *Microfluidics and Nanofluidics*, vol. 6, no. 4, pp. 571–576, 2009.

[110] N. D. J. Price C. P., *Principles and Practice of Immunoassay*. Macmillan reference Ltd., 1997.

[111] A. H. Wu, "A selected history and future of immunoassay development and applications in clinical chemistry," *Clinica Chimica Acta*, vol. 369, no. 2, pp. 119 – 124, 2006. Special issue celebrating the 50th anniversary of Clinica Chimica Acta.

[112] D. Wild, ed., *The immunoassay handbook*. Elsevier, 2005.

[113] N. D. Price, C.P., *Principles and Practice of Immunoassay*. Grove's Dictionaries; 2 Sub edition, 1991.

[114] G. Burns, A. Kurrle-Weittenhiller, J. Karl, W. Dieter Engel, A. Gromping, K.-S. Boos, and D. Seidel, "A simple turbidimetric assay designed for the routine screening as well as therapeutic monitoring of native ldl particles," *Clinica Chimica Acta*, vol. 303, no. 1-2, pp. 155–165, 2001.

[115] L. Lewellen and H. McCurdy, "A novel procedure for the analysis of drugs in whole blood by homogeneous enzyme immunoassay," *Journal of Analytical Toxicology*, vol. 12, no. 5, pp. 260–264, 1988.

[116] E. Loomans, A. van Doornmalen, J. Wat, and G. Zaman, "High-throughput screening with immobilized metal ion affinity-based fluorescence polarization detection, a homogeneous assay for protein kinases.," *Assay Drug Dev Technol*, vol. 1, no. 3, pp. 445–453, 2003.

[117] E. Ullman, H. Kirakossian, A. Switchenko, J. Ishkanian, M. Ericson, C. Wartchow, M. Pirio, J. Pease, B. Irvin, S. Singh, R. Singh, R. Patel, A. Dafforn, D. Davalian, C. Skold, N. Kurn, and D. Wagner, "Luminescent oxygen channeling assay (loci(tm)): Sensitive, broadly applicable homogeneous immunoassay method," *Clinical Chemistry*, vol. 42, no. 9, pp. 1518–1526, 1996.

[118] S. Miraglia, , J. Mellentin-Michelotti, L. Evangelista, C. Smith, I. Gunawan, K. Lohman, E. Goldberg, B. Manian, and P.-M. Yuan, "Homogeneous cell- and bead-based assays for high throughput screening using fluorometric microvolume assay technology," *Journal of Biomolecular Screening*, vol. 4, no. 4, pp. 193–204, 1999.

[119] J. H. Leuvering, B. C. Goverde, P. J. Thal, and A. H. Schuurs, "A homogeneous sol particle immunoassay for human chorionic gonadotrophin using monoclonal antibodies," *Journal of Immunological Methods*, vol. 60, no. 1-2, pp. 9–23, 1983.

[120] T. H. Aoki, M. Satoh, K. Mizuki, and H. Watabe, "A homogeneous assay for relative affinity of binding proteins using a green fluorescent protein tag and membrane disk," *Analytical Biochemistry*, vol. 344, no. 1, pp. 25–32, 2005.

[121] R. Lee, M. Trans, M. Nocerini, and M. Liang, "A high-throughput hybridoma selection method using fluorometric microvolume assay technology," *Journal of Biomolecular Screening*, vol. 13, no. 3, pp. 210–217, 2008.

[122] R. S. Yalow and S. A. Berson, "Immunoassay of endogenous plasma insulin in man," *Journal of Clinical Investigation*, vol. 39, no. 7, pp. 1157–1175, 1960.

[123] E. Engvall and P. Perlmann, "Enzyme-linked immunosorbent assay (elisa) quantitative assay of immunoglobulin-g," *Immunochemistry*, vol. 8, no. 9, p. 871, 1971.

[124] B. Vanweeme and A. H. W. Schuurs, "Immunoassay using antigen-enzyme conjugates," *Febs Letters*, vol. 15, no. 3, p. 232, 1971.

[125] J. M. Singer and C. M. Plotz, "The latex fixation test: I. application to the serologic diagnosis of rheumatoid arthritis," *The American Journal of Medicine*, vol. 21, no. 6, pp. 888–892, 1956.

[126] J. Molina-Bolivar and F. Galisteo-Gonzalez, "Latex immunoagglutination assays," *Journal of Macromolecular Science - Polymer Reviews*, vol. 45, no. 1, pp. 59–98, 2005.

[127] F. Lacharme, C. Vandevyver, and M. A. M. Gijs, "Full on-chip nanoliter immunoassay by geometrical magnetic trapping of nanoparticle chains," *Analytical Chemistry*, vol. 80, no. 8, pp. 2905–2910, 2008.

[128] G. Degre, E. Brunet, A. Dodge, and P. Tabeling, "Improving agglutination tests by working in microfluidic channels," *Lab on a Chip*, vol. 5, no. 6, pp. 691–694, 2005.

[129] Y. Moser, T. Lehnert, and M. A. M. Gijs, "On-chip immuno-agglutination assay with analyte capture by dynamic manipulation of superparamagnetic beads," *Lab on a Chip*, vol. 9, no. 22, pp. 3261–3267, 2009.

[130] R. Afshar, Y. Moser, T. Lehnert, and M. A. M. Gijs, "Magnetic particle dosing and size separation in a microfluidic channel," *Sensors and Actuators B: Chemical,*, p. DOI: 10.1016/j.snb.2009.08.044, 2009.

[131] G. H. Zhang J., Tan K.L., "Characterization of the polymerization of su-8 photoresist and its applications in micro-electro-mechanical systems (mems)," *Polymer Testing*, vol. 20, no. 6, pp. 693–701, 2001.

[132] Y. Moser, *Dynamic Actuation of Magnetic Beads for Immunoassays on-chip*. PhD thesis, EPFL, 2010.

Curriculum Vitae

Rana Afshar

Date of birth: March 7, 1981

Avenue Floréal, 5, CH-1006, Lausanne

Rana.afshar@gmail.com, +41 78 811 50 74

Education

- **PhD in Microtechnology - 2007 - 2011**

  Microsystems laboratory 2 (LMIS2),

  Ecole Polytechnique Fédérale de Lausanne (EPFL), Switzerland

  Subject: Separation and focusing of magnetic beads for agglutination tests

- **Master of micro and nanotechnology (Molecular science) - 2005-2007**

  University of Neuchâtel IMT (institute of microtechnology)

- **Bachelor of chemical engineering 1999-2003**

  Polytechnic University of Tehran

Professional experiences

- **Teaching assistant in microsystem group, EPFL - 2007-2011**

  Teaching responsibilities for practical courses

- **Process engineer in chemical engineering company) - 2003-2005**

  Sales engineer (Eshteale Arak co, Iran)

- **Summer training at microsystems laboratory 1, EPFL - 7.2007-10.2007**

  Electro-deposition of Pd

Peer-reviewed papers

– R. Afshar, Y. Moser, T. Lehnert, and M. A. M. Gijs, *3-dimensional magnetic focusing of superparamagnetic beads for on-chip agglutination assays*, Analytical chemistry, DOI: 0.1021/ac102813x, 2011.

– R. Afshar, Y. Moser, T. Lehnert, and M. A. M. Gijs, *Magneto-Microfluidic Three-Dimensional Focusing of Magnetic Particles,* AIP Conference Proceedings, vol. 1311, no. 1, pp. 161166, 2010.

– R. Afshar, Y. Moser, T. Lehnert, and M. A. M. Gijs, *Magnetic particle dosing and size separation in a microfluidic channel,* Sensors and Actuators B: Chemical, DOI: 10.1016/j.snb.2009.08.044, 2009.

Conference contributions

– R. Afshar, Y. Moser, T. Lehnert, M.A.M. Gijs, *Magnetic particle dosing, release and separation in a microfluidic chip with magnetic actuation*, MicroTAS 2010, Groningen, Netherlands.

– R. Afshar, Y. Moser, T. Lehnert, M.A.M. Gijs, *Magnet-Microfluidic Three-Dimensional Focusing of Magnetic Particles*, 8th International Conference on the Scientific and Clinical Applications of Magnetic Carriers 2010, Rostock, Germany

– R. Afshar, T. Lehnert, Y. Moser, and M.A.M. Gijs. *Magnetic bead dosing, release and separation in a microfluidic chip with magnetic actuation*, Transducers 2009, Denver, USA

– Y. Moser, T. Lehnert, E. Dupont, R. Afshar, and M.A.M. Gijs, *Active superparamagnetic bead manipulation for immunoassays on-chip*, MicroTAS 2008, San Diego, USA

– Y. Moser, T. Lehnert, R. Afshar, G. Sinicco, and M.A.M. Gijs. *Active superparamagnetic bead manipulation on-chip*. 7th International Conference on Scientific and Clinical Applications of Magnetic Carriers 2008, Vancouver, Canada

– R. Afshar, Y. Moser, T. Lehnert, and M.A.M. Gijs. Microfluidic chip for the separation of magnetic beads. Digest Nanotech 2007, Montreux, Switzerland